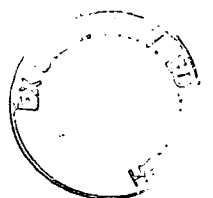


A Numerical Method for Perturbative QCD Calculations

Mark Anthony Sookraj Ramtohol



Doctor of Philosophy
The University of Edinburgh
2004



Abstract

Standard methods for performing analytic perturbative calculations for the process of $e^+e^- \rightarrow q\bar{q}$ up to $\mathcal{O}(\alpha_s)$ are explained and the results given. An emphasis is given to the organisation of calculations using the Cutkosky cutting rules and the renormalisation of the massive quark propagator.

Methods for numerical integration are presented including those used in VEGAS. The numerical methods used in the Beowulf program for calculating infra-red safe observables for jet events from electron-positron collisions are also explained. Cancellations of singularities required for numerical calculations are demonstrated using an example in ϕ^3 theory both numerically and graphically. Renormalisation by subtraction of appropriate integrals is also covered.

Adaptations of the Beowulf procedure required for the inclusion of massive fermions are developed and explained. An alternative method for including the quark self energy and its related cuts using scalar decomposition, numerically equivalent integrals and its spinor structure is introduced. The methods are used to calculate the $\mathcal{O}(\alpha_s)$ corrections to the process $e^+e^- \rightarrow q\bar{q}$ using VEGAS. Drawbacks of the smearing function required in the numerical integration due to the corrections dependence on the mass and centre of mass energy are discussed. Results of the $\mathcal{O}(\alpha_s)$ cross section using the numerical method verify the procedure. The method will then be used to see the effects of mass on the thrust distribution and when using the Durham and JADE jet algorithms.

Declaration

This thesis has been composed by myself. The method described for the inclusion of massive fermions in numerical perturbative calculations and the results obtained from the numerical calculations are all my own work. The computer program used to generate the results uses the VEGAS numerical integration routine created by Peter Lepage and is based upon the Beowulf program created by Davison Soper. This work has not been submitted for any other degree or professional qualification other than for the doctorate of philosophy.

Mark A. S. Ramtohul.

Acknowledgements

There are a number of people who I would like to thank that have helped me throughout the time I have worked on this thesis. I would like to thank my supervisor Michael Krämer for giving me this project and for all his help, support and guidance especially when putting the thesis together. I am very grateful for the time, technical assistance and encouragement Thomas Binoth has given me throughout the project. I would like to thank Dave Soper for setting up the project that my work is based upon and the useful discussions and suggestions for development of the method.

Within the School of Physics, there have been many people who have supported me during my study in Edinburgh. The Particle Physics Theory group both staff and students who have always been very friendly, with assistance at the knock of a door. Of the students in the group I would particularly like to thank Derek Hepburn and Varda Hood who welcomed me to their office and were willing to listen to me on a daily basis. I would also like to thank the ‘condensed matter crew’ and other lecturers in the school who have made me feel at home in the department.

I would like to thank my friends outside of the physics community who have showed interest in my work although the details may have been a bit beyond them. Finally I would like to thank my parents, Gooroodutt and Kathleen, and my brother Andrew who constantly drive me onwards and have always been there for me.

Contents

| | |
|---|-----------|
| 1. Introduction | 1 |
| 2. Analytic Framework | 5 |
| 2.1. Quantum Field Theory | 5 |
| 2.2. Calculating the Born Cross Section | 8 |
| 2.3. $\mathcal{O}(\alpha_s)$ Correction | 15 |
| 2.4. Massive Quarks | 27 |
| 3. Numerical Methods | 31 |
| 3.1. Monte-Carlo Integration | 31 |
| 3.1.1. Sampling Techniques | 32 |
| 3.1.2. Choosing Coordinate Systems | 33 |
| 3.2. An Example in ϕ^3 Theory | 36 |
| 3.2.1. Soft Singularities | 42 |
| 3.2.2. Collinear Singularities | 46 |
| 3.2.3. Scattering Singularity | 50 |
| 3.3. Visualisation of Singularity Cancellations | 51 |

Contents

| | |
|--|------------|
| 3.4. Dealing with UV Singularities | 67 |
| 3.5. Treatment of Scattering Singularities | 70 |
| 4. Numerical Calculations | 75 |
| 4.1. Integrands with Massive Fermions | 75 |
| 4.1.1. Vertex Correction | 76 |
| 4.1.2. Self Energy Correction | 82 |
| 4.1.3. Comparison to the Massless Case | 87 |
| 4.2. Cancellation of Singularities Revisited | 87 |
| 4.2.1. Vertex Graph | 87 |
| 4.2.2. Self Energy Graph | 89 |
| 4.3. Obtaining Numerical Results | 91 |
| 4.4. Infra-Red Safe Observables | 104 |
| 4.5. Ground Work for Future Calculations | 112 |
| 5. Conclusions | 117 |
| A. Feynman Rules | 121 |
| A.1. ϕ^3 Rules | 121 |
| A.2. Standard Rules | 122 |
| A.3. Cutkosky Cutting Rules in the Feynman Gauge | 123 |
| B. Integrand Algebra | 125 |
| B.1. Gamma Matrices in n Dimensions | 125 |
| B.2. Feynman Parameters | 125 |

| | |
|--|------------|
| B.3. n Dimensional Integrals | 126 |
| B.4. Gamma Functions | 126 |
| B.5. Colour Factors | 127 |
| C. Binned Thrust Values | 129 |

1. Introduction

Like all research in physics, this thesis has grown from the vast amount of work performed by many physicists. Without the basis given by them, the material developed here would be at most a mathematical challenge. However using the theories and models already constructed, the method assembled in this thesis could be used and adapted to help make predictions and verify results from experiments that could give a deeper insight into the building blocks of the universe.

The work described is constructed within the framework of particle physics theory. In particular, the phenomenological aspect of calculating quantities using the accepted models formulated in the language of quantum field theory that can be verified using experiments. All the results presented have been generated using the Standard Model of particle physics with special interest in Quantum Chromodynamics (QCD) and have been obtained previously using methods that will be described again in this thesis. So what does this work offer that has not already been obtained?

To help answer this question, it is useful to understand the motivation behind the recent work of Davison Soper [1]. His work grew from the methods developed by Ellis, Ross and Terrano [2] for performing calculations using a combined analytic and numerical approach. Mainly on the grounds of versatility, Soper sought a purely numerical approach to the problem. Thus Beowulf was created, a computer program that uses a 'bare hands' approach akin to the fabled hero from the story of the same name.

The Beowulf program has gradually developed around the core theme of perturbative QCD. Preliminary versions used numerical integration to calculate the properties

1. Introduction

of three jet processes as found in the detectors of electron-positron colliders using the next to leading order approximation of perturbative QCD. As the program has matured the methods for choosing suitable contours of integration and the organisation of sampling methods used in the numerical integration [3] have been adapted.

The two biggest changes to the program make moves towards calculating more physical processes. Firstly Beowulf was adapted to have a representation for the gluons that did not transmit unphysical polarisations into the final state particles [4]. There is freedom to choose the way gluons are represented as they are gauge particles. This allows them to be parametrised in a multitude of ways. However, for any particular calculation with a fixed parametrisation a result is gained that is independent of this choice if gauge invariant calculations are performed. A simple yet unphysical choice of gauge that was employed in the earlier versions is the Feynman gauge and so the physical Coulomb gauge that requires more intensive calculations was chosen in preference.

This leads directly onto the second adaptation. The motivation behind having physical polarisation states for the gluon was so that more physical jets could be simulated [5, 6]. To do this, a move away from inclusive fixed orders in perturbation theory is made by including parton showering. By doing this, a step towards modelling jets similar to those found in experiments is made where many particles cluster to form jets.

Another feature to be considered, and the motivation behind this work, is the effect of mass on jet calculations. The effectiveness of perturbative QCD as a predictive tool is reliant upon experiments performed at high energies. This is due to a property called asymptotic freedom where the coupling constant of the strong force, g , that determines the strength of the force and acts as an expansion parameter of the perturbative series, decreases with increasing energy. At sufficiently high energies the coupling constant is small enough to warrant a perturbative expansion. This leads to smaller corrections as the order of the perturbative series increases. The upshot is that for the lighter quarks; up, down, strange and charm, the energies are much greater than the masses and so the effects of their mass are negligible. However, if jets based on bottom and top parent quarks are produced, then the mass effects are more prominent. To reduce errors in calculations, increase predictive power and gain better understanding of results from

experiments, it is important to include this characteristic. The introduction of mass also leads to the examination of other possible models such as super-symmetric theories so that they can be compared to the results obtained through the Standard Model.

The work that follows will illustrate how massive quarks may be included into a numerical procedure for calculating jet properties. To test this method a less complicated process concerning the $\mathcal{O}(\alpha_s)$ correction of electron-positron annihilation into two jets was chosen. In chapter two aspects of quantum field theory, analytic calculations and results pertinent to the verification of the numerical method for this process will be presented. Chapter three explains the concepts of numerical integration and how they are used in this context. Results and interpretations of the numerical procedure, comparisons with analytic procedures and implications for the incorporation of the concept into Beowulf will be given in chapter four. Finally in chapter five the practicalities and applicability of the method for introducing massive fermions will be summed up with a discussion of possibilities for future work.

2. Analytic Framework for Calculations of Quark-Antiquark Production from Electron-Positron Annihilation up to $\mathcal{O}(\alpha_s)$

When developing a technique for calculating using a computer it is useful to have known results to compare against. As the perturbative calculation of $e^+e^- \rightarrow q\bar{q}$ is well known, it is a suitable candidate for comparison with the numerical technique. In this chapter the principles behind the analytic calculations will be discussed, technical details that support the development of a numerical procedure presented and the results to check the numerical procedure will be given.

2.1. Quantum Field Theory

The Standard Model of particle physics has had much success in describing the nature and interactions of the sub atomic particles [7]. Using quantum field theory to describe the strong, weak and electromagnetic forces as interactions of gauge bosons with the quarks and leptons is a major achievement. Most importantly, it has survived the tests set out by experiments. Extensions to the Standard Model have mainly come in the form of supersymmetric theories which are again field theories. Seeing that quantum field theories play a major role in our understanding of the fundamental nature of matter, it is important to develop effective tools to test the models created and make

2. Analytic Framework

predictions using these theories.

Given a specific quantum field theory, a suitable procedure for calculating processes must be chosen. Asymptotic freedom of QCD and naturally small coupling constants of the electroweak theory have led to perturbative calculations taking a prominent role in calculating high-energy scattering processes. Analytic calculations have progressively been performed to higher orders in perturbation theory. The procedures for creating the required terms in perturbative calculations is fairly straight forward, even mechanical due to the Feynman rules (Appendix A). The main difficulties and developments in calculations have been in the techniques for preparing and evaluating the integrals that need to be performed. While analytic calculations using techniques such as Feynman parameters and dimensional regularisation are very effective, integrals for high order calculations become increasingly more challenging and result in functions that require numerical evaluation.

Although the Feynman rules may provide a way of constructing the amplitudes required for the process, technical issues can hamper the calculations. As the Standard Model is renormalisable, consistent interpretable finite answers can be produced. Intermediate divergent results still need to be handled with care. This applies both to high energy ultra-violet divergences (UV), low energy infra-red divergences (IR) and mass singularities. Changing the integrals so that they are performed in n dimensions can regulate these divergences [8]. While the IR divergences and mass singularities cancel for inclusive calculations of electron positron annihilations, the UV divergences have to be removed through renormalisation. Although the renormalisation schemes of minimal subtraction (MS) [9] and modified minimal subtraction (\overline{MS}) have been developed through the dimensional regularisation procedure, there is still a degree of freedom in choosing what to use. The freedom of choice is restricted however by the Ward identities [10] that give the relationships between renormalisation terms used for renormalising different UV divergent graphs in both the electroweak and strong theories. There is also a matter of preference how renormalisation schemes are implemented. One could choose to use only renormalised propagators and vertices, thus avoiding loop diagrams or use loop diagrams and find the suitable counter terms afterwards. Using different renormalisation schemes leads to effects that manifest as higher order corrections.

When making calculations using Quantum Electrodynamics (QED) and QCD, the similarities between them are very useful. Unless the Feynman diagrams to be used contain the triple or quartic gluon vertices then the algebraic differences between the two theories are caused by the coupling constants, and the Lie algebra used in QCD due to its non-Abelian $SU(3)$ nature. These differences produce overall factors for this subset of processes. Although these theories may look very similar it is important to keep in mind the physical differences between them. While the leptons can exist as free particles, the quarks and the gluon, collectively the partons, are only detected via their formation of hadrons in the form of jets. This relies on the principle of confinement that requires all partons to form hadrons. Perturbation theory in QCD deals with the initial partons as the non-perturbative creation of hadrons is factored out. Calculations tell us about the high energy scattering process and the basic characteristics of the jets produced but not the detailed nature of the jets themselves or how they are formed. Models are needed in QCD to describe the evolution of partons into hadrons. Characteristics of the strong coupling constant also limits the region of centre of mass energies for which the perturbative methods are valid for QCD as the coupling is high for small energies.

The analytic properties of the scattering matrices can help in the organisation and calculation of scattering processes. High order corrections of propagators, vertices and general N-point functions can be related to scattering processes through the optical theorem [7]. This basically states that a Feynman diagram of a given order in perturbation theory with N external particles (N-point function) can be related to the sum of all the possible scattering processes that contain the same order of coupling in total and have the same initial states as the N-point functions legs. Standard processes involving the corrections due to decays of particles or the scattering of two particles correspond to corrections of a two-point function (propagator) or a four-point function respectively with pairs of identical particles. The analytic properties also allow this to be performed on a subpart of a particular amplitude as well. By relating high energy processes to N-point functions it is easy to categorise the required graph topologies to be included and provides a simple way of calculating higher order corrections.

Given the relation between N-point functions and scattering processes it would be useful to have a simple method for determining the required scattering matrices. This

2. Analytic Framework

is given through Cutkosky's cutting rules [11] which were developed as a consequence of looking at the analytic properties of scalar amplitudes and using the optical theorem. Through the Cutkosky rules the expressions of the Feynman diagrams that have loops are related to the expressions of scattering processes. When separating an N-point function into two amplitudes a line is drawn through the pictorial representation of the N-point function effectively cutting the diagram. This was first considered using scalar particles leading to a relationship between a propagator and a cut propagator. Adapted Feynman rules can be applied to cut diagrams or cutting rules can be used to adapt the expression for the N-point function.

2.2. Calculating the Born Cross Section

To put some of the theory mentioned in context it is useful to apply it to the simple calculation of the Born cross section [7, 12, 13]. When an electron and positron collide they can annihilate and produce a multitude of possible particles. The collection of particles created will conserve the quantum numbers and kinematic properties of the initial state. One particular production channel is via an intermediate virtual photon. The photon then decays into a particle-antiparticle pair that interact through the electromagnetic force and satisfy the initial conditions. Further decays are then possible although the case when only a muon anti-muon pair is created is the Born process (Fig. 2.1).

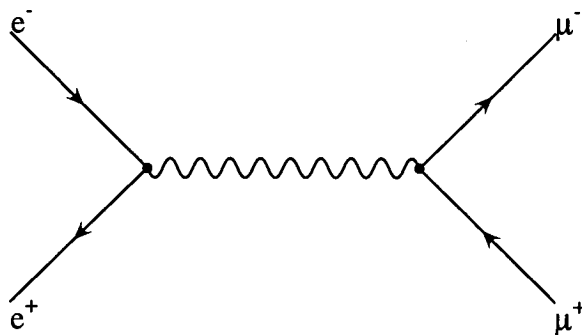


Figure 2.1.: The Born process, $e^+e^- \rightarrow \mu^+\mu^-$.

This is the simplest Feynman diagram to produce a muon-antimuon pair as the

Standard Model does not allow for vertices that change lepton generation. In addition it has the least possible vertices for this process and so the fewest interactions meaning the lowest order and fundamental underlying process. It is also a process that solely involves the electromagnetic force. The similarity between quarks and leptons can be demonstrated by replacing the muon-antimuon pair with a quark-antiquark pair. This is possible as the quarks interact through the electromagnetic force as well as the strong force. Figure 2.2 shows that diagrammatically it is basically the same structure and

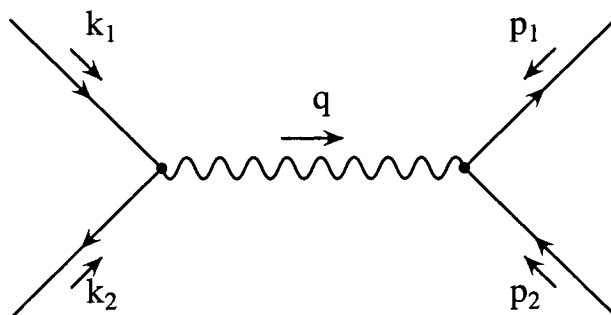


Figure 2.2.: Lowest order production of a quark-antiquark pair from electron-positron annihilation.

again it is the simplest diagram to produce quarks through the electromagnetic force as there are no vertices that mix lepton and quark generations. The differences can be seen in the algebraic representations and their physical differences as mentioned earlier. Rather than proceeding to calculate the $e^+e^- \rightarrow \mu^+\mu^-$ the $e^+e^- \rightarrow q\bar{q}$ calculation will be performed as it will be the QCD corrections that are required for this thesis and it forms the basis for the remaining work. This will be referred to as the Born cross section throughout the rest of the thesis. Also to keep the calculation simple, massless quarks will be used for the moment although it is the aim to use massive quarks eventually.

Determining the required integral for this process using the Feynman rules (Appendix A) is a fairly simple procedure. Each line and vertex in the diagram corresponds to an algebraic expression that is written in order, going against the direction of the fermion flow as represented by the arrows on the fermion lines. To find the scattering matrix the amplitude has to be multiplied by its hermitian conjugate. This is effectively done by reversing the order of the original amplitude, changing factors of i to $-i$ and conjugating the spinors. By keeping track of the spinor indices, this leads to an

2. Analytic Framework

integrand that consists of two traces:

$$\begin{aligned}
\mathcal{M} &= \left(\bar{u}(p_1)(iQe\gamma^\mu)v(p_2) \left(\frac{-ig_{\mu\nu}}{q^2} \right) \bar{v}(k_2)(ie\gamma^\nu)u(k_1) \right) \\
|\mathcal{M}|^2 &= \left(\bar{u}(p_1)(iQe\gamma^\mu)v(p_2) \left(\frac{-ig_{\mu\nu}}{q^2} \right) \bar{v}(k_2)(ie\gamma^\nu)u(k_1) \right) \\
&\quad \times \left(\bar{u}(k_1)(-ie\gamma^\sigma)v(k_2) \left(\frac{ig_{\rho\sigma}}{q^2} \right) \bar{v}(p_2)(-iQe\gamma^\rho)u(p_1) \right) \\
&= \text{Tr}(\bar{u}(p_1)(iQe\gamma^\mu)v(p_2)\bar{v}(p_2)(-iQe\gamma^\rho)u(p_1)) \\
&\quad \times \text{Tr}(\bar{v}(k_2)(ie\gamma^\nu)u(k_1)\bar{u}(k_1)(-ie\gamma^\sigma)v(k_2)) \times \frac{-ig_{\mu\nu}}{q^2} \times \frac{ig_{\rho\sigma}}{q^2} \\
&= \frac{Q^2 e^4}{q^4} \text{Tr}(\bar{u}(p_1)\gamma^\mu v(p_2)\bar{v}(p_2)\gamma^\rho u(p_1)) \text{Tr}(\bar{v}(k_2)\gamma_\mu u(k_1)\bar{u}(k_1)\gamma_\rho v(k_2)) .
\end{aligned} \tag{2.1}$$

The integrand can be further simplified by using spinor algebra, properties of the gamma matrices and the trace (Appendix B). For an inclusive calculation all possible spin states of the final state particles are included and an average of the spin states of the initial state particles as the initial particles are usually unpolarised. There is also a numerical colour factor due to the quarks carrying the colour quantum number. Using these properties the scattering matrix becomes,

$$\begin{aligned}
|\mathcal{M}|^2 &= \frac{Q^2 e^4}{q^4} \text{Tr}(\not{p}_1 \gamma^\mu \not{p}_2 \gamma^\rho) \text{Tr}(\not{k}_2 \gamma_\mu \not{k}_1 \gamma_\rho) \\
&= \frac{4N_c Q^2 e^2}{q^4} (p_1^\mu p_2^\rho - p_1 \cdot p_2 g^{\mu\rho} + p_1^\rho p_2^\mu) (k_{2\mu} k_{1\rho} - k_2 \cdot k_1 g_{\mu\rho} + k_{2\rho} k_{1\mu}) \\
&= \frac{4N_c Q^2 e^4}{q^4} (2p_1 \cdot k_2 p_2 \cdot k_1 + 2p_1 \cdot k_1 p_2 \cdot k_2 + (n-4)p_1 \cdot p_2 k_1 \cdot k_2) . \tag{2.2}
\end{aligned}$$

Using standard scattering theory the cross section is found by integrating the scattering matrix just determined over Lorentz invariant phase space and dividing this answer by a flux factor. To simplify calculations it is easier to work in the centre of mass frame which gives the virtual photon an energy E_{cm} but no three-momentum. The incoming momenta will be taken to lie along the z-axis (beam axis) and the outgoing

2.2. Calculating the Born Cross Section

momenta will be at an angle θ to the z-axis in the y-z plane:

$$k_1 = \frac{E_{cm}}{2}(1, 0, 0, 1) \quad (2.3)$$

$$k_2 = \frac{E_{cm}}{2}(1, 0, 0, -1) \quad (2.4)$$

$$p_1 = \frac{E_{cm}}{2}(1, 0, \sin \theta, \cos \theta) \quad (2.5)$$

$$p_2 = \frac{E_{cm}}{2}(1, 0, -\sin \theta, -\cos \theta) \quad (2.6)$$

$$(2.7)$$

Using these relations the cross section is given by,

$$\begin{aligned} \sigma_0 &= \frac{1}{2E_{k_1}2E_{k_2}|v_{\vec{k}_1} - v_{\vec{k}_2}|} \\ &\times \int \frac{d^{n-1}\vec{p}_1}{2E_{p_1}(2\pi)^{n-1}} \int \frac{d^{n-1}\vec{p}_2}{2E_{p_2}(2\pi)^{n-1}} |\mathcal{M}|^2 (2\pi)^n \delta(p_1 + p_2 - k_1 - k_2) \\ &= \frac{1}{2E_{cm}^2} \int \frac{d^{n-1}\vec{p}_1}{2E_{p_1}(2\pi)^{n-1}} \int \frac{d^{n-1}\vec{p}_2}{2E_{p_2}(2\pi)^{n-1}} |\mathcal{M}|^2 (2\pi)^{n-1} \delta(p_1 + p_2 - k_1 - k_2) \\ &= \frac{1}{2E_{cm}^2} \int \frac{d^{n-1}\vec{p}_1}{2E_{p_1}2E_{p_2}(2\pi)^{n-1}} |\mathcal{M}|^2 (2\pi) \delta(E_{p_1} + E_{p_2} - E_{cm}) \\ &= \frac{1}{2E_{cm}^2} \int d\Omega \int d|\vec{p}_1| |\vec{p}_1|^{n-4} \frac{1}{16\pi^2} |\mathcal{M}|^2 \delta(2|\vec{p}_1| - E_{cm}) \\ &= \frac{1}{2E_{cm}^2} \int d\Omega \frac{1}{32\pi^2} \left(\frac{E_{cm}}{2}\right)^{n-4} |\mathcal{M}|^2 \end{aligned} \quad (2.8)$$

The calculations performed have used momentum conservation of the two particle final state and the relationship between the energies of the particles to the centre of mass energy, E_{cm} . Using the expressions gained the form of the squared scattering matrix has to be modified and the remaining angular integrals performed. As no poles have been created in the calculation so far, it is safe to perform the remaining calculations with $n = 4$ and so the angular integrals are just those used in spherical

2. Analytic Framework

polar coordinates:

$$\begin{aligned}
\sigma_0 &= \frac{1}{2E_{cm}^2} \int d\phi \int d\cos\theta \frac{1}{32\pi^2} \frac{4N_c Q^2 e^4}{E_{cm}^4} \\
&\quad \times \left(2 \left(\frac{E_{cm}}{2} \right)^4 (1 + \cos\theta)^2 + 2 \left(\frac{E_{cm}}{2} \right)^4 (1 - \cos\theta)^2 \right) \\
&= \frac{1}{2E_{cm}^2} \int d\phi \int d\cos\theta \frac{1}{32\pi^2} N_c Q^2 e^4 (1 + \cos^2\theta) \\
&= \frac{1}{2E_{cm}^2} \int d\cos\theta \frac{1}{16\pi} N_c Q^2 e^4 (1 + \cos^2\theta) \\
&= \frac{1}{2E_{cm}^2} \frac{1}{16\pi} N_c Q^2 e^4 \left(2 + \frac{2}{3} \right) \\
&= \frac{4N_c Q^2 \pi \alpha^2}{3E_{cm}^2} . \tag{2.9}
\end{aligned}$$

To complete this example, the number of generations of quarks to be included in the calculation needs to be considered. When the centre of mass energy passes through the threshold for the production of a generation of quarks the cross section gains a contribution from it. This would require the centre of mass energy to be much greater than twice the mass of the heaviest quark. As massless quarks have been used, those that would be produced at a given centre of mass energy needs to be included. The difference in contribution comes from the charge of the quarks contributing. The charge for the up, charm and top quark is $\frac{2}{3}$ while for the down, strange and bottom quarks it is $-\frac{1}{3}$. With this information the cross section can be written in terms of the cross section R for $e^+e^- \rightarrow \mu^+\mu^-$ given the type of quarks, i , to be used.

$$\begin{aligned}
\sigma_0 &= N_c \sum_i Q_i^2 \frac{4\pi\alpha^2}{3E_{cm}^2} \\
&= N_c \sum_i Q_i^2 R . \tag{2.10}
\end{aligned}$$

Extending this calculation to the next order in perturbation theory will increase the accuracy of the calculation. Since the final state particles can interact via the strong force it is natural to consider the quantum corrections due to QCD, although it is also possible to look at the electroweak corrections. One reason for considering the strong interactions is that they will have a dominant effect due to the size of the coupling compared to that of the electroweak coupling constants. Another reason is that it is a simpler effect to consider as at the next level of perturbation theory it only affects the final state particles. This means that the corrections will not be affected by the initial state particles and so they only contribute to the angular distribution and an overall

2.2. Calculating the Born Cross Section

factor in the cross section. With this in mind it is possible to simplify the integrands further by ignoring the initial state particle when determining higher order corrections produced by the strong force on the total cross section.

Removing the initial electron-positron collision from the scattering diagram leaves a process that looks like the decay of a virtual photon into a quark-antiquark pair (Fig.2.3). Instead of having the spinor structure of the electron-positron scattering

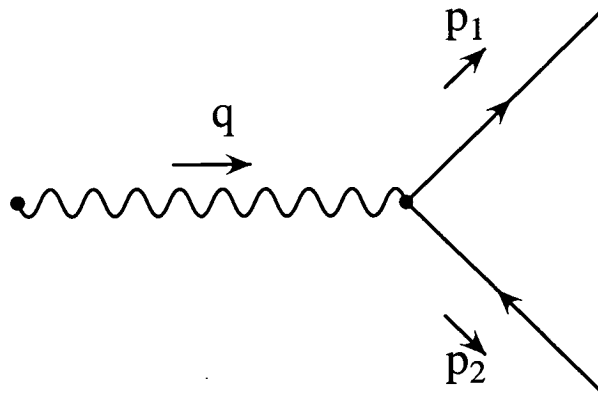


Figure 2.3.: Decay of a virtual photon into a quark-antiquark pair.

there is a simple polarisation vector for the photon. The decay itself is defined in much the same way as a scattering process with its Lorentz invariant integrals and integrand but now with a prefactor that is inversely proportional to the mass of the decaying particle. As it is the ratio between the lower and higher order corrections we wish to calculate and the flux factor does not change, it suffices to calculate the remaining

2. Analytic Framework

Lorentz invariant part, I_0 :

$$\begin{aligned}\mathcal{M}_0 &= \bar{u}(p_1) (-iQe\gamma^\mu \epsilon_\mu) v(p_2) \\ &= -iQe\epsilon_\mu \bar{u}(p_1) \gamma^\mu v(p_2)\end{aligned}\tag{2.11}$$

$$\begin{aligned}|\mathcal{M}_0|^2 &= Q^2 e^2 \epsilon_\mu \epsilon_\nu^* \text{Tr}(\bar{u}(p_1) \gamma^\mu v(p_2) \bar{v}(p_2) \gamma^\nu u(p_1)) \\ &= -Q^2 e^2 \text{Tr}(\not{p}_1 \gamma^\mu \not{p}_2 \gamma_\mu) \\ &= 8N_c Q^2 e^2 p_1 \cdot p_2\end{aligned}\tag{2.12}$$

$$\begin{aligned}I_0 &= \int \frac{d^3 \vec{p}_1}{2E_1 (2\pi)^3} \int \frac{d^3 \vec{p}_2}{2E_2 (2\pi)^3} |\mathcal{M}_0|^2 (2\pi)^3 \delta(p_1 + p_2 - q) \\ &= \int d\Omega \frac{1}{32\pi^2} |\mathcal{M}_0|^2 \\ &= \frac{1}{8\pi} 8N_c Q^2 e^2 \left(\frac{E_{cm}^2}{2} \right) \\ &= \frac{N_c Q^2 e^2 E_{cm}^2}{2\pi}\end{aligned}\tag{2.13}$$

For comparison, it is useful to see how this calculation is set up using the Cutkosky cutting rules. If the contraction of the photon was not performed then this diagram would basically be the quark loop contribution to the correction of the photon propagator, $\Pi^{\mu\nu}$, and this is how it will be viewed. Given this and the requirement that the cut should give a quark-antiquark pair produced from a virtual photon, only a single cut can be used (Fig. 2.4). Applying the Feynman rules for cut diagrams (Appendix

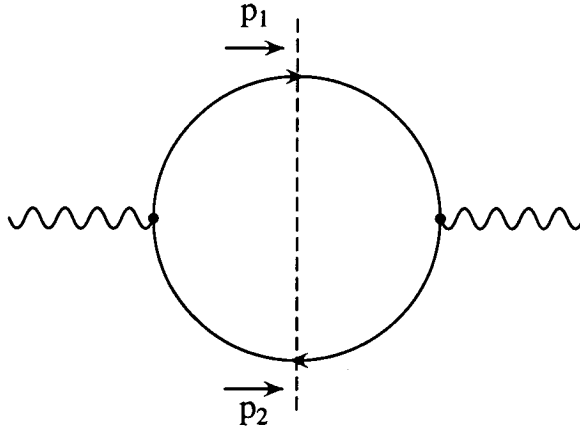


Figure 2.4.: Cut of the quark loop correction to the photon propagator.

A) the form of the integrand is easily found:

$$\begin{aligned}
 I_0 &= \epsilon_\mu \epsilon_\nu \Pi_{cut}^{\mu\nu} \\
 &= \epsilon_\mu \epsilon_\nu \int \frac{d^4 p_1}{(2\pi)^4} - \text{Tr}((-iQe\gamma^\mu)(\not{p}_1)(iQe\gamma^\nu)(-\not{p}_2)) \\
 &\quad (2\pi)\theta(p_1^0)\delta(p_1^2)(2\pi)\theta(p_2^0)\delta(p_2^2) \\
 &= \int \frac{d^3 \vec{p}_1}{(2\pi)^3} 8N_c Q^2 e^2 p_1 \cdot p_2 \left(\frac{1}{2E_{p_1}} \right) (2\pi)\theta(p_2^0)\delta((E_{cm} - |\vec{p}_1|)^2 - |\vec{p}_1|^2) \\
 &= \int d\Omega \frac{1}{32\pi^2} 8N_c Q^2 e^2 \left(\frac{E_{cm}^2}{2} \right) \\
 &= \frac{N_c Q^2 e^2 E_{cm}^2}{2\pi} .
 \end{aligned} \tag{2.14}$$

The calculation demonstrates the equivalence of the two methods and shows how a scattering calculation can be related to a particular topology of a higher order correction.

2.3. $\mathcal{O}(\alpha_s)$ Correction

As expected the lowest order calculation was free from divergences as it was a tree-level calculation and so had no quantum corrections. Going beyond this order, it is inevitable that divergences due to loop momenta will occur. Dimensional regularisation that was superfluously used before, now takes a more important role. The integrands to be considered do not have UV divergences if the dimension of the integrand is less than four. On the other hand individual integrands do not have IR divergences or mass singularities if the dimension is greater than four. To regulate the divergences the integrations can be performed in an arbitrary number of dimensions, n . It is convenient to take the number of dimensions to be $n = 4 - 2\epsilon$ where the -2ϵ will regulate the divergences as ϵ can be both positive or negative. The divergences will appear as powers of $\frac{1}{\epsilon}$ although it is easy to distinguish the terms at $\mathcal{O}(\alpha_s)$ that belong to the UV divergences by the calculations being performed as will be seen later.

As mentioned previously the MS and \overline{MS} renormalisation schemes are suited to the results produced by dimensional regularisation. The MS scheme is most straight forward to apply as it removes the $\frac{1}{\epsilon}$ poles while the \overline{MS} scheme when using $n = 4 - 2\epsilon$ requires subtracting $\frac{1}{\epsilon} - \log(4\pi) + \gamma_E$ where γ_E is the Euler gamma constant. This

2. Analytic Framework

scheme will be used as it is more convenient to apply in both the analytic and numerical calculations.

Determination of the strong corrections to the decay of the photon can be approached by finding the required amplitudes or by cutting the two loop strong corrections of the photon propagator. The constituent amplitudes can be separated into three types; graphs used in the calculation of the Born cross section, graphs containing strong loop corrections and graphs with gluon emission. There are basically two topologies of graphs with loop corrections. One contains the ‘self energy’ of the quark or antiquark and the other the vertex correction. Of the two graphs, the one containing the self energy has the most interesting properties. For the moment it is useful to consider the self energy diagram (Fig.2.5). As the gluon is a gauge boson there is a degree of

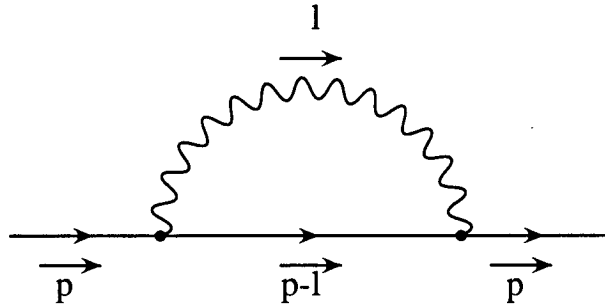


Figure 2.5.: Self energy strong correction of the quark propagator.

choice how the gluon is represented in terms of Feynman rules. Once a particular choice of gauge has been chosen then it is fixed for any further calculation. To begin with, this diagram will be calculated in an arbitrary gauge using the machinery of Feynman parameters:

$$\begin{aligned}
 i\Sigma(p) &= \int \frac{d^n l}{(2\pi)^n} \frac{(ig\gamma^\mu T^a)i(\not{p}-\not{l})(ig\gamma^\nu T^a)}{((p-l)^2 + i\epsilon)} \cdot \frac{-i}{l^2 + i\epsilon} \left(g_{\mu\nu} + \eta \frac{l_\mu l_\nu}{l^2} \right) \\
 &= -g^2 T^a T^a \int \frac{d^n l}{(2\pi)^n} \frac{\gamma^\mu (\not{p}-\not{l}) \gamma^\nu}{((p-l)^2 + i\epsilon)(l^2 + i\epsilon)} \cdot \left(g_{\mu\nu} + \eta \frac{l_\mu l_\nu}{l^2} \right) \\
 &= -g^2 T^a T^a \int \frac{d^n l}{(2\pi)^n} \frac{(2-n)(\not{p}-\not{l})}{((p-l)^2 + i\epsilon)(l^2 + i\epsilon)} + \eta \frac{\not{l}(\not{p}-\not{l})\not{l}}{((p-l)^2 + i\epsilon)(l^2 + i\epsilon)^2} \\
 &= -g^2 T^a T^a \int_0^1 dx \int \frac{d^n l}{(2\pi)^n} \frac{(2-n)(\not{p}-\not{l})}{(x(p-l)^2 + (1-x)l^2 + i\epsilon)^2} \\
 &\quad + \eta \frac{2(1-x)\not{l}(\not{p}-\not{l})\not{l}}{(x(p-l)^2 + (1-x)l^2 + i\epsilon)^3} .
 \end{aligned} \tag{2.15}$$

A change of variables helps to continue this calculation:

$$\begin{aligned} K &= l - px \\ \Delta &= x(1-x)(-p^2) \quad . \end{aligned}$$

Terms linear in the integration variable may be ignored as the domain of integration is symmetric:

$$\begin{aligned} i\Sigma(p) &= -g^2 T^a T^a \not{p} \int_0^1 dx \int \frac{d^n K}{(2\pi)^n} \frac{(2-n)(1-x)}{(K^2 - \Delta + i\epsilon)^2} \\ &\quad + \eta \frac{2(1-x) \left(\frac{(2-n)}{n} K^2(1-x) - 2xK^2 + x^2(1-x)p^2 \right)}{(K^2 - \Delta + i\epsilon)^3} \quad . \end{aligned} \quad (2.16)$$

The final evaluation can be performed using a Wick rotation that effectively transforms the integrals from a Minkowski metric to a Euclidean metric:

$$\begin{aligned} i\Sigma(p) &= -ig^2 T^a T^a \not{p} \int_0^1 dx \int \frac{d^n K}{(2\pi)^n} \frac{(2-n)(1-x)}{(K^2 + \Delta)^2} \\ &\quad - \eta \frac{2(1-x) \left(-\frac{(2-n)}{n} K^2(1-x) + 2xK^2 + x^2(1-x)p^2 \right)}{(K^2 + \Delta)^3} \\ &= -ig^2 T^a T^a \not{p} \int_0^1 dx \Delta^{\frac{n}{2}-2} \Gamma\left(2 - \frac{n}{2}\right) (2-n)(1-x) \\ &\quad + \eta \left(\Delta^{\frac{n}{2}-2} \Gamma\left(2 - \frac{n}{2}\right) \left[\left(1 - \frac{n}{2}\right) (1-x)^2 - nx(1-x) \right] \right. \\ &\quad \left. - \Delta^{\frac{n}{2}-3} \Gamma\left(3 - \frac{n}{2}\right) x^2(1-x)^2 p^2 \right) \\ &= -ig^2 T^a T^a \not{p} (-p^2)^{\frac{n}{2}-2} \frac{2(1-n)\Gamma\left(2 - \frac{n}{2}\right) \Gamma\left(\frac{n}{2}\right)^2}{\Gamma(n)} (1+\eta) \quad . \end{aligned} \quad (2.17)$$

If η is set to -1 then the Landau gauge is chosen and it is clear that the self energy is equal to zero. More generally in dimensional regularisation if the quark propagator is put on-shell then it is equal to zero in any gauge [12]. This is due to cancellations between the UV and mass singularity of the self energy with zero remainder. Although this may be true, mass singularity cancellations will require a contribution from the self energy. In this current example, amplitudes containing the self energy can be ignored.

The vertex correction (Fig. 2.6) can't be thrown away so easily although there are no further tools necessary to perform the calculation. From this calculation onwards the Feynman gauge, $\eta = 0$ will be used for the gluons. Taking this into account the

2. Analytic Framework

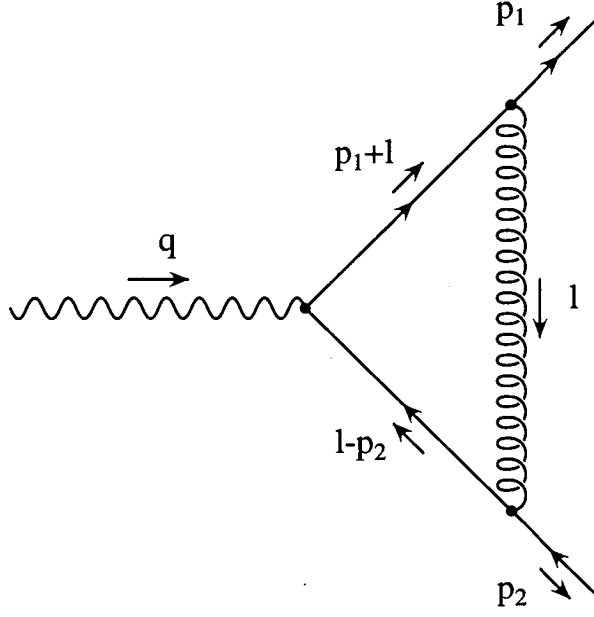


Figure 2.6.: $\mathcal{O}(\alpha_s)$ correction to the quark-antiquark-photon vertex.

calculations for the vertex correction can be performed:

$$\begin{aligned}
 V^\rho &= \int \frac{d^n l}{(2\pi)^n} (ig\gamma^\mu T^a) \frac{i(\not{p}_1 + \not{l})}{(p_1 + l)^2 + i\epsilon} (-ieQ\gamma^\rho) \frac{i(\not{l} - \not{p}_2)}{(l - p_2)^2 + i\epsilon} (ig\gamma^\nu T^a) \left(\frac{-ig_{\mu\nu}}{l^2 + i\epsilon} \right) \\
 &= -g^2 e Q T^a T^a \int \frac{d^n l}{(2\pi)^n} \frac{\gamma^\mu (\not{p}_1 + \not{l}) \gamma^\rho (\not{l} - \not{p}_2) \gamma_\mu}{((p_1 + l)^2 + i\epsilon)((l - p_2)^2 + i\epsilon)(l^2 + i\epsilon)} \\
 &= -g^2 e Q T^a T^a \int_0^1 dx \int_0^1 dy \int \frac{d^n l}{(2\pi)^n} \\
 &\quad \frac{2y(-2(\not{l} - \not{p}_2)\gamma^\rho(\not{p}_1 + \not{l}) - (n-4)(\not{p}_1 + \not{l})\gamma^\rho(\not{l} - \not{p}_2))}{(l^2 + 2xyp_1 \cdot l - 2(1-x)yp_2 \cdot l + i\epsilon)^3} \tag{2.18}
 \end{aligned}$$

$$K = l + xyp_1 - (1-x)yp_2 \tag{2.19}$$

$$\begin{aligned}
 \Delta &= 2x(1-x)y^2(-p_1 \cdot p_2) \\
 &= x(1-x)y^2(-E_{cm}^2) \tag{2.20}
 \end{aligned}$$

$$\begin{aligned}
 V^\rho &= -g^2 e Q T^a T^a \int_0^1 dx \int_0^1 dy \int \frac{d^n K}{(2\pi)^n} \\
 &\quad \frac{2y(2(1-y)\not{p}_2 \gamma^\rho \not{p}_1 - (2-n)x(1-x)y^2 \not{p}_2 \gamma^\rho \not{p}_1 + \frac{(2-n)^2}{n} K^2 \gamma^\rho)}{(K^2 - \Delta + i\epsilon)^3} \\
 &= -\frac{ig^2 e Q T^a T^a}{(4\pi)^{\frac{n}{2}}} \int_0^1 dx \int_0^1 dy \Delta^{\frac{n}{2}-2} \Gamma\left(2 - \frac{n}{2}\right) \gamma^\rho \frac{(n-2)^2}{2} y \\
 &\quad - \Delta^{\frac{n}{2}-3} \Gamma\left(3 - \frac{n}{2}\right) \not{p}_2 \gamma^\rho \not{p}_1 (2y(1-y) + (n-2)x(1-x)y^3) \\
 &= -\frac{ig^2 e Q T^a T^a \Gamma(1+\epsilon) \Gamma(1-\epsilon)^2}{(4\pi)^{2-\epsilon} \Gamma(2-2\epsilon)} \\
 &\quad \times \left[(-E_{cm}^2)^{-\epsilon} \gamma^\rho \left(\frac{1}{\epsilon} - 1\right) - (-E_{cm}^2)^{-1-\epsilon} \not{p}_2 \gamma^\rho \not{p}_1 \left(\frac{2}{\epsilon^2} + 1\right) \right] . \quad (2.21)
 \end{aligned}$$

The calculation demonstrates that powers of $\frac{1}{\epsilon}$ are produced at two stages of the calculation. Firstly when the momentum integrals are performed as seen by the factor of $\Gamma\left(2 - \frac{n}{2}\right)$ in equation (2.21) which is divergent as $n \rightarrow 4$. Secondly when the integrals over the Feynman parameters are carried out as can be seen by the $\frac{1}{\epsilon^2}$ pole generated in the second term. The former correspond to UV divergences and the latter due to IR and mass singularities that will be discussed later.

To conclude the calculation of the vertex correction requires finding the interference between this term and the tree-level decay process, evaluating the spinor algebra and performing the two particle phase space integrals. This provides the total virtual contribution, I^V , to the $\mathcal{O}(\alpha_s)$ calculation.

$$\begin{aligned}
 \mathcal{M}^V &= \bar{u}(p_1) V^\rho \epsilon_\rho v(p_2) \\
 \mathcal{M}^V \mathcal{M}_0^* &= Tr(\bar{u}(p_1) V^\rho \epsilon_\rho v(p_2) \bar{v}(p_2) (ieQ\gamma^\sigma \epsilon_\sigma) u(p_1)) \\
 &= -\frac{g^2 e^2 Q^2}{(4\pi)^{2-\epsilon}} \frac{N_c^2 - 1}{2} (-E_{cm}^2)^{1-\epsilon} \frac{\Gamma(1+\epsilon) \Gamma(1-\epsilon)^2}{\Gamma(2-2\epsilon)} \\
 &\quad \times 2(n-2) \left[\frac{2}{\epsilon^2} - \frac{1}{\epsilon} + 2 \right] \\
 &= (\mathcal{M}_0 \mathcal{M}^{V*})^* \quad (2.22)
 \end{aligned}$$

2. Analytic Framework

$$\begin{aligned}
I^V &= \int \frac{d^{n-1}\vec{p}_1}{2E_1(2\pi)^{n-1}} \int \frac{d^{n-1}\vec{p}_2}{2E_2(2\pi)^{n-1}} \\
&\quad \text{Re}(\mathcal{M}^V \mathcal{M}_0^* + \mathcal{M}_0 \mathcal{M}^{V*}) (2\pi)^n \delta(p_1 + p_2 - q) \\
&= \text{Re} \left[I_0 \frac{\alpha_s}{4\pi} \left(\frac{E_{cm}^2}{4\pi} \right)^{-\epsilon} \left(\frac{N_c^2 - 1}{2N_c} \right) \frac{\Gamma(1+\epsilon)\Gamma(1-\epsilon)^2}{\Gamma(1-2\epsilon)} \left[-\frac{4}{\epsilon^2} - \frac{6}{\epsilon} - 16 \right] \right] \\
&= I_0 \frac{\alpha_s}{4\pi} \left(\frac{N_c^2 - 1}{2N_c} \right) \text{Re} \left[-\frac{4}{\epsilon^2} - \frac{1}{\epsilon} \left(6 - 4\gamma_E - 4 \log \left(\frac{-E_{cm}^2}{4\pi} \right) \right) - 16 \right. \\
&\quad \left. + 6\gamma_E - 2 \left(\gamma_E^2 - \frac{\pi^2}{6} \right) + 6 \log \left(\frac{-E_{cm}^2}{4\pi} \right) - 4\gamma_E \log \left(\frac{-E_{cm}^2}{4\pi} \right) \right. \\
&\quad \left. - 2 \left(\log \left(\frac{-E_{cm}^2}{4\pi} \right) \right)^2 + O(\epsilon) \right] . \tag{2.23}
\end{aligned}$$

To obtain the final form of this correction, the log terms need to be analytically continued so that the argument of the logarithm is positive:

$$\log \left(\frac{-E_{cm}^2}{4\pi} \right) = \log \left(\frac{E_{cm}^2}{4\pi} \right) + i\pi \tag{2.24}$$

$$\begin{aligned}
\Rightarrow I^V &= I_0 \frac{\alpha_s}{4\pi} \left(\frac{N_c^2 - 1}{2N_c} \right) \text{Re} \left[-\frac{4}{\epsilon^2} - \frac{1}{\epsilon} \left(6 - 4\gamma_E - 4 \log \left(\frac{E_{cm}^2}{4\pi} \right) \right) - 16 + 6\gamma_E \right. \\
&\quad \left. - \frac{1}{3} (6\gamma_E^2 - 7\pi^2) + 6 \log \left(\frac{E_{cm}^2}{4\pi} \right) - 4\gamma_E \log \left(\frac{E_{cm}^2}{4\pi} \right) - 2 \left(\log \left(\frac{E_{cm}^2}{4\pi} \right) \right)^2 \right. \\
&\quad \left. + O(\epsilon) \right] . \tag{2.25}
\end{aligned}$$

The remaining amplitudes to consider for this process are the gluon emission graphs. Although these graphs have three particle final states, they are required to complete the $\mathcal{O}(\alpha_s)$ calculation. Physically they can contribute to the production of two jets in the regions where the gluon has a direction very similar to its parent quark or when they have very little energy at all. To isolate the contribution of this correction to the production of two jets a jet algorithm needs to be used that cuts out regions of phase space that would lead to three jet production. Two such algorithms are the JADE [14] and Durham algorithms [15], both of which look at the angles between the partons but differ in the way they treat their energies. The $\mathcal{O}(\alpha_s)$ calculation makes a contribution to the two jet and three jet events as seen in experiments. For the purposes of this calculation no jet algorithm will be used.

Although the graph contains no UV divergences the calculations still need to be performed using dimensional regularisation to regulate the IR and mass divergences. This is so that they will cancel with those obtained by the virtual gluon in the vertex

graph. There are only two possible real gluon emission amplitudes that contribute at this level; one where the quark emits the gluon, \mathcal{M}_1^R , and the other where the antiquark emits the gluon, \mathcal{M}_2^R , (Fig. 2.7). The amplitudes can then be found using the Feynman

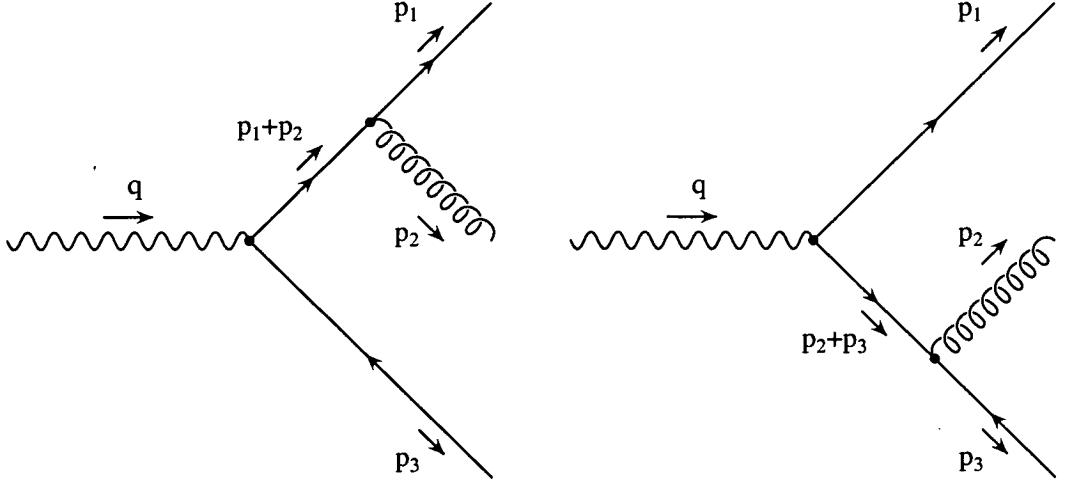


Figure 2.7.: Possible tree-level amplitudes with a quark-antiquark-gluon final state. \mathcal{M}_1^R on the left and \mathcal{M}_2^R on the right.

rules:

$$\begin{aligned} \mathcal{M}_1^R &= \bar{u}(p_1)(ig\gamma^\rho\epsilon_\rho T^a)\frac{i(\not{p}_1 + \not{p}_3)}{(p_1 + p_3)^2 + i\epsilon}(-ieQ\gamma^\mu\epsilon_\mu)v(p_2) \\ &= ig_eQT^a\frac{\bar{u}(p_1)\gamma^\rho(\not{p}_1 + \not{p}_3)\gamma^\mu v(p_2)}{(p_1 + p_3)^2 + i\epsilon}\epsilon_\rho\epsilon_\mu \end{aligned} \quad (2.26)$$

$$\begin{aligned} \mathcal{M}_2^R &= \bar{u}(-ieQ\gamma^\mu\epsilon_\mu)\frac{-i(\not{p}_2 + \not{p}_3)}{(p_2 + p_3)^2 + i\epsilon}(ig\gamma^\rho\epsilon_\rho T^a)v(p_2) \\ &= -ig_eQT^a\frac{\bar{u}(p_1)\gamma^\mu(\not{p}_2 + \not{p}_3)\gamma^\rho v(p_2)}{(p_2 + p_3)^2 + i\epsilon}\epsilon_\rho\epsilon_\mu \end{aligned} \quad (2.27)$$

Before performing the three particle phase space integrals the squared matrix elements need to be found. Combining the two amplitudes there are four possible terms,

2. Analytic Framework

however due to symmetry there are only three different terms produced,

$$\begin{aligned}
 |\mathcal{M}_1^R|^2 &= g^2 e^2 Q^2 T^a T^a \frac{\text{Tr}(\bar{u}(p_1) \gamma^\rho (\not{p}_1 + \not{p}_3) \gamma^\mu v(p_2) \bar{v}(p_2) \gamma_\mu (\not{p}_1 + \not{p}_3) \gamma_\rho u(p_1))}{(p_1 + p_3)^4} \\
 &= g^2 e^2 Q^2 T^a T^a \frac{2(n-2)^2 p_1 \cdot p_3 p_2 \cdot p_3}{(p_1 \cdot p_3)^2} \quad (2.28)
 \end{aligned}$$

$$\begin{aligned}
 |\mathcal{M}_2^R|^2 &= g^2 e^2 Q^2 T^a T^a \frac{\text{Tr}(\bar{u}(p_1) \gamma^\mu (\not{p}_2 + \not{p}_3) \gamma^\rho v(p_2) \bar{v}(p_2) \gamma_\rho (\not{p}_2 + \not{p}_3) \gamma_\mu u(p_1))}{(p_2 + p_3)^4} \\
 &= g^2 e^2 Q^2 T^a T^a \frac{2(n-2)^2 p_1 \cdot p_3 p_2 \cdot p_3}{(p_2 \cdot p_3)^2} \quad (2.29)
 \end{aligned}$$

$$\begin{aligned}
 \mathcal{M}_1^R \mathcal{M}_2^{R*} &= -g^2 e^2 Q^2 T^a T^a \frac{\text{Tr}(\bar{u}(p_1) \gamma^\rho (\not{p}_1 + \not{p}_3) \gamma^\mu v(p_2) \bar{v}(p_2) \gamma_\rho (\not{p}_2 + \not{p}_3) \gamma_\mu u(p_1))}{(p_1 + p_3)^2 (p_2 + p_3)^2} \\
 &= g^2 e^2 Q^2 T^a T^a \\
 &\quad \times \frac{2(n-2)[2(p_1 \cdot p_2)(p_1 \cdot p_2 + p_1 \cdot p_3 + p_2 \cdot p_3) + (n-4)(p_1 \cdot p_3)(p_2 \cdot p_3)]}{(p_1 \cdot p_3)(p_2 \cdot p_3)} \\
 &= \mathcal{M}_2^R \mathcal{M}_1^{R*} \quad (2.30)
 \end{aligned}$$

$$\begin{aligned}
 |\mathcal{M}_1^R + \mathcal{M}_2^R|^2 &= \frac{2(n-2)g^2 e^2 Q^2 T^a T^a}{(p_1 \cdot p_3)(p_2 \cdot p_3)} [(n-2)((p_1 \cdot p_3)^2 + (p_2 \cdot p_3)^2) \\
 &\quad + 4p_1 \cdot p_2 (p_1 \cdot p_2 + p_1 \cdot p_3 + p_2 \cdot p_3) + 2(n-4)(p_1 \cdot p_3)(p_2 \cdot p_3)] \\
 &= \frac{g^2 e^2 Q^2 T^a T^a (1-\epsilon)}{(p_1 \cdot p_3)(p_2 \cdot p_3)} [8(1-\epsilon)((p_1 \cdot p_3)^2 + (p_2 \cdot p_3)^2) \\
 &\quad + 16p_1 \cdot p_2 (p_1 \cdot p_2 + p_1 \cdot p_3 + p_2 \cdot p_3) + 16\epsilon(p_1 \cdot p_3)(p_2 \cdot p_3)] \quad (2.31)
 \end{aligned}$$

To evaluate the integrals it is useful to change variables using momentum conservation so that the integrand is written according to it's energy dependence. As will be seen, once momentum conservation is applied to the three particle phase space integrals, only energy related integrals will remain:

$$\begin{aligned}
 q &= p_1 + p_2 + p_3 \\
 p_1 \cdot p_2 &= \frac{E_{cm}^2}{2} \left(1 - \frac{2E_3}{E_{cm}}\right) = \frac{E_{cm}^2}{2} (1 - x_3) \\
 p_1 \cdot p_3 &= \frac{E_{cm}^2}{2} \left(1 - \frac{2E_2}{E_{cm}}\right) = \frac{E_{cm}^2}{2} (1 - x_2) \\
 p_2 \cdot p_3 &= \frac{E_{cm}^2}{2} \left(1 - \frac{2E_1}{E_{cm}}\right) = \frac{E_{cm}^2}{2} (1 - x_1) \\
 |\mathcal{M}_1^R + \mathcal{M}_2^R|^2 &= \frac{g^2 e^2 Q^2 T^a T^a (1-\epsilon)}{(1-x_1)(1-x_2)} [8(1-\epsilon)((1-x_1)^2 + (1-x_2)^2) \\
 &\quad + 16(x_1 + x_2 - 1) - 16\epsilon(1-x_1)(1-x_2)] \quad (2.32)
 \end{aligned}$$

Many of the integrals required for the three particle phase can be performed due to the momentum constraints and the angular independence of the decay. To perform

the remaining integrals, transformations used on the integrand have to be applied to the integration variables:

$$\begin{aligned}
 I^R &= \int \frac{d^{n-1}\vec{p}_1}{2E_1(2\pi)^{n-1}} \frac{d^{n-1}\vec{p}_2}{2E_2(2\pi)^{n-1}} \frac{d^{n-1}\vec{p}_3}{2E_3(2\pi)^{n-1}} |\mathcal{M}_1^R + \mathcal{M}_2^R|^2 (2\pi)^n \delta^n(q - p_1 - p_2 - p_3) \\
 &= \int \frac{d^{n-1}\vec{p}_1}{2E_1(2\pi)^{n-1}} \frac{d^{n-1}\vec{p}_2}{2E_2(2\pi)^{n-1}} |\mathcal{M}_1^R + \mathcal{M}_2^R|^2 \frac{2\pi}{2E_3} \delta(E_{cm} - E_1 - E_2 - E_3) \\
 &= \int \frac{d\Omega_{n-1}}{2(2\pi)^{n-1}} \frac{d\Omega_{n-2}}{2(2\pi)^{n-2}} \\
 &\quad \int dE_1 E_1^{n-3} \int dE_2 E_2^{n-3} \int d\theta_{12} \sin^{n-3} \theta_{12} |\mathcal{M}_1^R + \mathcal{M}_2^R|^2 \delta((q - p_1 - p_2 - p_3)^2) \\
 &= \frac{1}{(4\pi)^{\frac{n}{2}-\frac{1}{2}} \Gamma(\frac{n}{2}-\frac{1}{2})} \frac{1}{(4\pi)^{\frac{n}{2}-1} \Gamma(\frac{n}{2}-1)} \\
 &\quad \int dE_1 E_1^{n-3} \int dE_2 E_2^{n-3} \int d\theta_{12} \sin^{n-3} \theta_{12} |\mathcal{M}_1^R + \mathcal{M}_2^R|^2 \delta((q - p_1 - p_2 - p_3)^2)
 \end{aligned} \tag{2.33}$$

$$\begin{aligned}
 x_i &= \frac{2E_i}{E_{cm}} \\
 z &= \cos \theta_{12}
 \end{aligned}$$

$$\begin{aligned}
 I^R &= \frac{E_{cm}^{2n-4}}{(4\pi)^{n-1} 2^{n-2} \Gamma(n-2)} \int dx_1 x_1^{n-3} \int dx_2 x_2^{n-3} \\
 &\quad \int dz (1-z^2)^{\frac{n}{2}-2} |\mathcal{M}_1^R + \mathcal{M}_2^R|^2 \delta(E_{cm}^2 (1-x_1-x_2 + \frac{x_1 x_2}{2} (1-z))) \\
 &= \frac{E_{cm}^{2n-6}}{(4\pi)^{n-1} 2^{n-3} \Gamma(n-2)} \int dx_1 x_1^{n-4} \int dx_2 x_2^{n-4} \\
 &\quad \left(1 - \left(\frac{2-2x_1-2x_2+x_1 x_2}{x_1 x_2} \right)^2 \right)^{\frac{n}{2}-2} |\mathcal{M}_1^R + \mathcal{M}_2^R|^2 .
 \end{aligned} \tag{2.34}$$

A final transformation makes this integral easier to integrate:

$$\begin{aligned}
 x_2 &= 1 - vx_1 \\
 I^R &= \frac{E_{cm}^{2n-6}}{2(4\pi)^{n-1} \Gamma(n-2)} \\
 &\quad \times \int dx_1 \int dv x_1^{n-3} (1-x_1)^{\frac{n}{2}-2} v^{\frac{n}{2}-2} (1-v)^{\frac{n}{2}-2} |\mathcal{M}_1^R + \mathcal{M}_2^R|^2 \\
 |\mathcal{M}_1^R + \mathcal{M}_2^R|^2 &= \frac{g^2 e^2 Q^2 T^a T^a (1-\epsilon)}{x_1(1-x_1)v} [8(1-\epsilon)((1-x_1)^2 + v^2 x_1^2) \\
 &\quad + 16(1-v)x_1 - 16\epsilon x_1(1-x_1)v]
 \end{aligned}$$

2. Analytic Framework

$$\begin{aligned}
I^R &= I_0 \frac{\alpha_s}{4\pi} \left(\frac{E_{cm}^2}{4\pi} \right)^{-\epsilon} \frac{N_c^2 - 1}{2N_c} \frac{\Gamma(1 - \epsilon)^2}{\Gamma(1 - 3\epsilon)} \left[\frac{4}{\epsilon^2} + \frac{6}{\epsilon} + 19 \right] \\
&= I_0 \frac{\alpha_s}{4\pi} \frac{N_c^2 - 1}{2N_c} \left[\frac{4}{\epsilon^2} + \frac{1}{\epsilon} \left(6 - 4\gamma_E - 4 \log \left(\frac{E_{cm}^2}{4\pi} \right) \right) + 19 - 6\gamma_E + \frac{1}{3}(6\gamma_E^2 - 7\pi^2) \right. \\
&\quad \left. - 6 \log \left(\frac{E_{cm}^2}{4\pi} \right) + 4\gamma_E \log \left(\frac{E_{cm}^2}{4\pi} \right) + 2 \left(\log \left(\frac{E_{cm}^2}{4\pi} \right) \right)^2 + O(\epsilon) \right] . \quad (2.35)
\end{aligned}$$

To obtain the final result the contributions from the virtual gluon and real gluon emissions have to be included:

$$\begin{aligned}
I_1 &= I^V + I^R \\
&= 3I_0 \frac{\alpha_s}{4\pi} \left(\frac{N_c^2 - 1}{2N_c} \right) \quad (2.36)
\end{aligned}$$

$$\frac{I_1}{I_0} = \frac{\alpha_s}{\pi} \frac{\sigma_1}{\sigma_0} = \frac{\alpha_s}{\pi} \frac{3}{4} \left(\frac{N_c^2 - 1}{2N_c} \right) . \quad (2.37)$$

The above calculation can be performed again using the Cutkosky rules. Repeating the integrations is not very productive, but the organisation of the calculation is quite enlightening. Due to theorems by Bloch and Nordsieck [16], and Kinoshita [17], Lee and Nauenberg [18] each of the corrections to the photon propagator should be finite once UV renormalisation is performed. This is a general property for any order of any correction to this process. There are three corrections to the photon propagator that contribute to this process (Fig. 2.8). Within them can be identified each of the matrix

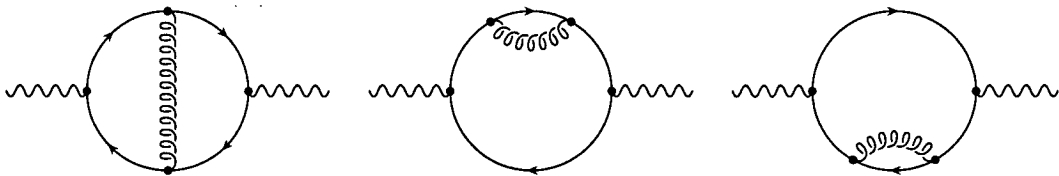


Figure 2.8.: $\mathcal{O}(\alpha_s)$ corrections to the photon propagator.

elements as calculated after cutting.

To begin with, consider the graph containing the vertex correction. Adding the results previously obtained for the corresponding cuts of this graph, $I_{Virtual}^{Vertex}$ and I_{Real}^{Vertex} (Fig. 2.9), the UV pole remains as expected. This term needs renormalising by suitable counter terms in an appropriate renormalisation scheme. At this order in perturbation theory the overall answer will be independent of renormalisation scheme. The \overline{MS}

renormalisation scheme was not used explicitly in the former calculation as the cancellations occurred between the IR and UV poles. However, the appropriate \overline{MS} counter terms, $I_{Counter}^{Vertex}$, should be applied to make the graph finite and can be represented graphically (Fig. 2.9). This then leads to a finite value for the graph with the vertex

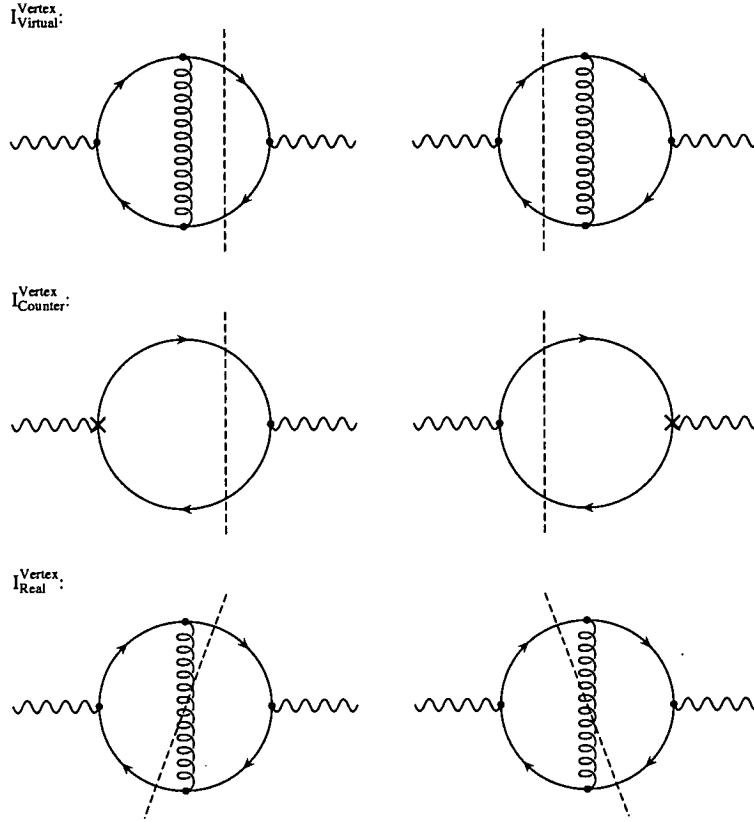


Figure 2.9.: Cuts of the two loop strong correction to the photon propagator that contains the vertex correction along with the renormalisation terms.

correction, $I_{\overline{MS}}^{Vertex}$:

$$\begin{aligned}
 I_{\overline{MS}}^{Vertex} &= I_{Virtual}^{Vertex} + I_{Counter}^{Vertex} + I_{Real}^{Vertex} \\
 &= I_0 \frac{2\alpha_s}{\pi} \left(\frac{N_c^2 - 1}{2N_c} \right) .
 \end{aligned} \tag{2.38}$$

Now consider the graph containing a self energy. Naively cutting the graph to obtain all two and three particle cuts leads to three possible cuts (Fig. 2.10). Two of these cuts contain self energies. Previously, these terms would be set to zero. This would lead to an overall divergent set of cuts due to the collinear singularity from the

2. Analytic Framework

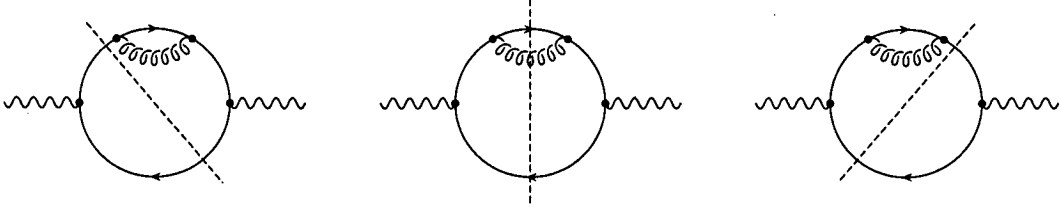


Figure 2.10.: Possible cuts of the two loop strong correction to the photon propagator containing the self energy graph.

three particle cut:

$$\begin{aligned}
 I_{Real}^{Self} &= \frac{E_{cm}^{2n-6}}{(4\pi)^{n-1} 2^{n-3} \Gamma(n-2)} \int dx_1 x_1^{n-4} \int dx_2 x_2^{n-4} \\
 &\quad \left(1 - \left(\frac{2 - 2x_1 - 2x_2 + x_1 x_2}{x_1 x_2} \right)^2 \right)^{\frac{n}{2}-2} |\mathcal{M}_1|^2 + |\mathcal{M}_2|^2 \\
 &= I_0 \left(\frac{\alpha_s}{4\pi} \right) \left(\frac{N_c^2 - 1}{2N_c} \right) \left(-5 - \frac{2}{\epsilon} + 2\gamma_E + 2 \log \left(\frac{E_{cm}^2}{4\pi} \right) \right) \quad (2.39)
 \end{aligned}$$

The $\frac{1}{\epsilon}$ term produced in equation 2.39 would cancel the UV pole generated by the vertex graph. As this graph should only have UV divergences, once the cuts are added together the $\frac{1}{\epsilon}$ pole should cancel with a $\frac{1}{\epsilon}$ pole produced by the renormalised self energy diagrams. However including both renormalised propagators leads to an over compensation of the mass divergences. In fact only a half of the self energy graph from each side of the cut is needed for the cancellation. Effectively, only one of the two particle cuts is required.

To resolve this apparent discrepancy, the Feynman rules need re-examination. The generation of matrix elements are derived from the expansion of the path integral. One of the constraints made is that only truncated diagrams are used. This removes the self energy diagram as it is a graph in itself i.e. can be cut to produce tree like graphs. However the self energy graph can be replaced with the first correction to the renormalised propagator. If using a renormalised Lagrangian then this corresponds to the wave function coefficient Z_2 in the counter term Lagrangian. The difference is that the self energy goes like Z_2 while the renormalised propagator goes like $\sqrt{Z_2}$. In the Taylor expansion of the counter terms, this gives rise to a factor of a half. Using both cuts and introducing the factor of half as given by the perturbative expansion gives the same result as before. The redundancy of the renormalisation scheme is due

to the poles created by the divergences cancelling between the graphs. However, it is important that cancellations between singularities occur between singularities of the same types. When using the numerical method this property will be required to give a smooth integrable function.

2.4. Massive Quarks

Having massive fermions complicates the calculation. The matrix elements are algebraically more intensive as the non-spinor structures of the mass terms are included in the Feynman rules. Terms generated due to the introduction of mass in the numerator all have even powers of the mass as the trace of an odd number of gamma matrices is zero, and the topologies of graphs to be considered only have two or four fermion propagators.

In terms of the IR and mass singularities the matrix elements become slightly simpler. The mass singularities appear due to vertices subtending massless particles. The introduction of mass to the quarks is sufficient to quell this singularity. Mass singularities can still occur in a QCD theory with massive quarks, but only when triple or quartic gluon vertices are present. There is also a reduction in the number of IR singularities caused by zero momentum (soft) massless particles as the mass gives the particle an energy even when it has zero three-momentum. In other words, the mass of the quark prevents it from becoming soft. Energy conservation prevents an infinite number of massive quarks from being produced, however an unlimited amount of zero momentum gluons is still allowed. As the bare matrix elements of the massless case are just a limiting case, it is of little surprise that the soft gluon cancellations still occur. Indeed the Bloch-Nordsieck and Kinoshita-Lee-Nauenberg theorems are generally true and can be attributed to the fact that the general numerator structure of every cut of a particular graph is the same and the above mentioned singularities arise from the denominator.

The mass is also another parameter of the theory that requires renormalising. This does not affect the renormalisation of the vertex correction as the terms proportional to the mass are all UV finite, and so its renormalisation is the same as the massless

2. Analytic Framework

case. This can easily be verified through power counting of the loop momentum as UV terms are generated by integrands with an over-all loop momenta of $\mathcal{O}(l^4)$ in the denominator:

$$\begin{aligned} V^\rho &= -g^2 e Q T^a T^a \int \frac{d^n l}{(2\pi)^n} \frac{\gamma^\mu (\not{p}_1 + \not{l} + m) \gamma^\rho (\not{l} - \not{p}_2 + m) \gamma_\mu}{((p_1 + l)^2 - m^2 + i\epsilon)((l - p_2)^2 - m^2 + i\epsilon)(l^2 + i\epsilon)} \\ &\rightarrow -g^2 e Q T^a T^a \int \frac{d^n l}{(2\pi)^n} \frac{\gamma^\mu \not{l} \gamma^\rho \not{l} \gamma_\mu}{(l^2 + i\epsilon)^3} . \end{aligned} \quad (2.40)$$

As before, the correction due to the self energy is a multiplicative factor. To show this, the corrections of the propagator need to be formalised. The full renormalised propagator to all orders in perturbation theory can be written as a sum of all the irreducible self energies. This corresponds to a geometric series that can be summed:

$$\begin{aligned} \Delta(p^2) &= \frac{i}{\not{p} - m} + \frac{i}{\not{p} - m} i\Sigma_f \frac{i}{\not{p} - m} + \frac{i}{\not{p} - m} i\Sigma_f \frac{i}{\not{p} - m} i\Sigma_f \frac{i}{\not{p} - m} \dots \\ &\rightarrow \frac{i}{\not{p} - m + \Sigma_f} . \end{aligned} \quad (2.41)$$

Now consider the \overline{MS} renormalised irreducible diagram Σ_f split into two parts, one corresponding to the wave function and one for the mass, each multiplied by a coefficient dependent on the incoming momentum:

$$\Sigma_f(p^2) = \not{p} A_f(p^2) - m B_f(p^2) \quad (2.42)$$

$$\begin{aligned} \Rightarrow \Delta(p^2) &= \frac{i}{\not{p} - m - \Sigma_f(p^2)} \\ &= \frac{i}{\not{p}(1 - A_f(p^2)) - m(1 - B_f(p^2))} . \end{aligned} \quad (2.43)$$

The mass of the propagator is no longer the bare mass m , but a new mass M . This is defined by saying that the pole of the propagator occurs when $\not{p} = M$. Thus a relationship between m and M can be determined choosing A_f and B_f to be of order g^2 :

$$M(1 - A_f(p^2))|_{p^2=M^2} = m(1 - B_f(p^2))|_{p^2=M^2} \quad (2.44)$$

$$M = m(1 + A_f(M^2) - B_f(M^2)) + \mathcal{O}(g^4) . \quad (2.45)$$

Performing a Taylor series expansion of the coefficients A_f and B_f , the residue of

the propagator can be determined:

$$\begin{aligned}
 \Delta(p^2) &= \frac{i}{\not{p}(1 - A_f(p^2)) - m(1 - B_f(p^2))} \\
 &= \frac{i}{\not{p} \left(1 - A_f(M^2) - (\not{p} - M) \left. \frac{\partial A}{\partial \not{p}} \right|_{p^2=M^2} \right) - m \left(1 - B_f(M^2) - (\not{p} - M) \left. \frac{\partial B}{\partial \not{p}} \right|_{p^2=M^2} \right)} \\
 &= \frac{i}{(\not{p} - M) \left(1 - A_f(M^2) - \not{p} \left. \frac{\partial A}{\partial \not{p}} \right|_{p^2=M^2} + m \left. \frac{\partial B}{\partial \not{p}} \right|_{p^2=M^2} \right)} \\
 &= \frac{iz_2}{\not{p} - M}
 \end{aligned}$$

$$\begin{aligned}
 \Rightarrow z_2 &= 1 + A_f(M^2) + \not{p} \left. \frac{\partial A}{\partial \not{p}} \right|_{p^2=M^2} - m \left. \frac{\partial B}{\partial \not{p}} \right|_{p^2=M^2} + O(g^4) \\
 z_2|_{p^2=M^2} &= 1 + A_f(M^2) + M \left. \frac{\partial A}{\partial \not{p}} \right|_{p^2=M^2} - m \left. \frac{\partial B}{\partial \not{p}} \right|_{p^2=M^2} + O(g^4) \\
 &= 1 + A_f(m^2) + m \left. \frac{\partial A}{\partial \not{p}} \right|_{p^2=m^2} - m \left. \frac{\partial B}{\partial \not{p}} \right|_{p^2=m^2} + O(g^4) \quad (2.46)
 \end{aligned}$$

$$\sqrt{z_2}|_{p^2=M^2} = 1 + \frac{1}{2} \left(A_f(m^2) + m \left. \frac{\partial A}{\partial \not{p}} \right|_{p^2=m^2} - m \left. \frac{\partial B}{\partial \not{p}} \right|_{p^2=m^2} \right) + O(g^4) \quad (2.47)$$

The correction to the quark propagator contributes to the calculation as a multiplicative factor of the massive Born term. Although z_2 is the residue of the propagator, only $\sqrt{z_2}$ is needed as the remaining $\sqrt{z_2}$ goes towards the fermion wave-function. Only the $\mathcal{O}(g^2)$ terms need to be included and they come with the factor of a half as stated earlier. The contribution of the self energy is less trivial than the massless case since there are now finite contributions. It should be noted that the derivative with respect to \not{p} of A and B renders them both UV finite as it increases the power of the loop momentum in the denominator. This means that the renormalisation term required in the actual calculation is the same as the massless renormalisation. Mass renormalisation at this order in perturbation theory only affects the way the mass is interpreted and provides a higher order effect if included in the correction terms.

Introducing massive fermions poses additional problems due to their effects on the phase space and the integrands themselves. The energy integrations of the massive particles now have a lower limit of m that leads to solutions in the form of logarithmic and dilogarithmic functions [19]. An interesting property of the analytic result is that

2. Analytic Framework

it is a function of the velocity of the massive particles,

$$v = \left(1 - \frac{4m^2}{s}\right)^{\frac{1}{2}}. \quad (2.48)$$

The analytic expression for the $\frac{\alpha_s}{\pi}$ coefficient, $\sigma_1(v)$, divided by the massless Born cross section $\sigma_0(v=1)$ is given by

$$\begin{aligned} \frac{\sigma_1(v)}{\sigma_0(v=1)} &= \left(\frac{N_c^2 - 1}{2N_c}\right) \frac{1}{2} \\ &\times \left\{ (1+v^2)(1-v^2) \left[3 \ln\left(\frac{1+v}{2}\right) \ln\left(\frac{1+v}{1-v}\right) \right. \right. \\ &\quad \left. \left. - 2 \ln v \ln\left(\frac{1+v}{1-v}\right) + 2 \text{Li}_2\left(\frac{1-v}{1+v}\right) + \text{Li}_2\left(\left(\frac{1-v}{1+v}\right)^2\right) \right] \right. \\ &\quad \left. + \left[\frac{11}{8}(1+v^2)(3-v^2) + \frac{1}{2}v^4 - 3v(3-v^2) \right] \ln\left(\frac{1+v}{1-v}\right) \right. \\ &\quad \left. + 6v(3-v^2) \ln\left(\frac{1+v}{2}\right) - 4v(3-v^2) \ln v + \frac{3}{4}v(5-3v^2) \right\} \quad (2.49) \end{aligned}$$

This expression will be used to check the results obtained from the numerical expression.

3. Numerical Methods for the Implementation of Perturbative Calculations

The previous chapter set the scene in terms of the types of integrals that need to be performed for high energy particle scattering. Analytic calculations are extremely useful, but they become laborious to evaluate due to the sheer number of terms and the forms of functions generated. Many of the functions obtained in higher order processes, such as the polylogarithms, can only be evaluated numerically. By considering these calculations using an almost purely numerical procedure from the outset, some of these problems may be alleviated. In contrast to the analytic method where the singularity structure of the IR and mass divergences have to be explicitly accounted for, the numerical procedure takes care of these divergences within the integrals [20]. Similarly, the UV divergences are handled by the subtraction of UV divergent integrals rather than subtracting $\frac{1}{\epsilon}$ poles. It also has the advantage of calculating many observables within the same program simultaneously. Here the principles behind Monte-Carlo integration will be discussed, how they are used in the Beowulf program and how they are used in the numerical integrations of the next chapter.

3.1. Monte-Carlo Integration

There are many methods of approximating the result of an integral. One method suitable to be performed with the aid of a computer is Monte-Carlo integration. The

3. Numerical Methods

basic principle behind this method is to evaluate the integrand at a series of random points within the domain of integration, and then take an average. This gives an approximation to the true value of the integral. As the number of points is increased the accuracy of the result also increases. Providing a suitable integrand is chosen, using a simple random scatter technique will result in the error decreasing proportional to the square root of the number of samples.

A classic example to illustrate this is the numerical evaluation for the value of π . A simple technique to do this is to take a unit square with a circle inscribed and randomly sample points within the square. The value returned is chosen to be one if the point lies within the boundaries of the circle else it is zero. The average of these points gives an approximation to area of the circle i.e. $\frac{\pi}{4}$. It is the fraction of the square taken up by the circle that is being calculated and as the square has unit area, the area of the circle is given directly. Obviously other areas of shapes can be calculated using suitable constraints within the square.

3.1.1. Sampling Techniques

More practical examples that we may wish to consider do not have the simple binary evaluation that the previous example had. The integrands are usually some function dependent on the domain of integration. When the value of the integrand has a large variation on the domain of integration, randomly sampling points may not be the most efficient method of estimating the integral. To improve the process, a more suitable choice of integration variable may be used. There also exists different ways of enhancing a Monte-Carlo integration, two of them are importance and stratified sampling [21].

The Beowulf code employs a tactic of choosing integration variables that match the shape of the integrand. This involves choosing multiple coordinate transformations or sampling methods, each of them catering for a specific feature of the integrand [3]. As the integrals to be considered consist of three-momenta each integrated over the whole of momentum space, there are an infinite number of ways to transform the momentum integrals into the space of a unit cube. Each of these transformations will squash or stretch the original momentum space in a different way. This changes the values that are sampled, however, the overall answer stays the same. A particular sampling

method is then chosen at random and the weighted average is taken. The parameters that distinguish the different transformations are tuned so that it produces the least error per sample thus increasing the efficiency of the integration.

Monte-Carlo integration routines such as VEGAS [22] deal with the integrands once they have been put into a unit hyper-cube. This is done by sampling the integrand inside the hyper-cube using techniques called importance and stratified sampling. Importance sampling is a variance minimisation technique. It involves slicing the sampling region along each dimension into a finite number of pieces thus creating many little sampling bins. Each bin is randomly sampled with the same probability. After each sample an estimate of the integration is calculated and the variance for each bin in every dimension is calculated. Over successive samples, regions that have greater variance are sampled more. This is done by changing the width of the divisions along each dimension. At the points along a particular dimension where there is greatest variance, the width of the division is decreased. This creates smaller boxes, but by keeping the probability of sampling a particular bin fixed the density of points in this region is effectively increased. Large variances are caused by high fluctuations in the integrand and so limiting the bin size reduces sampling space in this region and reduces variance.

Stratified sampling minimises variance in a slightly different way. Instead of changing the size of the bins keeping the number of points the same, the bins are kept the same size but the number of points are distributed differently. More points are given to the bins with greatest variance, thus increasing the density of points in that region of integration space, similar to the effect that importance sampling had. VEGAS is also capable of using this technique on individual bins but only when there are a sufficient number of points per sample. Thus VEGAS uses a combination of importance and stratified sampling, which allows it to tune itself to any suitable integrand given to it.

3.1.2. Choosing Coordinate Systems

For simplicity, Monte-Carlo integrations are usually performed by sampling points from a unit hypercube. This is because random number generators generally speaking produce numbers on the bounded region of 0 and 1. Thus a value can be chosen for each

3. Numerical Methods

dimension giving the coordinate for the point to sample. Unfortunately, most interesting integrals we wish to evaluate don't come in a multidimensional box. As mentioned the integrals evaluated here are momentum integrals extending over an infinite volume. After a change of coordinates for each momentum integral into a unit cube they are effectively combined to form a unit hypercube. A further complication is that from the outset, most of the integrals to be considered have points where the integrand appears to take infinite values. This can be seen when a factor in the denominator becomes zero in the integrands considered. However, all the integrals considered, as shown in the previous chapter will have finite answers. Heuristically, this can be reconciled by the fact that these values will 'average' over an infinite volume. This puts a constraint on the choice of coordinate system adopted in that it has to be 'good' i.e. one that transforms the integrand into a finite valued function over the unit hypercube.

To determine what type of coordinate system should be used, the type of singularities or places of enhancement need to be determined. The singularities that will be considered in three dimensions take the form of points, lines or closed surfaces in their original momentum coordinate systems. Cancellations that occur between different integrands reduce the number of singularities to deal with. Of these singularities, the only one that requires special attention in terms of the choice of coordinate system, are the point like singularities. These correspond to the IR singularities mentioned in the previous chapter. If a point like singularity is integrable, then it is sufficient to centre the coordinate system on the singularity and use spherical polar coordinates:

$$\int d^3\vec{l} = \int_0^\infty d|\vec{l}| \int_{-1}^1 d\cos\theta \int_0^{2\pi} d\phi |\vec{l}|^2 \quad . \quad (3.1)$$

From the above transformation, it is clear that any integrand that has a factor of $|\vec{l}|^2$ or less in the denominator that would superficially look problematic is removed by the factor of $|\vec{l}|^2$ from the Jacobian. This is the constraint for the overall integrand to be free from IR singularities once the two and three particle integrands are added together. A further transformation is required to change the domain of integration into

a cube:

$$|\vec{l}| = E \left(\frac{1}{x_1^A} - 1 \right)^B \quad (3.2)$$

$$\cos \theta = 2x_2 - 1 \quad (3.3)$$

$$\phi = 2\pi x_3 \quad (3.4)$$

$$\begin{aligned} \int_0^\infty d|\vec{l}| \int_{-1}^1 d \cos \theta \int_0^{2\pi} d\phi |\vec{l}|^2 &= \int_0^1 d^3 \vec{x} 4\pi ABE |\vec{l}|^2 \\ &\times \left(\left(\frac{|\vec{l}|}{E} \right)^{\frac{1}{B}} + 1 \right)^{1+\frac{1}{A}} \left(\frac{|\vec{l}|}{E} \right)^{1-\frac{1}{B}} \end{aligned} \quad (3.5)$$

Cancellations of multiple point like singularities in the domain of integration may at first sight pose a problem. Each cancellation will provide a $|\vec{l} - \vec{l}_i|^2$ factor in the denominator where \vec{l}_i specifies the position at which the cancellations take place and i labels each of the N points. How can one transformation take care of each point of cancellation? At this point a change of notation is useful. Instead of working in terms of the Jacobian, the inverse of the Jacobian is more useful. This will be labelled as $\rho_i(\vec{l})$ for each of the i points of cancellation. As the labelling suggests, the inverse of the Jacobian can be thought of as a density of integration points in a Monte-Carlo integration. To complete the task of catering for multiple singularities, it is necessary to multiply the integrand by 1 in a clever way:

$$\int d^3 \vec{l} A(\vec{l}) = \int d^3 \vec{l} \frac{\sum_{i=1}^N \alpha_i \rho_i}{\sum_{i=1}^N \alpha_i \rho_i} I(\vec{l}) \quad (3.6)$$

$$= \sum_{i=1}^N \int d^3 \vec{l} \frac{\alpha_i \rho_i}{\sum_{i=1}^N \alpha_i \rho_i} A(\vec{l}) \quad (3.7)$$

$$= \sum_{i=1}^N \int d^3 \vec{x}_i \frac{\alpha_i}{\sum_{i=1}^N \alpha_i \rho_i(\vec{x}_i)} A(\vec{l}(\vec{x}_i)) \quad (3.8)$$

This shows how an integrand that apparently has multiple soft singularities can be converted into multiple integrands that are free from singularities. Each of the integrals can be calculated separately then added together with it's associated weight. The current version of Beowulf treats this slightly differently as the different choices of coordinate system are sampled using the weights and then the overall answer determined.

To verify this procedure a test integral can be used whose value is predetermined. By modifying the normal distribution one can obtain a suitable integrand that exhibits

3. Numerical Methods

the required $\frac{1}{|\vec{l}|^2}$ structure:

$$\int d^3\vec{l} \frac{e^{-|\vec{l}|^2}}{\sqrt{\pi}} = 4\pi \quad (3.9)$$

To prepare for the integrands that will be considered later it is suitable to consider a slightly more complicated version of this integrand. The integrands to be considered will be functions of two-momenta and have three points of soft cancellations, as such an integrand of this type can be engineered. To match future notation the momenta used will be called \vec{l}_2 and \vec{l}_4 . The points of cancellation required are at $|\vec{l}_4| = 0$, $|\vec{l}_2| = 0$ and $|\vec{l}_2 + \vec{l}_4| = 0$. Using these conditions a suitable expression can be generated:

$$\frac{1}{(4\pi)^2} \int d^3\vec{l}_2 \int d^3\vec{l}_4 \frac{e^{-|\vec{l}_4|^2}}{2|\vec{l}_4|^2\sqrt{\pi}} \left(\frac{e^{-|\vec{l}_2|^2}}{2|\vec{l}_2|^2\sqrt{\pi}} + \frac{e^{-|\vec{l}_2+\vec{l}_4|^2}}{2|\vec{l}_2+\vec{l}_4|^2\sqrt{\pi}} \right) = 1 \quad (3.10)$$

The result can be easily verified by hand and implemented numerically using the coordinate transformations described with or without the help of VEGAS. Two separate numerical integrations need to be performed, one that centres on the pair of cancellation points $|\vec{l}_4| = 0$ and $|\vec{l}_2| = 0$, the other on the points $|\vec{l}_4| = 0$, $|\vec{l}_2 + \vec{l}_4| = 0$. These two sampling methods will now be referred to as method 1 and method 2 respectively as they will be used in the calculations to be performed later in the chapter and are the principle sampling methods used for the QCD case.

3.2. An Example in ϕ^3 Theory

The choice of coordinate systems used in the above example is almost identical to those required for the massless $e^+e^- \rightarrow q\bar{q}$ case. To gain an understanding of why no further transformations are required, it is useful to first consider a scalar version of this process. In particular, the graph containing a vertex correction in ϕ^3 theory (Fig. 3.1). This theory is useful as a toy model and one that was used to demonstrate the practicalities of the numerical method in the beginning stages of Beowulf [20]. It demonstrates how soft and collinear singularities appear and how they occur, while eliminating the complications introduced from non-trivial numerator structures.

The Feynman rules (Appendix A) obtained are very similar to those obtained in QED but with no spinor structure or gauge vertices. These may seem fairly drastic

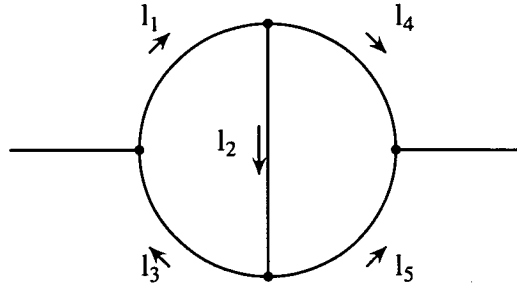


Figure 3.1.: Two loop correction to the scalar propagator.

changes, but when considering all singularity structures apart from UV singularities, they have no effect. The two loop scalar graph to be considered (Fig. 3.1) has the same denominator structure as the fermion case for each of the two and three particle cuts (Fig. 3.2):

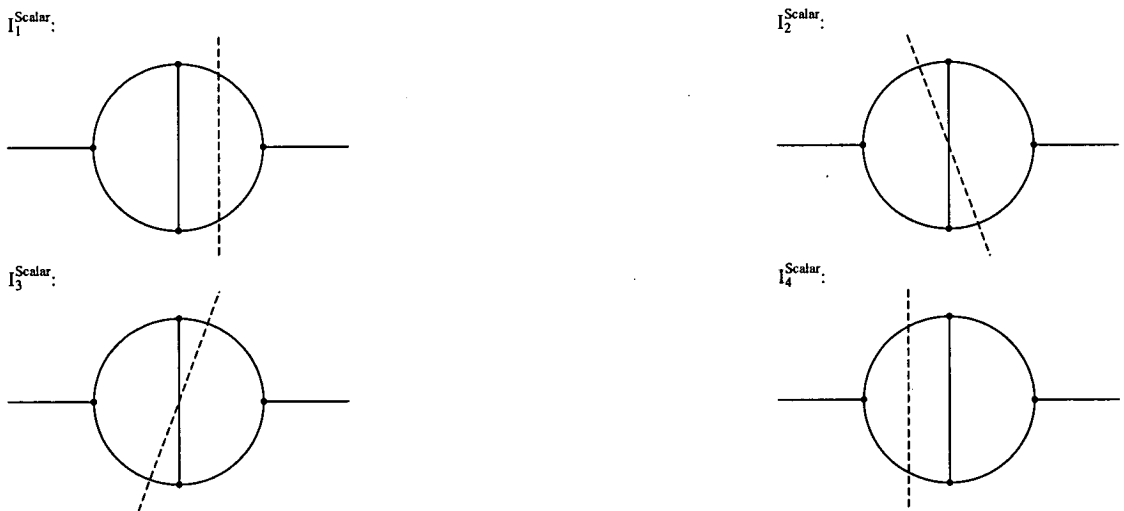


Figure 3.2.: Two and three particle cuts of the scalar two loop correction to the scalar propagator.

3. Numerical Methods

$$I_1^{Scalar} = \lambda^4 \int \frac{d^4 l_2}{(2\pi)^4} \int \frac{d^4 l_4}{(2\pi)^4} \int \frac{d^4 l_5}{(2\pi)^4} \frac{1}{(l_1^2 + i\epsilon)(l_2^2 + i\epsilon)(l_3^2 + i\epsilon)} \\ (2\pi)\delta(l_4^2)\theta(l_4^0)(2\pi)\delta(l_5^2)\theta(l_5^0)(2\pi)^4\delta^4(q - l_4 - l_5) \quad (3.11)$$

$$I_2^{Scalar} = \lambda^4 \int \frac{d^4 l_1}{(2\pi)^4} \int \frac{d^4 l_2}{(2\pi)^4} \int \frac{d^4 l_5}{(2\pi)^4} \frac{1}{(l_3^2 + i\epsilon)(l_4 - i\epsilon)} \\ (2\pi)\delta(l_1^2)\theta(l_1^0)(2\pi)\delta(l_2^2)\theta(-l_2^0)(2\pi)\delta(l_5^2)\theta(l_5^0)(2\pi)^4\delta^4(q - l_1 + l_2 - l_5) \quad (3.12)$$

$$I_3^{Scalar} = \lambda^4 \int \frac{d^4 l_2}{(2\pi)^4} \int \frac{d^4 l_3}{(2\pi)^4} \int \frac{d^4 l_4}{(2\pi)^4} \frac{1}{(l_1^2 + i\epsilon)(l_5 - i\epsilon)} \\ (2\pi)\delta(l_2^2)\theta(l_2^0)(2\pi)\delta(l_3^2)\theta(-l_3^0)(2\pi)\delta(l_4^2)\theta(l_4^0)(2\pi)^4\delta^4(q - l_2 + l_3 - l_4) \quad (3.13)$$

$$I_4^{Scalar} = \lambda^4 \int \frac{d^4 l_1}{(2\pi)^4} \int \frac{d^4 l_2}{(2\pi)^4} \int \frac{d^4 l_3}{(2\pi)^4} \frac{1}{(l_2^2 - i\epsilon)(l_4^2 - i\epsilon)(l_5^2 - i\epsilon)} \\ (2\pi)\delta(l_1^2)\theta(l_1^0)(2\pi)\delta(l_3^2)\theta(-l_3^0)(2\pi)^4\delta^4(q - l_1 + l_3) \quad (3.14)$$

To consider the integrals numerically, they need to be manipulated so that there are only three-momentum integrals left. Initially this is done by using the delta functions which put the propagators on shell and replaces the energies by three-momenta:

$$\int dp_0 \delta(p_0^2 - |\vec{p}|^2) \theta(p_0) = \frac{1}{2|\vec{p}|} \quad (3.15)$$

Looking at the integrands, it can be seen that there is one more delta function compared to the number of energy integrals in the three particle cuts. There are the same number of delta functions as energy integrals for the two particle cuts. However, the total conservation of energy delta function can not be eliminated by the loop energy integral. This is a typical property of loop momenta as they do not effect the overall conservation of four-momenta. These properties suggest that an integral over the total energy needs to be introduced to remove the final delta function. To do this, the integrand need to be multiplied by a function that integrates to one over the range of centre of mass energies $q^0 = \sqrt{s}$. The function will be referred to as the smearing function and will become a focus of attention later on:

$$\int d\sqrt{s} h(\sqrt{s}) = 1 \quad (3.16)$$

$$\begin{aligned}
 \Rightarrow I_1^{Scalar} &= \lambda^4 \int \frac{d^4 l_2}{(2\pi)^4} \int \frac{d^4 l_4}{(2\pi)^4} \int \frac{d^4 l_5}{(2\pi)^4} \int d\sqrt{s} \frac{h(\sqrt{s})}{(l_1^2 + i\epsilon)(l_2^2 + i\epsilon)(l_3^2 + i\epsilon)} \\
 &\quad (2\pi)\delta(l_4^2)\theta(l_4^0)(2\pi)\delta(l_5^2)\theta(l_5^0)(2\pi)^4\delta^4(q - l_4 - l_5) \\
 &= \lambda^4 \int \frac{d^4 l_2}{(2\pi)^4} \int \frac{d^3 \vec{l}_4}{(2\pi)^3} \frac{h(|\vec{l}_4| + |\vec{q} - \vec{l}_4|)}{2|\vec{l}_4|2|\vec{q} - \vec{l}_4|((l_2^0 + |\vec{l}_4|)^2 - |\vec{l}_2 + \vec{l}_4|^2 + i\epsilon)} \\
 &\quad \times \frac{1}{((l_2^0)^2 - |\vec{l}_2|^2 + i\epsilon)((l_2^0 - |\vec{q} - \vec{l}_4|)^2 - |\vec{l}_2 + \vec{l}_4 - \vec{q}|^2 + i\epsilon)} \quad (3.17)
 \end{aligned}$$

$$\begin{aligned}
 I_2^{Scalar} &= \lambda^4 \int \frac{d^4 l_1}{(2\pi)^4} \int \frac{d^4 l_2}{(2\pi)^4} \int \frac{d^4 l_5}{(2\pi)^4} \int d\sqrt{s} \frac{h(\sqrt{s})}{(l_3^2 + i\epsilon)(l_4^2 - i\epsilon)} \\
 &\quad (2\pi)\delta(l_1^2)\theta(l_1^0)(2\pi)\delta(l_2^2)\theta(-l_2^0)(2\pi)\delta(l_5^2)\theta(l_5^0)(2\pi)^4\delta^4(q - l_1 + l_2 - l_5) \\
 &= \lambda^4 \int \frac{d^3 \vec{l}_1}{(2\pi)^3} \int \frac{d^3 \vec{l}_2}{(2\pi)^3} \frac{h(|\vec{l}_1| + |\vec{l}_2| + |\vec{l}_2 - \vec{l}_1 + \vec{q}|)}{2|\vec{l}_1|2|\vec{l}_2|((|\vec{l}_2| + |\vec{l}_2 - \vec{l}_1 + \vec{q}|)^2 - |\vec{l}_1 - \vec{q}|^2 + i\epsilon)} \\
 &\quad \times \frac{1}{((|\vec{l}_1| + |\vec{l}_2|)^2 - |\vec{l}_1 - \vec{l}_2|^2 - i\epsilon)2|\vec{l}_2 - \vec{l}_1 + \vec{q}|} \quad (3.18)
 \end{aligned}$$

$$\begin{aligned}
 I_3^{Scalar} &= \lambda^4 \int \frac{d^4 l_2}{(2\pi)^4} \int \frac{d^4 l_3}{(2\pi)^4} \int \frac{d^4 l_4}{(2\pi)^4} \int d\sqrt{s} \frac{h(\sqrt{s})}{(l_1^2 + i\epsilon)(l_5^2 - i\epsilon)} \\
 &\quad (2\pi)\delta(l_2^2)\theta(l_2^0)(2\pi)\delta(l_3^2)\theta(-l_3^0)(2\pi)\delta(l_4^2)\theta(l_4^0)(2\pi)^4\delta^4(q - l_2 + l_3 - l_4) \\
 &= \lambda^4 \int \frac{d^3 \vec{l}_2}{(2\pi)^3} \int \frac{d^3 \vec{l}_4}{(2\pi)^3} \frac{h(|\vec{l}_2| + |\vec{l}_2 + \vec{l}_4 - \vec{q}| + |\vec{l}_4|)}{(|\vec{l}_2| + |\vec{l}_4|)^2 - |\vec{l}_2 + \vec{l}_4|^2 + i\epsilon} \frac{1}{2|\vec{l}_2|2|\vec{l}_2 + \vec{l}_4 - \vec{q}|} \\
 &\quad \times \frac{1}{2|\vec{l}_4|((|\vec{l}_2| + |\vec{l}_2 + \vec{l}_4 - \vec{q}|)^2 - |\vec{q} - \vec{l}_4|^2 - i\epsilon)} \quad (3.19)
 \end{aligned}$$

$$\begin{aligned}
 I_4^{Scalar} &= \lambda^4 \int \frac{d^4 l_1}{(2\pi)^4} \int \frac{d^4 l_2}{(2\pi)^4} \int \frac{d^4 l_3}{(2\pi)^4} \int d\sqrt{s} \frac{h(\sqrt{s})}{(l_2^2 - i\epsilon)(l_4^2 - i\epsilon)(l_5^2 - i\epsilon)} \\
 &\quad (2\pi)\delta(l_1^2)\theta(l_1^0)(2\pi)\delta(l_3^2)\theta(-l_3^0)(2\pi)^4\delta^4(q - l_1 + l_3) \\
 &= \lambda^4 \int \frac{d^3 \vec{l}_1}{(2\pi)^3} \int \frac{d^4 l_2}{(2\pi)^4} \frac{h(|\vec{l}_1| + |\vec{l}_1 - \vec{q}|)}{2|\vec{l}_1|((l_2^0)^2 - |\vec{l}_2|^2 - i\epsilon)2|\vec{l}_1 - \vec{q}|} \\
 &\quad \times \frac{1}{((|\vec{l}_1| - l_2^0)^2 - |\vec{l}_1 - \vec{l}_2|^2 - i\epsilon)((l_2^0 + |\vec{l}_1 - \vec{q}|)^2 - |\vec{l}_2 - \vec{l}_1 + \vec{q}|^2 - i\epsilon)} \quad (3.20)
 \end{aligned}$$

Once all delta functions have been removed, there remains a final integral to perform over the loop momenta of the two-particle cuts i.e. I_1^{Scalar} and I_4^{Scalar} . To perform this integral a knowledge of complex analysis is useful. The residues of the integrand need to be found and then the result is simply $2\pi i$ times the sum of the residues. Each of the propagators has two poles but only one must be used in the calculation. Due to causality constraints, we must choose either the positive or the negative energy solution. Thankfully, the Feynman rules include the $i\epsilon$ prescription that specify which pole to include. For each pair of poles, the positive energy solution will be taken. Finally, care must be taken with the direction that the contour travels around the pole as a minus

3. Numerical Methods

sign is incurred if the contour travels clockwise:

$$\int dp_0 \frac{1}{p^2 + i\epsilon} = -\frac{2\pi i}{2|\vec{p}|} \quad (3.21)$$

The overall effect of the integration applied to this example is to gain an integrand for each of the propagators in the loop put on-shell (Fig. 3.3):

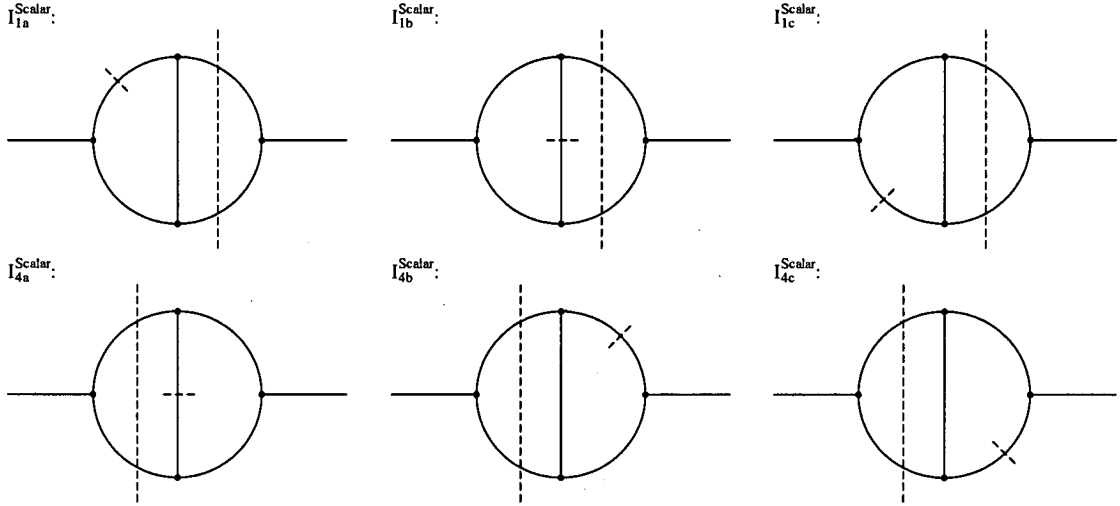


Figure 3.3.: Two particle cuts of the scalar two loop correction to the scalar propagator with one propagator put on-shell in each uncut loop.

$$I_{1a}^{Scalar} = \lambda^4 \int \frac{d^3\vec{l}_2}{(2\pi)^3} \int \frac{d^3\vec{l}_4}{(2\pi)^3} \frac{h(|\vec{l}_4| + |\vec{q} - \vec{l}_4|)}{2|\vec{l}_4|2|\vec{q} - \vec{l}_4|2|\vec{l}_2 + \vec{l}_4|((|\vec{l}_2 + \vec{l}_4| - |\vec{l}_4|)^2 - |\vec{l}_2|^2 + i\epsilon)} \times \frac{1}{((|\vec{l}_2 + \vec{l}_4| - |\vec{l}_4| - |\vec{q} - \vec{l}_4|)^2 - |\vec{l}_2 + \vec{l}_4 - \vec{q}|^2 + i\epsilon)} \quad (3.22)$$

$$I_{1b}^{Scalar} = \lambda^4 \int \frac{d^3\vec{l}_2}{(2\pi)^3} \int \frac{d^3\vec{l}_4}{(2\pi)^3} \frac{h(|\vec{l}_4| + |\vec{q} - \vec{l}_4|)}{2|\vec{l}_4|2|\vec{q} - \vec{l}_4|((|\vec{l}_2| + |\vec{l}_4|)^2 - |\vec{l}_2 + \vec{l}_4|^2 + i\epsilon)} \times \frac{1}{2|\vec{l}_2|((|\vec{l}_2| - |\vec{q} - \vec{l}_4|)^2 - |\vec{l}_2 + \vec{l}_4 - \vec{q}|^2 + i\epsilon)} \quad (3.23)$$

$$I_{1c}^{Scalar} = \lambda^4 \int \frac{d^3\vec{l}_2}{(2\pi)^3} \int \frac{d^3\vec{l}_4}{(2\pi)^3} \frac{h(|\vec{l}_4| + |\vec{q} - \vec{l}_4|)}{2|\vec{l}_4|2|\vec{q} - \vec{l}_4|((|\vec{q} - \vec{l}_4| + |\vec{l}_2 + \vec{l}_4 - \vec{q}| + |\vec{l}_4|)^2 - |\vec{l}_2 + \vec{l}_4|^2 + i\epsilon)} \times \frac{1}{((|\vec{q} - \vec{l}_4| + |\vec{l}_2 + \vec{l}_4 - \vec{q}|)^2 - |\vec{l}_2|^2 + i\epsilon)2|\vec{l}_2 + \vec{l}_4 - \vec{q}|} \quad (3.24)$$

$$\begin{aligned}
 I_{4a}^{Scalar} &= \lambda^4 \int \frac{d^3\vec{l}_1}{(2\pi)^3} \int \frac{d^3\vec{l}_2}{(2\pi)^3} \frac{h(|\vec{l}_1| + |\vec{l}_1 - \vec{q}|)}{2|\vec{l}_1|2|\vec{l}_2|2|\vec{l}_1 - \vec{q}|((|\vec{l}_1| - |\vec{l}_2|)^2 - |\vec{l}_1 - \vec{l}_2|^2 - i\epsilon)} \\
 &\quad \times \frac{1}{((|\vec{l}_2| + |\vec{l}_1 - \vec{q}|)^2 - |\vec{l}_2 - \vec{l}_1 + \vec{q}|^2 - i\epsilon)} \quad (3.25)
 \end{aligned}$$

$$\begin{aligned}
 I_{4b}^{Scalar} &= \lambda^4 \int \frac{d^3\vec{l}_1}{(2\pi)^3} \int \frac{d^3\vec{l}_2}{(2\pi)^3} \frac{h(|\vec{l}_1| + |\vec{l}_1 - \vec{q}|)}{2|\vec{l}_1|((|\vec{l}_1| + |\vec{l}_1 - \vec{l}_2|)^2 - |\vec{l}_2|^2 - i\epsilon)2|\vec{l}_1 - \vec{q}|2|\vec{l}_1 - \vec{l}_2|} \\
 &\quad \times \frac{1}{((|\vec{l}_1| + |\vec{l}_1 - \vec{l}_2| + |\vec{l}_1 - \vec{q}|)^2 - |\vec{l}_2 - \vec{l}_1 + \vec{q}|^2 - i\epsilon)} \quad (3.26)
 \end{aligned}$$

$$\begin{aligned}
 I_{4c}^{Scalar} &= \lambda^4 \int \frac{d^3\vec{l}_1}{(2\pi)^3} \int \frac{d^3\vec{l}_2}{(2\pi)^3} \frac{h(|\vec{l}_1| + |\vec{l}_1 - \vec{q}|)}{2|\vec{l}_1|((|\vec{l}_1 - \vec{l}_2 - \vec{q}| - |\vec{l}_1 - \vec{q}|)^2 - |\vec{l}_2|^2 - i\epsilon)2|\vec{l}_1 - \vec{q}|} \\
 &\quad \times \frac{1}{((|\vec{l}_1| - |\vec{l}_1 - \vec{l}_2 - \vec{q}| + |\vec{l}_1 - \vec{q}|)^2 - |\vec{l}_1 - \vec{l}_2|^2 - i\epsilon)2|\vec{l}_1 - \vec{l}_2 - \vec{q}|} \quad (3.27)
 \end{aligned}$$

At this point in the procedure there are eight expressions. Each of these expressions consist of integrands that depend on the incoming momenta, \vec{q} , and two other three-momenta that are integrated over. To make things simpler, the calculations may be performed in the centre of mass frame $\vec{q} = 0$. Finally using momentum conservation, all of the expressions can be written in terms of \vec{l}_2 and \vec{l}_3 . This is carried out by integrating over a momentum conserving delta function:

$$\begin{aligned}
 \int \frac{d^3\vec{l}_1}{(2\pi)^3} \int \frac{d^3\vec{l}_2}{(2\pi)^3} f(\vec{l}_1, \vec{l}_2) &= \int \frac{d^3\vec{l}_1}{(2\pi)^3} \int \frac{d^3\vec{l}_2}{(2\pi)^3} \int \frac{d^3\vec{l}_4}{(2\pi)^3} f(\vec{l}_1, \vec{l}_2) (2\pi)^3 \delta(\vec{l}_1 - \vec{l}_2 - \vec{l}_4) \\
 &= \int \frac{d^3\vec{l}_2}{(2\pi)^3} \int \frac{d^3\vec{l}_4}{(2\pi)^3} f(\vec{l}_2 + \vec{l}_4, \vec{l}_2) \quad (3.28)
 \end{aligned}$$

$$\begin{aligned}
 I_{1a}^{Scalar} &= \lambda^4 \int \frac{d^3\vec{l}_2}{(2\pi)^3} \int \frac{d^3\vec{l}_4}{(2\pi)^3} \frac{h(2|\vec{l}_4|)}{2|\vec{l}_4|2|\vec{l}_4|2|\vec{l}_2 + \vec{l}_4|((|\vec{l}_2 + \vec{l}_4| - |\vec{l}_4|)^2 - |\vec{l}_2|^2 + i\epsilon)} \\
 &\quad \times \frac{1}{((|\vec{l}_2 + \vec{l}_4| - 2|\vec{l}_4|)^2 - |\vec{l}_2 + \vec{l}_4|^2 + i\epsilon)} \quad (3.29)
 \end{aligned}$$

$$\begin{aligned}
 I_{1b}^{Scalar} &= \lambda^4 \int \frac{d^3\vec{l}_2}{(2\pi)^3} \int \frac{d^3\vec{l}_4}{(2\pi)^3} \frac{h(2|\vec{l}_4|)}{2|\vec{l}_4|2|\vec{l}_4|((|\vec{l}_2| + |\vec{l}_4|)^2 - |\vec{l}_2 + \vec{l}_4|^2 + i\epsilon)} \\
 &\quad \times \frac{1}{2|\vec{l}_2|((|\vec{l}_2| - |\vec{l}_4|)^2 - |\vec{l}_2 + \vec{l}_4|^2 + i\epsilon)} \quad (3.30)
 \end{aligned}$$

$$\begin{aligned}
 I_{1c}^{Scalar} &= \lambda^4 \int \frac{d^3\vec{l}_2}{(2\pi)^3} \int \frac{d^3\vec{l}_4}{(2\pi)^3} \frac{h(2|\vec{l}_4|)}{2|\vec{l}_4|2|\vec{l}_4|((2|\vec{l}_4| + |\vec{l}_2 + \vec{l}_4|)^2 - |\vec{l}_2 + \vec{l}_4|^2 + i\epsilon)} \\
 &\quad \times \frac{1}{((|\vec{l}_4| + |\vec{l}_2 + \vec{l}_4|)^2 - |\vec{l}_2|^2 + i\epsilon)2|\vec{l}_2 + \vec{l}_4|} \quad (3.31)
 \end{aligned}$$

3. Numerical Methods

$$\begin{aligned}
I_2^{Scalar} &= \lambda^4 \int \frac{d^3\vec{l}_2}{(2\pi)^3} \int \frac{d^3\vec{l}_4}{(2\pi)^3} \frac{h(|\vec{l}_2 + \vec{l}_4| + |\vec{l}_2| + |\vec{l}_4|)}{2|\vec{l}_2 + \vec{l}_4|2|\vec{l}_2|((|\vec{l}_2| + |\vec{l}_4|)^2 - |\vec{l}_2 + \vec{l}_4|^2 + i\epsilon)} \\
&\quad \times \frac{1}{((|\vec{l}_2 + \vec{l}_4| + |\vec{l}_2|)^2 - |\vec{l}_4|^2 - i\epsilon)2|\vec{l}_4|} \tag{3.32}
\end{aligned}$$

$$\begin{aligned}
I_3^{Scalar} &= \lambda^4 \int \frac{d^3\vec{l}_2}{(2\pi)^3} \int \frac{d^3\vec{l}_4}{(2\pi)^3} \frac{h(|\vec{l}_2| + |\vec{l}_2 + \vec{l}_4| + |\vec{l}_4|)}{(|\vec{l}_2| + |\vec{l}_4|)^2 - |\vec{l}_2 + \vec{l}_4|^2 + i\epsilon} 2|\vec{l}_2|2|\vec{l}_2 + \vec{l}_4| \\
&\quad \times \frac{1}{2|\vec{l}_4|((|\vec{l}_2| + |\vec{l}_2 + \vec{l}_4|)^2 - |\vec{l}_4|^2 - i\epsilon)} \tag{3.33}
\end{aligned}$$

$$\begin{aligned}
I_{4a}^{Scalar} &= \lambda^4 \int \frac{d^3\vec{l}_2}{(2\pi)^3} \int \frac{d^3\vec{l}_4}{(2\pi)^3} \frac{h(2|\vec{l}_2 + \vec{l}_4|)}{2|\vec{l}_2 + \vec{l}_4|2|\vec{l}_2|2|\vec{l}_2 + \vec{l}_4|((|\vec{l}_2 + \vec{l}_4| - |\vec{l}_2|)^2 - |\vec{l}_4|^2 - i\epsilon)} \\
&\quad \times \frac{1}{((|\vec{l}_2| + |\vec{l}_2 + \vec{l}_4|)^2 - |\vec{l}_4|^2 - i\epsilon)} \tag{3.34}
\end{aligned}$$

$$\begin{aligned}
I_{4b}^{Scalar} &= \lambda^4 \int \frac{d^3\vec{l}_2}{(2\pi)^3} \int \frac{d^3\vec{l}_4}{(2\pi)^3} \frac{h(2|\vec{l}_2 + \vec{l}_4|)}{2|\vec{l}_2 + \vec{l}_4|((|\vec{l}_2 + \vec{l}_4| + |\vec{l}_4|)^2 - |\vec{l}_2|^2 - i\epsilon)2|\vec{l}_2 + \vec{l}_4|2|\vec{l}_4|} \\
&\quad \times \frac{1}{((2|\vec{l}_2 + \vec{l}_4| + |\vec{l}_4|)^2 - |\vec{l}_4|^2 - i\epsilon)} \tag{3.35}
\end{aligned}$$

$$\begin{aligned}
I_{4c}^{Scalar} &= \lambda^4 \int \frac{d^3\vec{l}_1}{(2\pi)^3} \int \frac{d^3\vec{l}_2}{(2\pi)^3} \frac{h(2|\vec{l}_2 + \vec{l}_4|)}{2|\vec{l}_2 + \vec{l}_4|((|\vec{l}_4| - |\vec{l}_2 + \vec{l}_4|)^2 - |\vec{l}_2|^2 - i\epsilon)2|\vec{l}_2 + \vec{l}_4|} \\
&\quad \times \frac{1}{((2|\vec{l}_2 + \vec{l}_4| - |\vec{l}_4|)^2 - |\vec{l}_4|^2 - i\epsilon)2|\vec{l}_4|} \tag{3.36}
\end{aligned}$$

The expressions are now in a form that can be integrated numerically and so the singularity structures need to be examined before choosing suitable coordinate systems. In each of the integrands there is a combination of soft, collinear and scattering singularities. As mentioned previously, the soft singularities are point-like while the collinear and scattering singularities are lines and surfaces in three-momentum space. For the remainder of the chapter the factor of λ^4 will be neglected as the analysis does not depend on it.

3.2.1. Soft Singularities

Soft singularities can occur whenever a massless particle has zero three-momentum. This leads to zero factors in the denominator that can cause an infinite integrand. In this case there are only two momentum variables \vec{l}_2 and \vec{l}_4 . If \vec{l}_4 is taken to be fixed and non zero then the variable \vec{l}_2 can be varied so that either $|\vec{l}_2|$ or $|\vec{l}_2 + \vec{l}_4|$ tends to zero. Considering the first case when \vec{l}_2 is small then expansions of the other factors in the denominator can be made. Taking \vec{u}_2 to be the direction of \vec{l}_2 and \vec{u}_4 to be

the direction of \vec{l}_4 , the greatest multiplicative power of δ in the denominator can be examined:

$$|\vec{l}_2| \rightarrow \delta \quad (3.37)$$

$$|\vec{l}_2 + \vec{l}_4| \rightarrow |\vec{l}_4| + \delta \vec{u}_2 \cdot \vec{u}_4 \quad (3.38)$$

$$\frac{1}{|\vec{l}_2|} \approx \frac{1}{\delta} \quad (3.39)$$

$$\frac{1}{2|\vec{l}_2 + \vec{l}_4|} \approx \frac{1}{2|\vec{l}_4|} \quad (3.40)$$

$$\frac{1}{((|\vec{l}_2 + \vec{l}_4| - |\vec{l}_4|)^2 - |\vec{l}_2|^2)} \approx \frac{1}{\delta^2((\vec{u}_2 \cdot \vec{u}_4)^2 - 1)} \quad (3.41)$$

$$\frac{1}{((|\vec{l}_2 + \vec{l}_4| - 2|\vec{l}_4|)^2 - |\vec{l}_2 + \vec{l}_4|^2)} \approx -\frac{1}{4\delta|\vec{l}_4|\vec{u}_2 \cdot \vec{u}_4} \quad (3.42)$$

$$\frac{1}{(|\vec{l}_2| + |\vec{l}_4|)^2 - |\vec{l}_2 + \vec{l}_4|^2)} \approx \frac{1}{2\delta|\vec{l}_4|(1 - \vec{u}_2 \cdot \vec{u}_4)} \quad (3.43)$$

$$\frac{1}{(|\vec{l}_2| - |\vec{l}_4|)^2 - |\vec{l}_2 + \vec{l}_4|^2)} \approx -\frac{1}{2\delta|\vec{l}_4|(1 + \vec{u}_2 \cdot \vec{u}_4)} \quad (3.44)$$

$$\frac{1}{((|\vec{l}_2 + \vec{l}_4| + 2|\vec{l}_4|)^2 - |\vec{l}_2 + \vec{l}_4| + 2|)} \approx \frac{1}{8\delta|\vec{l}_4|} \quad (3.45)$$

$$\frac{1}{((|\vec{l}_2 + \vec{l}_4| + |\vec{l}_4|)^2 - |\vec{l}_2|^2)} \approx \frac{1}{4|\vec{l}_4|^2} \quad (3.46)$$

$$\frac{1}{((|\vec{l}_2 + \vec{l}_4| + |\vec{l}_2|)^2 - |\vec{l}_4|^2)} \approx \frac{1}{2\delta|\vec{l}_4|(1 + \vec{u}_2 \cdot \vec{u}_4)} \quad (3.47)$$

$$\frac{1}{((2|\vec{l}_2 + \vec{l}_4| + |\vec{l}_4|)^2 - |\vec{l}_4|^2)} \approx \frac{1}{8|\vec{l}_4|^2} \quad (3.48)$$

$$\frac{1}{((|\vec{l}_2 + \vec{l}_4| - |\vec{l}_2|)^2 - |\vec{l}_4|^2)} \approx -\frac{1}{2\delta|\vec{l}_4|(1 - \vec{u}_2 \cdot \vec{u}_4)} \quad (3.49)$$

All the integrands, A^{Scalar} , of the expressions for the graph can be formed out of

3. Numerical Methods

the above factors. This gives the highest order soft singularity:

$$A_{1a}^{Scalar} \approx \frac{h(2|\vec{l}_4|)}{32\delta^3|\vec{l}_4|^4(1 - (\vec{u}_2 \cdot \vec{u}_4)^2)\vec{u}_2 \cdot \vec{u}_4} \quad (3.50)$$

$$A_{1b}^{Scalar} \approx -\frac{h(2|\vec{l}_4|)}{32\delta^3|\vec{l}_4|^4(1 - (\vec{u}_2 \cdot \vec{u}_4)^2)} \quad (3.51)$$

$$A_{1c}^{Scalar} \approx \frac{h(2|\vec{l}_4|)}{256|\vec{l}_4|^7} \quad (3.52)$$

$$A_2^{Scalar} \approx \frac{h(2|\vec{l}_4|)}{32\delta^3|\vec{l}_4|^4(1 - (\vec{u}_2 \cdot \vec{u}_4)^2)} \quad (3.53)$$

$$A_3^{Scalar} \approx \frac{h(2|\vec{l}_4|)}{32\delta^3|\vec{l}_4|^4(1 - (\vec{u}_2 \cdot \vec{u}_4)^2)} \quad (3.54)$$

$$A_{4a}^{Scalar} \approx -\frac{h(2|\vec{l}_4|)}{32\delta^3|\vec{l}_4|^4(1 - (\vec{u}_2 \cdot \vec{u}_4)^2)} \quad (3.55)$$

$$A_{4b}^{Scalar} \approx -\frac{h(2|\vec{l}_4|)}{32\delta^3|\vec{l}_4|^4(1 - (\vec{u}_2 \cdot \vec{u}_4)^2)\vec{u}_2 \cdot \vec{u}_4} \quad (3.56)$$

$$A_{4c}^{Scalar} \approx \frac{h(2|\vec{l}_4|)}{256|\vec{l}_4|^7} \quad (3.57)$$

Only two of the above expressions are finite as \vec{l}_2 goes to zero, they are A_{1c}^{Scalar} and A_{4c}^{Scalar} . All the other integrands contain a factor of δ^3 in the denominator. However there are intricate cancellations between the cuts. When the integrands are added together cancellations occur between A_{1a}^{Scalar} and A_{4b}^{Scalar} , and the group of integrands A_{1b}^{Scalar} , A_2^{Scalar} , A_3^{Scalar} and A_{4a}^{Scalar} . After the addition there still remain terms with δ^2 in the denominator, but these terms are integrable singularities that the momentum dependence of the measure takes care of.

A similar procedure can be used to examine the soft case when $|\vec{l}_2 + \vec{l}_4|$ goes soft for fixed \vec{l}_4 . This time the momentum concerned is an external momentum for the cut with the vertex correction on the right hand side. Not surprisingly, the strong soft singularities appear in the three expressions corresponding to this cut. To show that

the soft singularities cancel, the first order expansions need to be kept:

$$|\vec{l}_2 + \vec{l}_4| = \delta \quad (3.58)$$

$$\begin{aligned} |\vec{l}_2| &= |\vec{l}_2 + \vec{l}_4 - \vec{l}_4| \\ &\approx |\vec{l}_4| - |\vec{l}_2 + \vec{l}_4| \vec{u}_{24} \cdot \vec{u}_4 \\ &= |\vec{l}_4| - \delta \vec{u}_{24} \cdot \vec{u}_4 \end{aligned} \quad (3.59)$$

$$A_{1a}^{Scalar} \approx \frac{h(2|\vec{l}_4|)}{64\delta^2 |\vec{l}_4|^5 (\vec{u}_{24} \cdot \vec{u}_4 - 1)} \quad (3.60)$$

$$A_{1b}^{Scalar} \approx \frac{h(2|\vec{l}_4|)}{32\delta^2 |\vec{l}_4|^5 ((\vec{u}_{24} \cdot \vec{u}_4)^2 - 1)} \quad (3.61)$$

$$A_{1c}^{Scalar} \approx \frac{h(2|\vec{l}_4|)}{64\delta^2 |\vec{l}_4|^5 (\vec{u}_{24} \cdot \vec{u}_4 + 1)} \quad (3.62)$$

$$A_2^{Scalar} \approx \frac{h(2|\vec{l}_4|)}{64\delta^2 |\vec{l}_4|^5} \quad (3.63)$$

$$A_3^{Scalar} \approx \frac{h(2|\vec{l}_4|)}{64\delta^2 |\vec{l}_4|^5} \quad (3.64)$$

$$A_{4a}^{Scalar} \approx \frac{h(2\delta)}{32\delta^4 |\vec{l}_4|^2 (|\vec{l}_4| - \delta \vec{u}_{24} \cdot \vec{u}_4) ((\vec{u}_{24} \cdot \vec{u}_4)^2 - 1)} \quad (3.65)$$

$$A_{4b}^{Scalar} \approx \frac{h(2\delta)}{64\delta^4 |\vec{l}_4|^2 (\vec{u}_{24} \cdot \vec{u}_4 - 1) (\delta - |\vec{l}_4|)} \quad (3.66)$$

$$A_{4c}^{Scalar} \approx \frac{h(2\delta)}{64\delta^4 |\vec{l}_4|^2 (\vec{u}_{24} \cdot \vec{u}_4 + 1) (\delta + |\vec{l}_4|)} \quad (3.67)$$

$$A_{4a}^{Scalar} + A_{4b}^{Scalar} + A_{4c}^{Scalar} \approx \frac{h(2\delta)}{32\delta^2 |\vec{l}_4|^5} \quad (3.68)$$

Finally, the soft characteristics when \vec{l}_4 is small need to be examined. Here \vec{l}_2 is

3. Numerical Methods

kept at a fixed non-zero value:

$$|\vec{l}_4| = \delta \quad (3.69)$$

$$|\vec{l}_2 + \vec{l}_4| \approx |\vec{l}_2| + \delta \vec{u}_2 \cdot \vec{u}_4 \quad (3.70)$$

$$A_{1a}^{Scalar} \approx \frac{h(2\delta)}{64\delta^4 |\vec{l}_2|^2 (1 - \vec{u}_2 \cdot \vec{u}_4) (|\vec{l}_2| - 2\delta(1 - \vec{u}_2 \cdot \vec{u}_4))} \quad (3.71)$$

$$A_{1b}^{Scalar} \approx \frac{h(2\delta)}{32\delta^4 |\vec{l}_2|^3 ((\vec{u}_2 \cdot \vec{u}_4)^2 - 1)} \quad (3.72)$$

$$A_{1c}^{Scalar} \approx \frac{h(2\delta)}{64\delta^4 |\vec{l}_2|^2 (1 + \vec{u}_2 \cdot \vec{u}_4) (|\vec{l}_2| + 2\delta(1 + \vec{u}_2 \cdot \vec{u}_4))} \quad (3.73)$$

$$A_{1a}^{Scalar} + A_{1b}^{Scalar} + A_{1c}^{Scalar} \approx 0 \quad (3.74)$$

$$A_2^{Scalar} \approx \frac{h(2|\vec{l}_2|)}{64\delta^2 |\vec{l}_2|^5 (1 - \vec{u}_2 \cdot \vec{u}_4)} \quad (3.75)$$

$$A_3^{Scalar} \approx \frac{h(2|\vec{l}_2|)}{64\delta^2 |\vec{l}_2|^5 (1 - \vec{u}_2 \cdot \vec{u}_4)} \quad (3.76)$$

$$A_{4a}^{Scalar} \approx \frac{h(2|\vec{l}_2|)}{64\delta^2 |\vec{l}_2|^5 ((\vec{u}_2 \cdot \vec{u}_4)^2 - 1)} \quad (3.77)$$

$$A_{4b}^{Scalar} \approx \frac{h(2|\vec{l}_2|)}{64\delta^2 |\vec{l}_2|^5 (\vec{u}_2 \cdot \vec{u}_4 - 1)} \quad (3.78)$$

$$A_{4c}^{Scalar} \approx \frac{h(2|\vec{l}_2|)}{64\delta^2 |\vec{l}_2|^5 (1 + \vec{u}_2 \cdot \vec{u}_4)} \quad (3.79)$$

For the soft cancellations with small \vec{l}_4 or $\vec{l}_2 + \vec{l}_4$, the smearing function can help to make the integrand less singular, however it is not required to do so. The directional vectors, \vec{u} , point towards other singular features of the expressions that will be dealt with in the next section.

3.2.2. Collinear Singularities

Collinear singularities occur when the momenta of two or more on-shell massless particles emerging from a vertex lie parallel or anti-parallel to each other. If one or both of the particles has a mass then these singularities disappear. They are called mass singularities for this reason.

As a nice coordinate system has already been chosen it would be useful if all remnants of the collinear singularities disappeared on the addition of the cuts. Superficially, it would seem that only graphs with three particle cuts could carry collinear singularities

as they naturally possess on-shell particles emerging from the same vertex. However, the graphs with two particle cuts also contribute. This is due to the internal momenta flowing round the loop being put on-shell. It is sufficient to consider the collinearity of the two independent momenta by writing one of the vectors in terms of another along with a transverse part. The transverse part is taken to be small and the components are expanded about the magnitude of the small transverse momenta:

$$\vec{l}_2 = x\vec{l}_4 + \vec{l}_T \quad (3.80)$$

$$|\vec{l}_2| = |x\vec{l}_4 + \vec{l}_T| \quad (3.81)$$

$$= (x^2|\vec{l}_4|^2 + |\vec{l}_T|^2)^{\frac{1}{2}} \quad (3.82)$$

$$\approx |x||\vec{l}_4| \left(1 + \frac{|\vec{l}_T|^2}{2x^2|\vec{l}_4|^2} \right) \quad (3.83)$$

$$|\vec{l}_2 + \vec{l}_4| = |(1+x)\vec{l}_4 + \vec{l}_T| \quad (3.84)$$

$$= ((1+x)^2|\vec{l}_4|^2 + |\vec{l}_T|^2)^{\frac{1}{2}} \quad (3.85)$$

$$\approx |1+x||\vec{l}_4| \left(1 + \frac{|\vec{l}_T|^2}{2(1+x)^2|\vec{l}_4|^2} \right) \quad (3.86)$$

By examining the factors in the denominator it is possible to attribute the collinear singularities to three possible terms. These factors in turn have collinear regions for different ranges of x :

$$\begin{aligned} |\vec{l}_4| - |\vec{l}_2 + \vec{l}_4| - |\vec{l}_2| &\approx |\vec{l}_4| - |1+x||\vec{l}_4| \left(1 + \frac{|\vec{l}_T|^2}{2(1+x)^2|\vec{l}_4|^2} \right) - |x||\vec{l}_4| \left(1 + \frac{|\vec{l}_T|^2}{2x^2|\vec{l}_4|^2} \right) \\ &= -\frac{|\vec{l}_T|^2}{2(1+x)|\vec{l}_4|^2} + \frac{|\vec{l}_T|^2}{2x|\vec{l}_4|^2}, \quad -1 < x < 0 \end{aligned} \quad (3.87)$$

$$\begin{aligned} |\vec{l}_4| - |\vec{l}_2 + \vec{l}_4| + |\vec{l}_2| &\approx |\vec{l}_4| - |1+x||\vec{l}_4| \left(1 + \frac{|\vec{l}_T|^2}{2(1+x)^2|\vec{l}_4|^2} \right) + |x||\vec{l}_4| \left(1 + \frac{|\vec{l}_T|^2}{2x^2|\vec{l}_4|^2} \right) \\ &= -\frac{|\vec{l}_T|^2}{2(1+x)|\vec{l}_4|^2} + \frac{|\vec{l}_T|^2}{2x|\vec{l}_4|^2}, \quad 0 < x < \infty \end{aligned} \quad (3.88)$$

$$\begin{aligned} |\vec{l}_4| + |\vec{l}_2 + \vec{l}_4| - |\vec{l}_2| &\approx |\vec{l}_4| + |1+x||\vec{l}_4| \left(1 + \frac{|\vec{l}_T|^2}{2(1+x)^2|\vec{l}_4|^2} \right) - |x||\vec{l}_4| \left(1 + \frac{|\vec{l}_T|^2}{2x^2|\vec{l}_4|^2} \right) \\ &= -\frac{|\vec{l}_T|^2}{2(1+x)|\vec{l}_4|^2} + \frac{|\vec{l}_T|^2}{2x|\vec{l}_4|^2}, \quad -\infty < x < -1. \end{aligned} \quad (3.89)$$

The integrands can now be categorised according to what collinear factors they have in the denominator (Tab. 3.1).

Cancellations must occur between integrands that have collinear singularities in the

3. Numerical Methods

| Integrand | $-\infty < x < -1$ | $-1 < x < 0$ | $0 < x < \infty$ |
|-------------------|--------------------|--------------|------------------|
| A_{1a}^{Scalar} | No | Yes | Yes |
| A_{1b}^{Scalar} | Yes | Yes | Yes |
| A_{1c}^{Scalar} | Yes | No | No |
| A_2^{Scalar} | No | Yes | Yes |
| A_3^{Scalar} | No | Yes | Yes |
| A_{4a}^{Scalar} | Yes | Yes | Yes |
| A_{4b}^{Scalar} | No | Yes | Yes |
| A_{4c}^{Scalar} | Yes | No | No |

Table 3.1.: Table showing singularities in each integrand.

same regions. To examine this further, the integrands can be expanded in the collinear regions and the highest order cancelling terms determined:

$$-\infty < x < -1:$$

$$A_{1b}^{Scalar} \approx \frac{h(2|\vec{l}_4|)}{32x|\vec{l}_T|^2|\vec{l}_4|^5} \quad (3.90)$$

$$A_{1c}^{Scalar} \approx -\frac{h(2|\vec{l}_4|)}{32x|\vec{l}_T|^2|\vec{l}_4|^5} \quad (3.91)$$

$$A_{4a}^{Scalar} \approx \frac{h(2|1+x||\vec{l}_4|)}{32x(1+x)^2|\vec{l}_T|^2|\vec{l}_4|^5} \quad (3.92)$$

$$A_{4c}^{Scalar} \approx -\frac{h(2|1+x||\vec{l}_4|)}{32x(1+x)^2|\vec{l}_T|^2|\vec{l}_4|^5} \quad (3.93)$$

$$-1 < x < 0:$$

$$A_{1a}^{Scalar} \approx \frac{h(2|\vec{l}_4|)}{32x|\vec{l}_T|^2|\vec{l}_4|^5} \quad (3.94)$$

$$A_{1b}^{Scalar} \approx \frac{h(2|\vec{l}_4|)}{32x|\vec{l}_T|^2|\vec{l}_4|^5} \quad (3.95)$$

$$A_2^{Scalar} \approx -\frac{h(2|\vec{l}_4|)}{32x|\vec{l}_T|^2|\vec{l}_4|^5} \quad (3.96)$$

$$A_3^{Scalar} \approx -\frac{h(2|\vec{l}_4|)}{32x|\vec{l}_T|^2|\vec{l}_4|^5} \quad (3.97)$$

$$A_{4a}^{Scalar} \approx \frac{h(2|1+x||\vec{l}_4|)}{32x(1+x)^2|\vec{l}_T|^2|\vec{l}_4|^5} \quad (3.98)$$

$$A_{4b}^{Scalar} \approx -\frac{h(2|1+x||\vec{l}_4|)}{32x(1+x)^2|\vec{l}_T|^2|\vec{l}_4|^5} \quad (3.99)$$

$0 < x < \infty$:

$$A_{1a}^{Scalar} \approx \frac{h(2|\vec{l}_4|)}{32x|\vec{l}_T|^2|\vec{l}_4|^5} \quad (3.100)$$

$$A_{1b}^{Scalar} \approx -\frac{h(2|\vec{l}_4|)}{32x|\vec{l}_T|^2|\vec{l}_4|^5} \quad (3.101)$$

$$A_2^{Scalar} \approx \frac{h(2|1+x||\vec{l}_4|)}{32x(1+x)^2|\vec{l}_T|^2|\vec{l}_4|^5} \quad (3.102)$$

$$A_3^{Scalar} \approx \frac{h(2|1+x||\vec{l}_4|)}{32x(1+x)^2|\vec{l}_T|^2|\vec{l}_4|^5} \quad (3.103)$$

$$A_{4a}^{Scalar} \approx -\frac{h(2|1+x||\vec{l}_4|)}{32x(1+x)^2|\vec{l}_T|^2|\vec{l}_4|^5} \quad (3.104)$$

$$A_{4b}^{Scalar} \approx -\frac{h(2|1+x||\vec{l}_4|)}{32x(1+x)^2|\vec{l}_T|^2|\vec{l}_4|^5} \quad (3.105)$$

Combining the integrands in their respective regions, it can be seen that no factors of $|\vec{l}_T|$ remain in the denominator. The form of the integrands also suggest that pairs of amplitudes when combined without expanding may leave integrands free from collinear singularities in a particular region. Where the smearing function is dependent on different momenta, the combination can only take place exactly on the line of collinearity:

$-\infty < x < -1$:

$$\begin{aligned} A_{1b}^{Scalar} + A_{1c}^{Scalar} &= \frac{h(2|\vec{l}_4|)(4|\vec{l}_2 + \vec{l}_4||\vec{l}_4| + |\vec{l}_2|(|\vec{l}_4| + |\vec{l}_2 + \vec{l}_4| + |\vec{l}_2|))}{32|\vec{l}_2 + \vec{l}_4||\vec{l}_2||\vec{l}_4|^3(|\vec{l}_4| + |\vec{l}_2 + \vec{l}_4| + |\vec{l}_2|)(|\vec{l}_4| + |\vec{l}_2 + \vec{l}_4| - |\vec{l}_2|)} \\ &\quad \times \frac{1}{(|\vec{l}_4| + |\vec{l}_2 + \vec{l}_4| - |\vec{l}_2|)(|\vec{l}_4| + |\vec{l}_2 + \vec{l}_4|)} \end{aligned} \quad (3.106)$$

$$\begin{aligned} A_{4a}^{Scalar} + A_{4c}^{Scalar} &= \frac{h(2|1+x||\vec{l}_4|)(4|\vec{l}_4||\vec{l}_2 + \vec{l}_4| + |\vec{l}_2|(|\vec{l}_4| + |\vec{l}_2 + \vec{l}_4| + |\vec{l}_2|))}{32|\vec{l}_2||\vec{l}_4||\vec{l}_2 + \vec{l}_4|^3(|\vec{l}_4| + |\vec{l}_2 + \vec{l}_4| + |\vec{l}_2|)(|\vec{l}_4| - |\vec{l}_2 + \vec{l}_4| + |\vec{l}_2|)} \\ &\quad \times \frac{1}{(|\vec{l}_4| - |\vec{l}_2 + \vec{l}_4| - |\vec{l}_2|)(|\vec{l}_4| + |\vec{l}_2 + \vec{l}_4|)} \end{aligned} \quad (3.107)$$

3. Numerical Methods

$$-1 < x < 0$$

$$A_{1a}^{Scalar} + A_2^{Scalar} = \frac{h(2|\vec{l}_4|)(|\vec{l}_2|(|\vec{l}_2| + |\vec{l}_2 + \vec{l}_4| + |\vec{l}_4|) + 2|\vec{l}_2||\vec{l}_4| + 4|\vec{l}_4|^2)}{32|\vec{l}_2||\vec{l}_2 + \vec{l}_4||\vec{l}_4|^3(|\vec{l}_2 + \vec{l}_4| - |\vec{l}_4| - |\vec{l}_2|)(|\vec{l}_2| + |\vec{l}_4| + |\vec{l}_2 + \vec{l}_4|)^2} \\ \times \frac{1}{(|\vec{l}_4| - |\vec{l}_2 + \vec{l}_4|)} \quad (3.108)$$

$$A_{1b}^{Scalar} + A_3^{Scalar} = \frac{h(2|\vec{l}_4|)(|\vec{l}_2 + \vec{l}_4| - |\vec{l}_4|)}{8|\vec{l}_2||\vec{l}_2 + \vec{l}_4||\vec{l}_4|^2((|\vec{l}_2| + |\vec{l}_4|)^2 - |\vec{l}_2 + \vec{l}_4|^2)(|\vec{l}_4| + |\vec{l}_2 + \vec{l}_4| - |\vec{l}_2|)} \\ \times \frac{1}{(|\vec{l}_2| + |\vec{l}_4| + |\vec{l}_2 + \vec{l}_4|)} \quad (3.109)$$

$$A_{4a}^{Scalar} + A_{4b}^{Scalar} = \frac{h(2|1+x||\vec{l}_4|)(4|\vec{l}_4||\vec{l}_2 + \vec{l}_4| + |\vec{l}_2|(|\vec{l}_2 + \vec{l}_4| - |\vec{l}_2| - |\vec{l}_4|))}{32|\vec{l}_2||\vec{l}_4||\vec{l}_2 + \vec{l}_4|^3(|\vec{l}_2 + \vec{l}_4| - |\vec{l}_2| - |\vec{l}_4|)(|\vec{l}_2| + |\vec{l}_4| + |\vec{l}_2 + \vec{l}_4|)} \\ \times \frac{1}{(|\vec{l}_4| + |\vec{l}_2 + \vec{l}_4| - |\vec{l}_2|)(|\vec{l}_2 + \vec{l}_4| - |\vec{l}_4|)} \quad (3.110)$$

$$0 < x < \infty$$

$$A_{1a}^{Scalar} + A_{1b}^{Scalar} = \frac{h(2|\vec{l}_4|)(4|\vec{l}_2 + \vec{l}_4||\vec{l}_4| + |\vec{l}_2|(|\vec{l}_4| - |\vec{l}_2 + \vec{l}_4| - |\vec{l}_2|))}{32|\vec{l}_2||\vec{l}_2 + \vec{l}_4||\vec{l}_4|^3(|\vec{l}_4| - |\vec{l}_2 + \vec{l}_4| - |\vec{l}_2|)(|\vec{l}_4| + |\vec{l}_2 + \vec{l}_4| + |\vec{l}_2|)} \\ \times \frac{1}{(|\vec{l}_4| + |\vec{l}_2 + \vec{l}_4| - |\vec{l}_2|)(|\vec{l}_4| - |\vec{l}_2 + \vec{l}_4|)} \quad (3.111)$$

$$A_2^{Scalar} + A_{4b}^{Scalar} = \frac{h(2|1+x||\vec{l}_4|)}{32|\vec{l}_4||\vec{l}_2||\vec{l}_2 + \vec{l}_4|^3(|\vec{l}_4| - |\vec{l}_2 + \vec{l}_4| - |\vec{l}_2|)(|\vec{l}_4| + |\vec{l}_2 + \vec{l}_4| + |\vec{l}_2|)^2} \\ \times \frac{2(|\vec{l}_2 + \vec{l}_4| + |\vec{l}_2|)^2 + 2|\vec{l}_2 + \vec{l}_4|^2 + |\vec{l}_2|(|\vec{l}_4| - |\vec{l}_2 + \vec{l}_4| - |\vec{l}_2|)}{(|\vec{l}_2 + \vec{l}_4| - |\vec{l}_4|)} \quad (3.112)$$

$$A_3^{Scalar} + A_{4a}^{Scalar} = \frac{h(2|1+x||\vec{l}_4|)(|\vec{l}_4| + |\vec{l}_2 + \vec{l}_4|)}{8|\vec{l}_4||\vec{l}_2||\vec{l}_2 + \vec{l}_4|^2(|\vec{l}_4| - |\vec{l}_2 + \vec{l}_4| - |\vec{l}_2|)(|\vec{l}_4| + |\vec{l}_2 + \vec{l}_4| + |\vec{l}_2|)^2} \\ \times \frac{1}{(|\vec{l}_4| + |\vec{l}_2 + \vec{l}_4| - |\vec{l}_2|)} \quad (3.113)$$

As can be seen, the factor in the denominator that would produce a collinear singularity in a particular region cancels on the addition of pairs of integrands.

3.2.3. Scattering Singularity

The final type of singularity that could warrant a change of coordinate system is the scattering singularity. This singularity is so named as it occurs whenever two on-shell particles scatter within a diagram to produce other on-shell particles. This type of singularity can only occur within graphs that have loops. For this configuration, there is only one possible source of scattering singularity and that is when the two propagators extending from the source are on-shell and produce the two on-shell final state particles.

3.3. Visualisation of Singularity Cancellations

In the centre of mass frame, the characteristic factor in the denominator is $2|\vec{l}_4| - 2|\vec{l}_2 + \vec{l}_4|$. This can be understood as two particles colliding, producing two more particles, with each pair being back to back. Geometrically, this factor is zero on a sphere in loop three-momentum space centred on $\vec{l}_2 = \vec{l}_4$ with radius $|\vec{l}_4|$. There only exists two integrands, A_{1a}^{Scalar} and A_{4b}^{Scalar} , one from either side of the cut that contain this factor. When these two integrands are added together the singularity disappears:

$$A_{1a}^{Scalar} + A_{4b}^{Scalar} = -\frac{h(2|\vec{l}_4|)(|\vec{l}_4| + |\vec{l}_2 + \vec{l}_4|)}{32|\vec{l}_4|^3|\vec{l}_2 + \vec{l}_4|^3((|\vec{l}_2 + \vec{l}_4| - |\vec{l}_4|)^2 - |\vec{l}_2|^2)} \quad (3.114)$$

This simplifies the numerical procedure as no contour deformation is required as will be explained later.

3.3. Visualisation of Singularity Cancellations and Verification of the Numerical Procedure

The analytic justification of the cancellation of singularities is thorough and shows that the integrals are viable. Before carrying out the numerical procedure it is useful to visualise the integrand to be evaluated. As the integral is 6 dimensional, it is impossible to view the whole integrand in a single image. This problem can be overcome by considering one or two dimensional slices of the integrand. To see how the singularities cancel it is useful to choose slices that contain each type of cancellation. There are two ways this can be done, either by viewing a small section of momentum space, or by looking at the integrand after the transformations are made for the purposes of numerical integration. The former gives a view that is easy to interpret from the original integrand while the latter gives an idea of the shape of the integral to be evaluated.

Before considering what the integrand looks like, the smearing function to be used must be decided. This is because it alters the weight of the contribution from each integrand depending on the momentum that is flowing through the external legs of each cut. A way of combining the integrands with equal weight in a region of momentum space is by using a ‘top hat’ smearing function. This is basically a function that is a combination of the standard theta functions. If the region of integration to be

3. Numerical Methods

considered starts at $\sqrt{s} = E_a$ and ends at $\sqrt{s} = E_b$ then the function required is

$$h(\sqrt{s}) = \frac{\theta(\sqrt{s} - E_a) - \theta(\sqrt{s} - E_b)}{E_b - E_a} \quad (3.115)$$

By increasing the width of the top hat, the common non-zero contributions from each cut in momentum space increase. Taking a top hat smearing function centred on $\sqrt{s} = 100$ GeV with a width of 40 GeV the region of loop momentum space that has contributions from each cut at various magnitudes of external momentum whose directions lie along the l_2^1 axis are shown in Fig. 3.4 and 3.5.

The most interesting regions of momentum space for the scalar case is the part of momentum space where soft collinear and scattering singularity cancellations occur. To see how each of the cuts contribute to the integrand while avoiding effects due to change of coordinates, a very wide top hat function that includes $\sqrt{s} = 0$ can be used (Fig. 3.6).

An alternative smearing function that has been used in the Beowulf program can be applied here. It is a function that is non-zero over the whole of momentum space and is based on the radial transformation used in the choice of momenta:

$$\begin{aligned} \sqrt{s} &= E \left(\frac{1}{X^A} - 1 \right)^B \\ \int_0^\infty d\sqrt{s} h(\sqrt{s}) &= \int_0^1 dX \frac{h(\sqrt{s}) A B E \left(\left(\frac{\sqrt{s}}{E} \right)^{\frac{1}{B}} + 1 \right)^{1+\frac{1}{A}}}{\left(\frac{\sqrt{s}}{E} \right)^{\frac{1}{B}-1}} \\ &= 1 \end{aligned} \quad (3.116)$$

$$\rightarrow h(\sqrt{s}) = \frac{\left(\frac{\sqrt{s}}{E} \right)^{\frac{1}{B}-1}}{A B E \left(\left(\frac{\sqrt{s}}{E} \right)^{\frac{1}{B}} + 1 \right)^{1+\frac{1}{A}}} \quad (3.117)$$

The peak of the smearing function can be found by differentiating the smearing function with respect to the centre of mass energy and so finding the maximum of the function. This then allows the parameters E , A and B to be fixed for the required

3.3. Visualisation of Singularity Cancellations

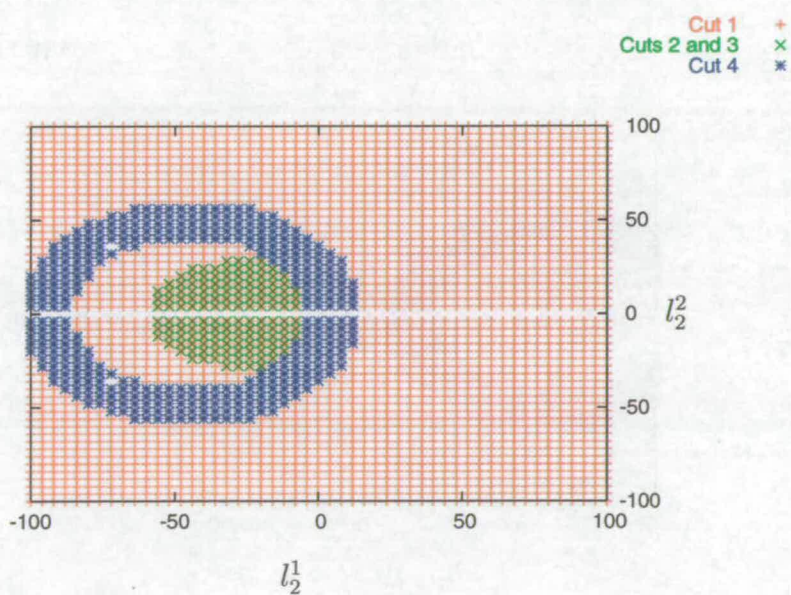
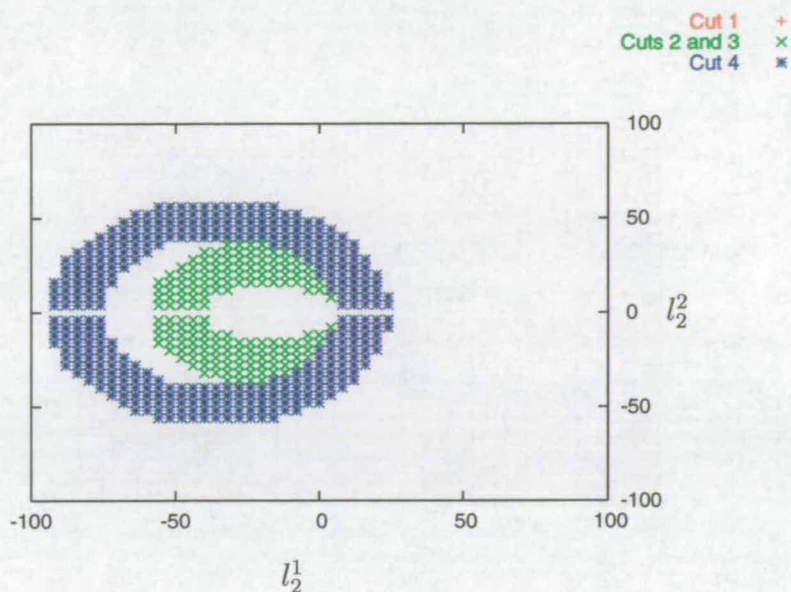


Figure 3.4.: Plots of integration regions for each of the main cuts in the l_2^1, l_2^2 plane using $\sqrt{s} = 100$ GeV and a top hat smearing function of width 40 GeV. Plots given for external momentum of magnitude 35 GeV (top) and 45 GeV (bottom).

3. Numerical Methods

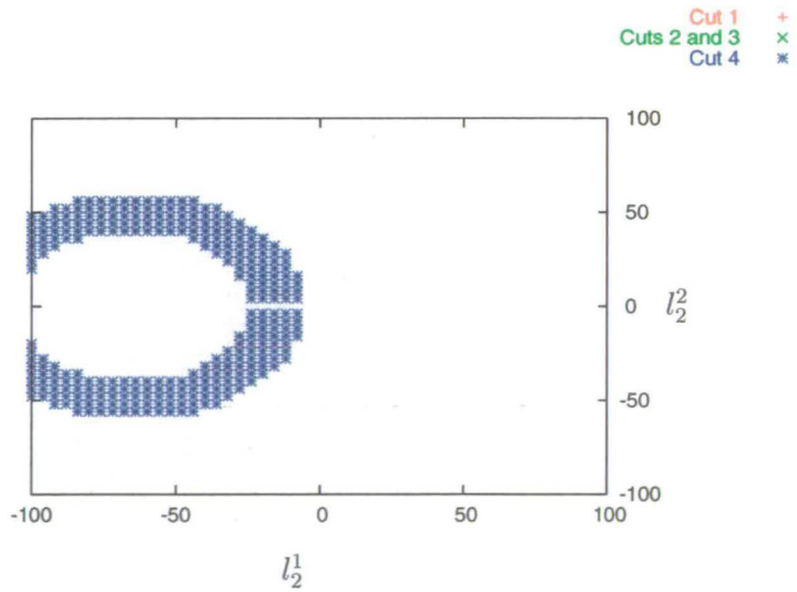
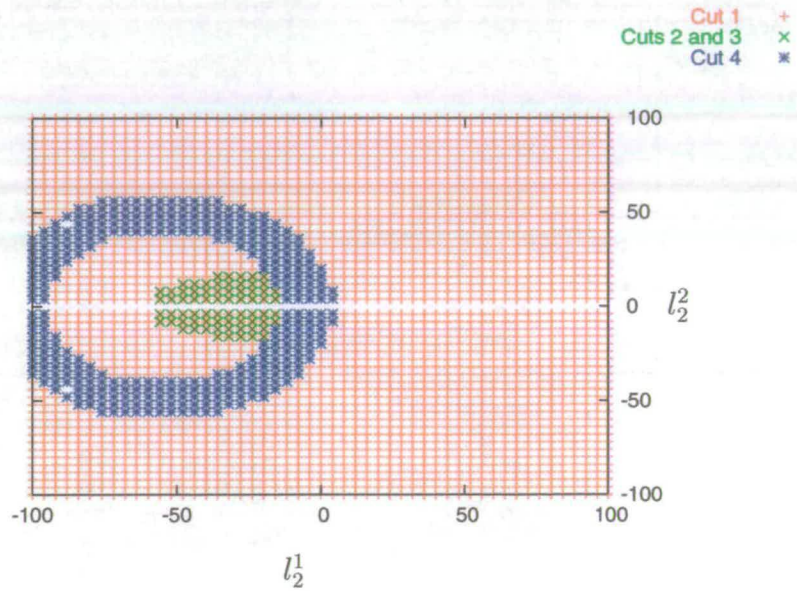


Figure 3.5.: Plots of integration regions for each of the main cuts in the l_2^1, l_2^2 plane using $\sqrt{s} = 100$ GeV and a top hat smearing function of width 40 GeV. Plots given for external momentum of magnitude 55 GeV (top) and 65 GeV (bottom).

3.3. Visualisation of Singularity Cancellations

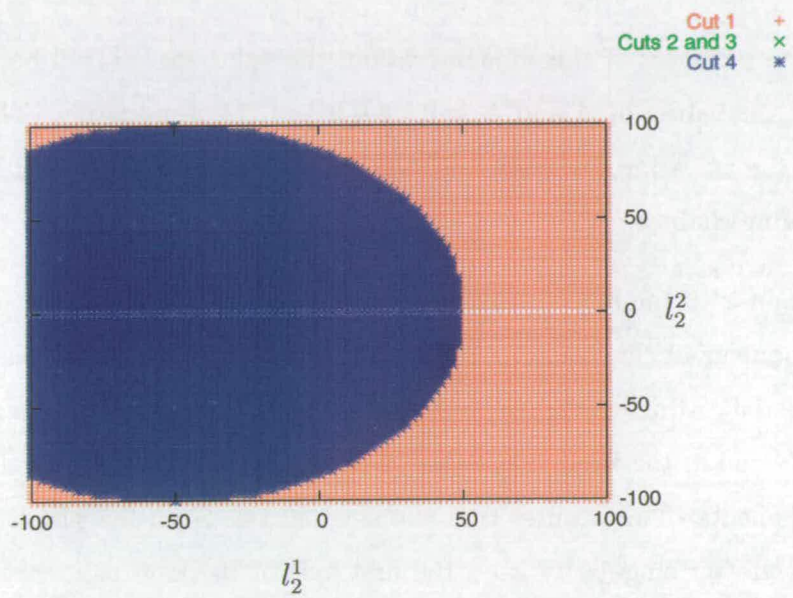


Figure 3.6.: Plot of integration region for each of the main cuts in the l_2^1, l_2^2 plane using $\sqrt{s} = 100$ GeV and a top hat smearing function of width 200 GeV. Plots given for external momentum of magnitude 50 GeV.

3. Numerical Methods

energy:

$$\begin{aligned} \left. \frac{\partial h(\sqrt{s})}{\partial \sqrt{s}} \right|_{\sqrt{s}_{peak}} &= \frac{\left(\frac{\sqrt{s}}{E}\right)^{\frac{1}{B}-2}}{ABE \left(\left(\frac{\sqrt{s}}{E}\right)^{\frac{1}{B}} + 1\right)^{2+\frac{1}{A}}} \\ &\times \left[\left(\frac{1}{B} - 1\right) - \left(1 + \frac{1}{AB}\right) \left(\frac{\sqrt{s}}{E}\right)^{\frac{1}{B}} \right] \Bigg|_{\sqrt{s}_{peak}} \\ &= 0 \end{aligned} \quad (3.118)$$

$$\Rightarrow E = \sqrt{s}_{peak} \left(\frac{1+AB}{A(1-B)} \right)^B \quad (3.119)$$

For the purposes of this demonstration, the value for \sqrt{s} will be taken to be 100 GeV and the values of A and B will be 0.9 and 0.1 respectively. The effects on the shape of the smearing function due to changing the parameters will be considered in the following chapter.

To begin with the momentum picture of the integrand will be considered. The first two components of the loop momentum \vec{l}_2 can be used to form the basis of the slice to be considered. After making this choice it is useful to make a choice for \vec{l}_4 that has a non-zero value in the first component of the momentum and zero value for the other two components. This ensures that the singularities lie in the plane to be considered and the collinear singularity is on the first axis of the loop momentum. By choosing the size of \vec{l}_4 to be 50 GeV, taking a section of \vec{l}_2 that lies between -100 GeV and 100 GeV in both the components mentioned the integrands can be evaluated using a very wide top hat function as described previously. The pictures presented in figures 3.7, 3.8, 3.9 and 3.10 show both the positive and negative contributions of the integrand by ignoring the majority of points within the red parallelogram as they have very small values.

The most prominent feature of each of the integrands are the soft singularities that can be seen as peaks. As noted previously not all cuts have both of the soft singularities and this can be correlated to the pictures given. One can also clearly see the scattering singularities in A_{1a} and A_{4b} , and the collinear singularities in each of the integrands although they are not as prominent. By combining the integrands one can see that the scattering and collinear singularities disappear leaving only the two soft singularities. Even the strength of their singular nature has decreased as expected, however, they are

3.3. Visualisation of Singularity Cancellations

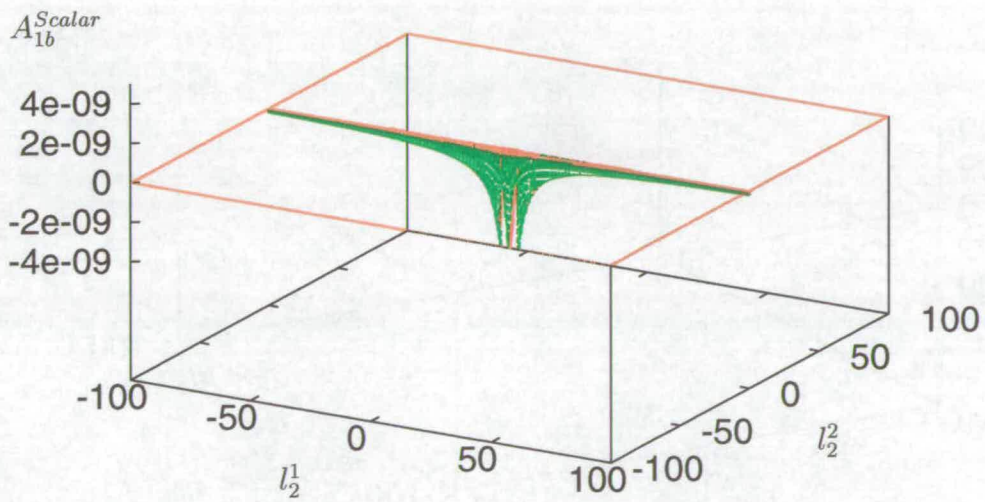
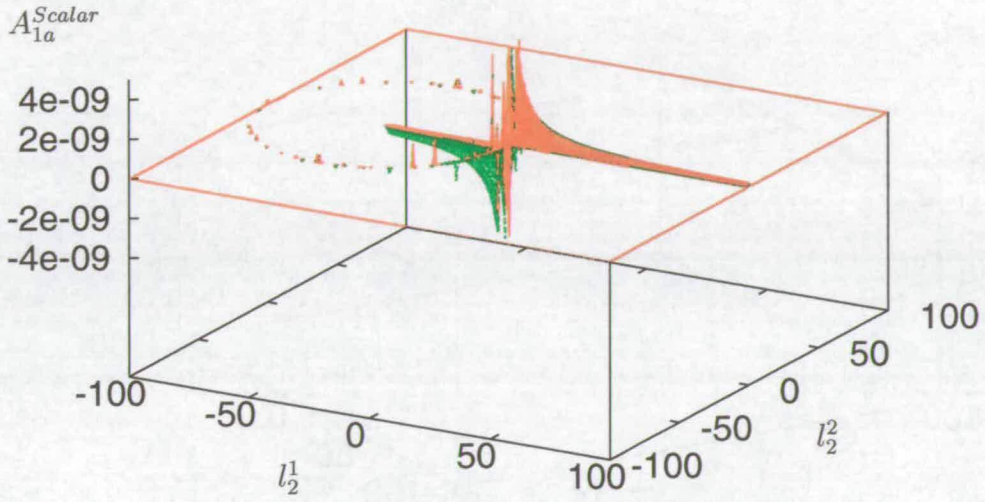


Figure 3.7.: Scalar integrands A_{1a} and A_{1b} evaluated in a cross section of momentum space.

3. Numerical Methods

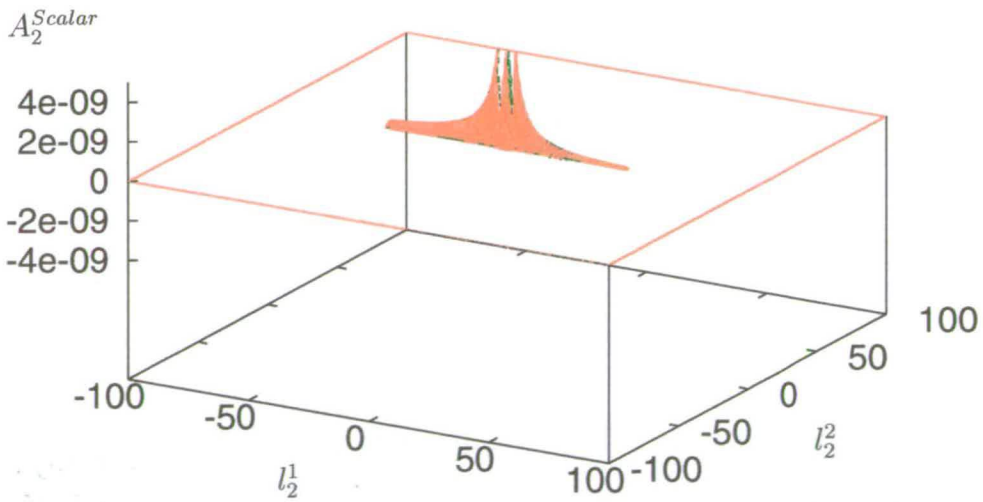
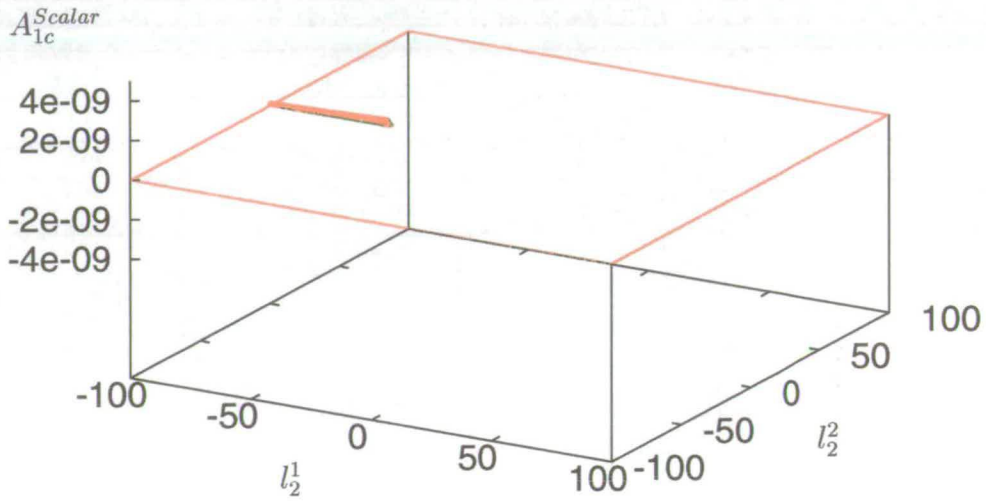


Figure 3.8.: Scalar integrands A_{1c} and A_2 evaluated in a cross section of momentum space.

3.3. Visualisation of Singularity Cancellations

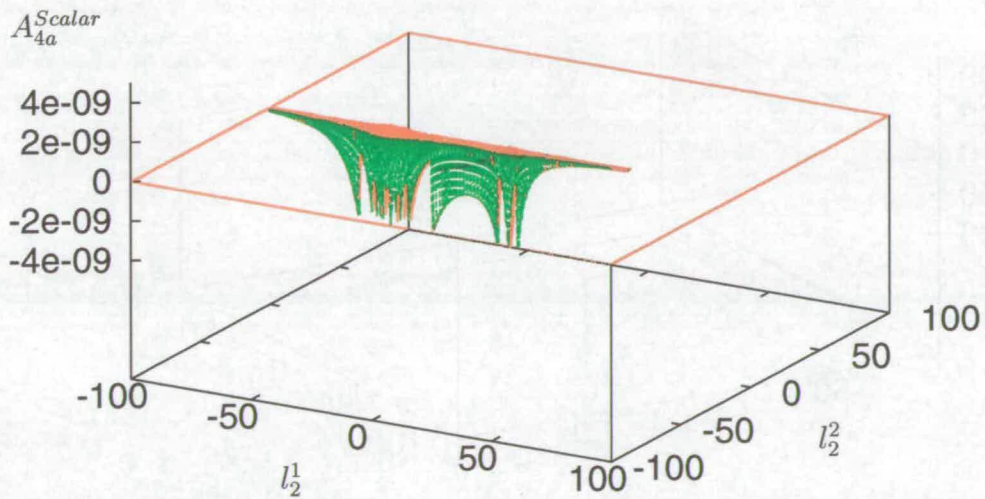
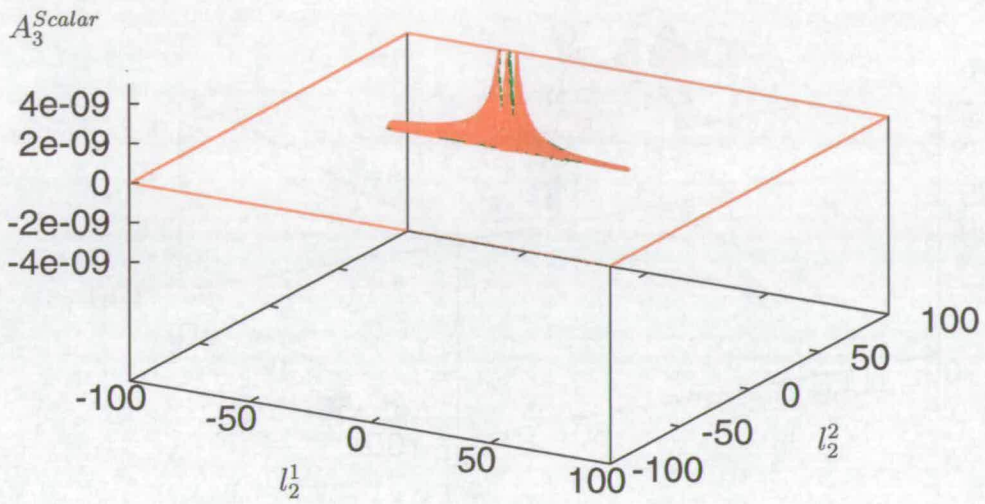


Figure 3.9.: Scalar integrands A_3 and A_{4a} evaluated in a cross section of momentum space.

3. Numerical Methods

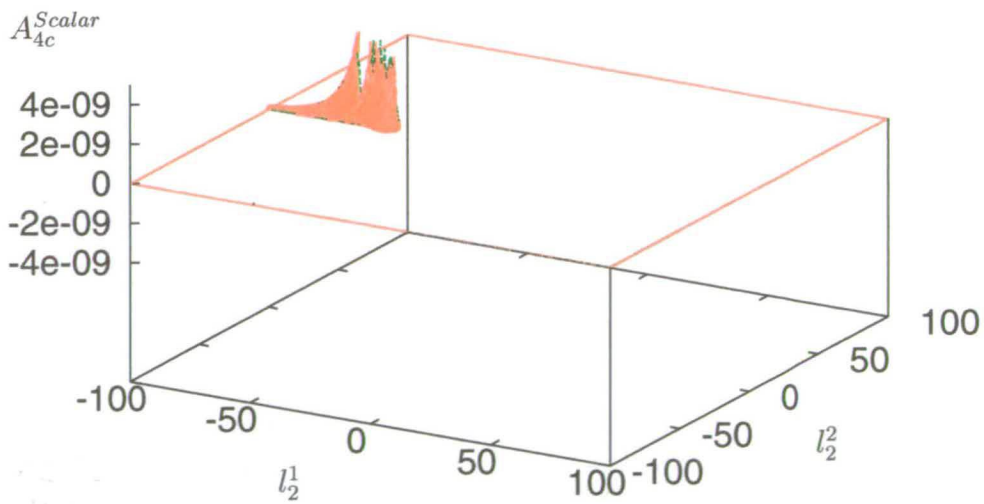
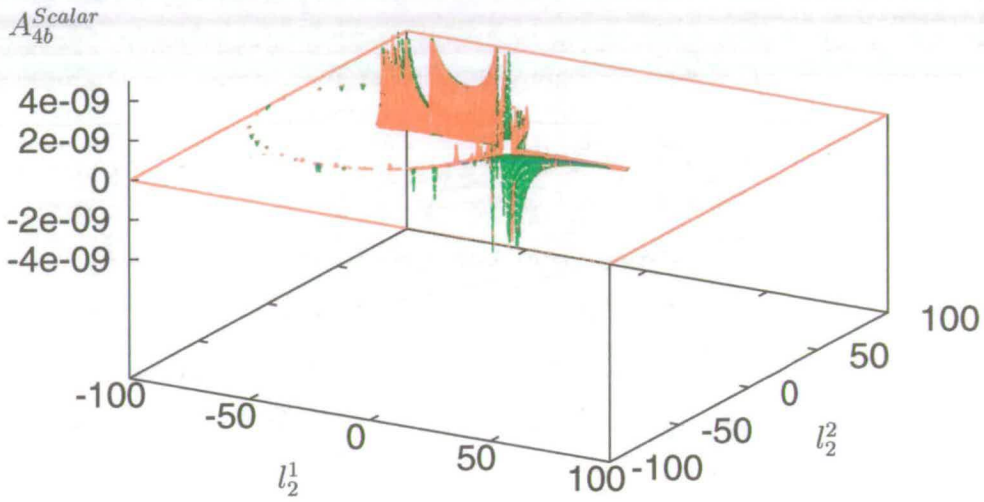


Figure 3.10.: Scalar integrands A_{4b} and A_{4c} evaluated in a cross section of momentum space.

still peaks that go to infinity as the coordinate transformation has not been performed yet (Fig. 3.11).

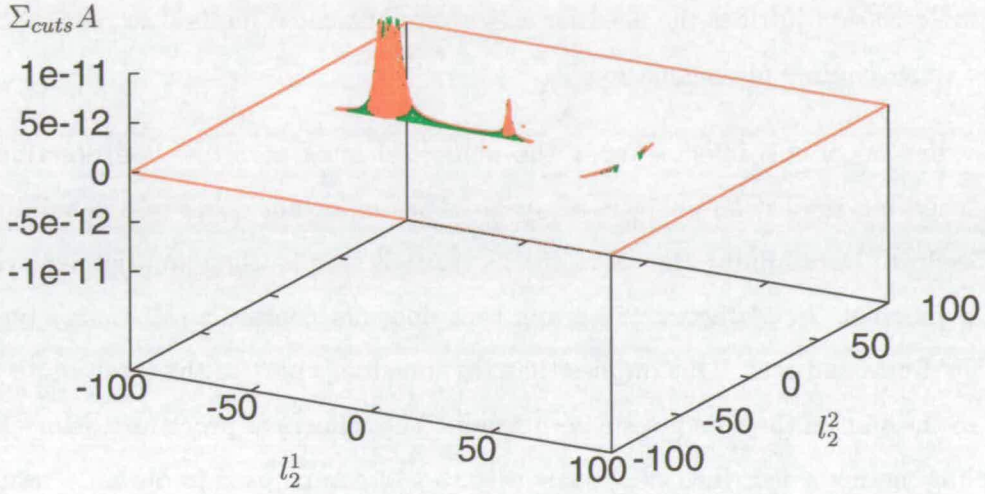


Figure 3.11.: Combined scalar integrands evaluated in a cross section of momentum space.

Creating an image of the transformed integral is a little different. As the integrand is now constrained in a six dimensional unit hypercube, a full two dimensional slice can be viewed. One of the momenta, \vec{l}_4 , can be specified again, this time it has to be specified using the appropriate transformed variables that will be denoted by \vec{z} . The other two transformations required to determine the loop momentum \vec{l}_2 that centre the coordinate systems on $|\vec{l}_2| = 0$ and $|\vec{l}_2 + \vec{l}_4| = 0$ will use the variables \vec{x} and \vec{y} respectively. In all three transformations the first component is related to the size of the momentum, the second component to the azimuthal angle and the third component to the polar angle. If \vec{l}_4 is chosen so that the soft pole lies on the axis of the third component of \vec{l}_2 , then it is sensible to choose x_1 and x_2 or y_1 and y_2 to represent the plane. This is because there is an axial symmetry about the collinear singularity, that can be seen in the previous images. An idea of how the integrand changes over the integration space can be gained by using a smooth smearing function peaked at 100 GeV and taking sections setting $z_2 = 0$ and $z_3 = 0$ for \vec{l}_4 , using a different value of z_1

3. Numerical Methods

for \vec{l}_4 in each slice (Fig. 3.12, 3.13, 3.14 and 3.15).

It can be deduced from the different sections that the integrand is finite over the integration domain as stated previously. Enhancements do occur where the soft singularities were previously positioned. The different sections also highlight how the integrand varies over the domain of integration. Although a simple Monte-Carlo method could be used, the variation justifies the need for a more sophisticated method to reduce the amount of time required for calculation.

The evaluation of this integral using the numerical integration method described and cross checking against an analytic result gives an important check on the validity of the procedure. Determining the value of this graph is simple using an argument via the optical theorem. In ϕ^3 theory any graph that does not contain a self energy type graph is UV finite and real. This implies that the imaginary part of the total graph is zero and so the sum of the cuts gives a zero result. The numerical procedure using the two sampling methods described previously (Sec. 3.1.2) can be used to obtain a result for I^{Scalar} . Method 1 needs a loop momentum coordinate transformation of,

$$\begin{aligned} |\vec{l}_2| &= E \left(\frac{1}{x_1} - 1 \right) \\ \cos \theta &= 2x_2 - 1 \\ \phi &= 2\pi x_3 \quad , \end{aligned} \tag{3.120}$$

while method 2 uses a loop momentum coordinate transformation of,

$$\begin{aligned} |\vec{l}_2 + \vec{l}_4| &= E \left(\frac{1}{y_1} - 1 \right) \\ \cos \theta &= 2y_2 - 1 \\ \phi &= 2\pi y_3 \quad . \end{aligned} \tag{3.121}$$

These transformations respectively produce Jacobians or inverse densities,

$$\begin{aligned} \frac{1}{\rho_1} &= 4\pi E |\vec{l}_2|^2 \left(\frac{|\vec{l}_2|}{E} + 1 \right)^2 \\ \frac{1}{\rho_2} &= 4\pi E |\vec{l}_2 + \vec{l}_4|^2 \left(\frac{|\vec{l}_2 + \vec{l}_4|}{E} + 1 \right)^2 \quad . \end{aligned} \tag{3.122}$$

The energy scale, E , in the above transformations is arbitrary and will be taken to be $|\vec{l}_4|$ to reduce the number of input parameters introduced.

3.3. Visualisation of Singularity Cancellations

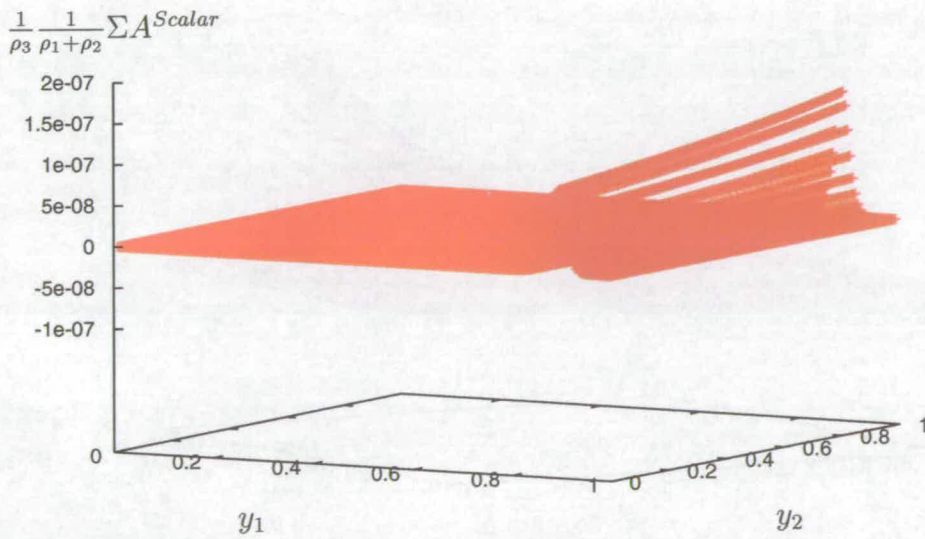
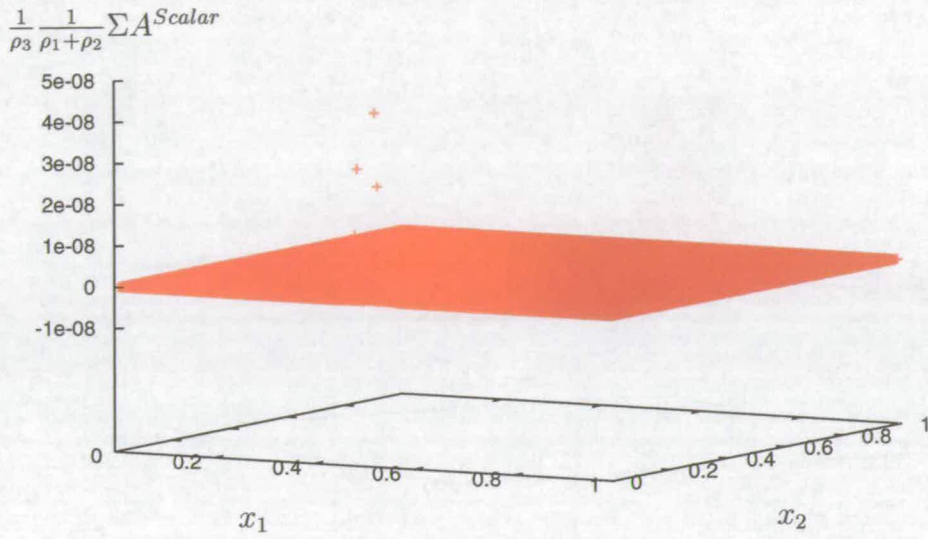


Figure 3.12.: Sections of the scalar integrand in the true sample space with $z_1 = 0.2$.

3. Numerical Methods

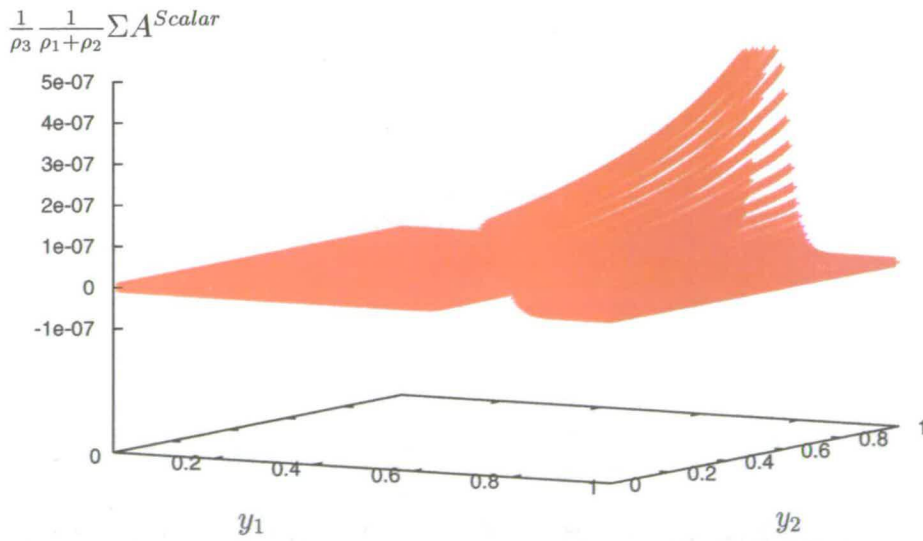
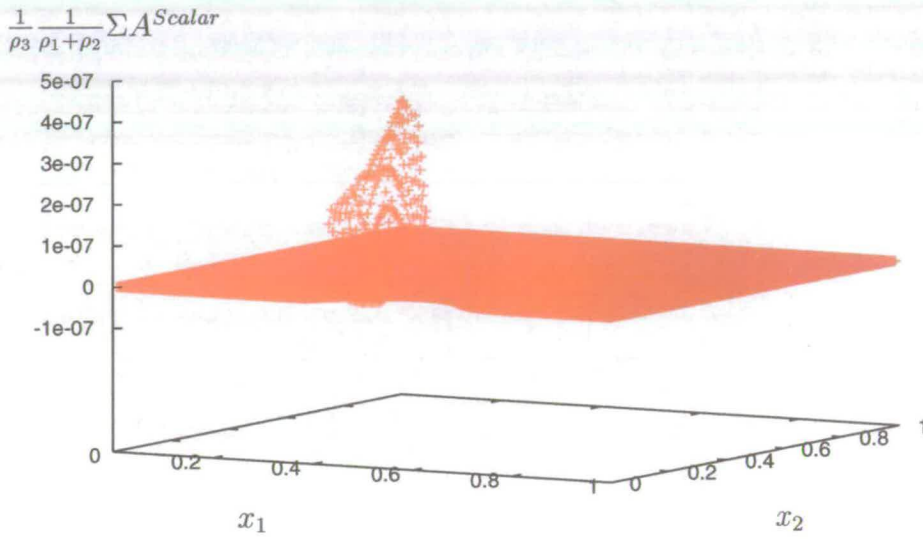


Figure 3.13.: Sections of the scalar integrand in the true sample space with $z_1 = 0.4$.

3.3. Visualisation of Singularity Cancellations

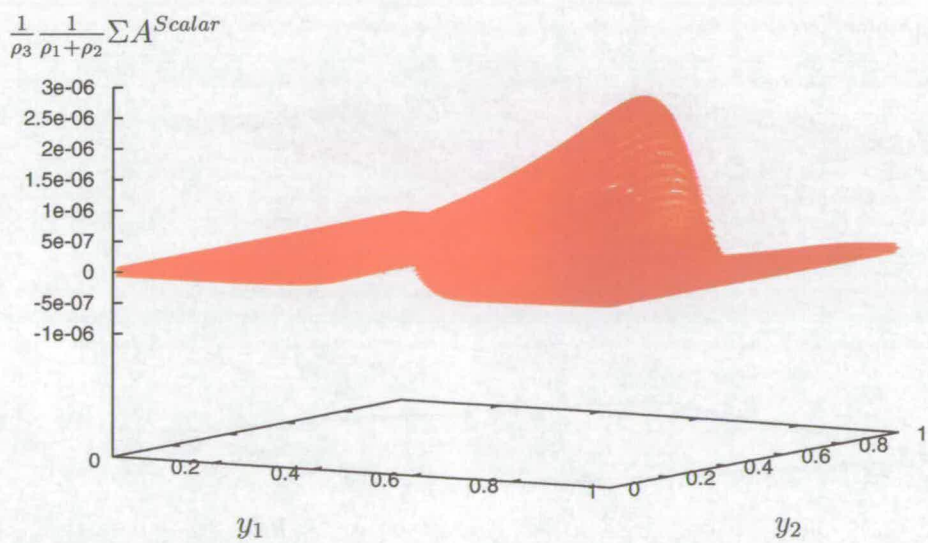
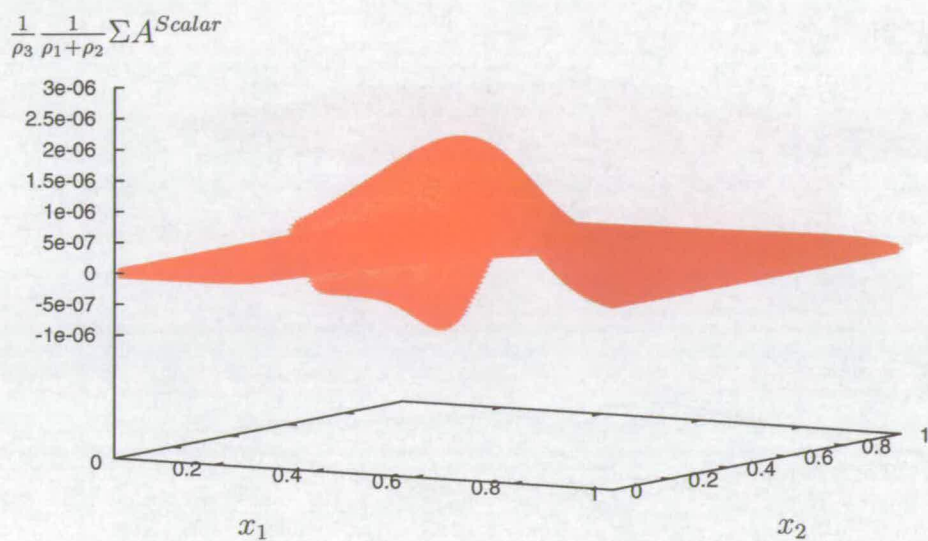


Figure 3.14.: Sections of the scalar integrand in the true sample space with $z_1 = 0.6$.

3. Numerical Methods

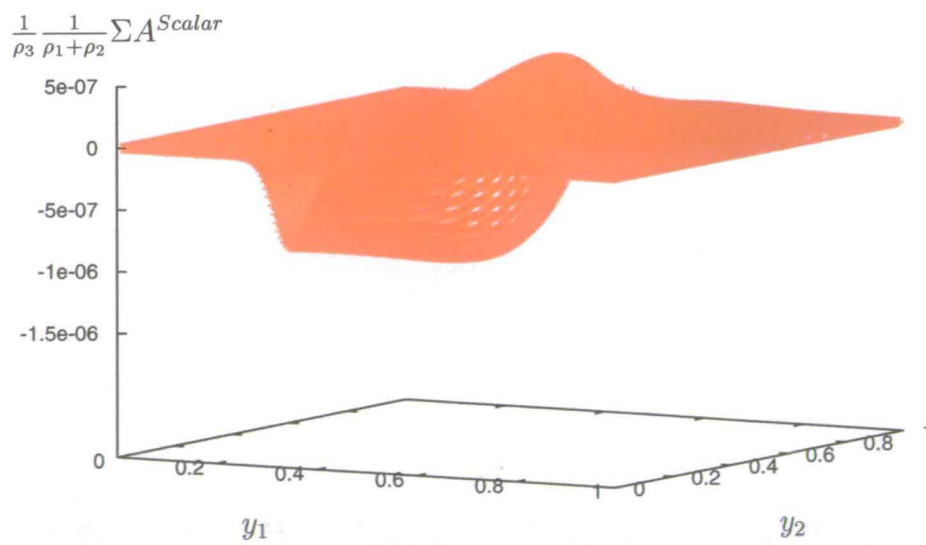
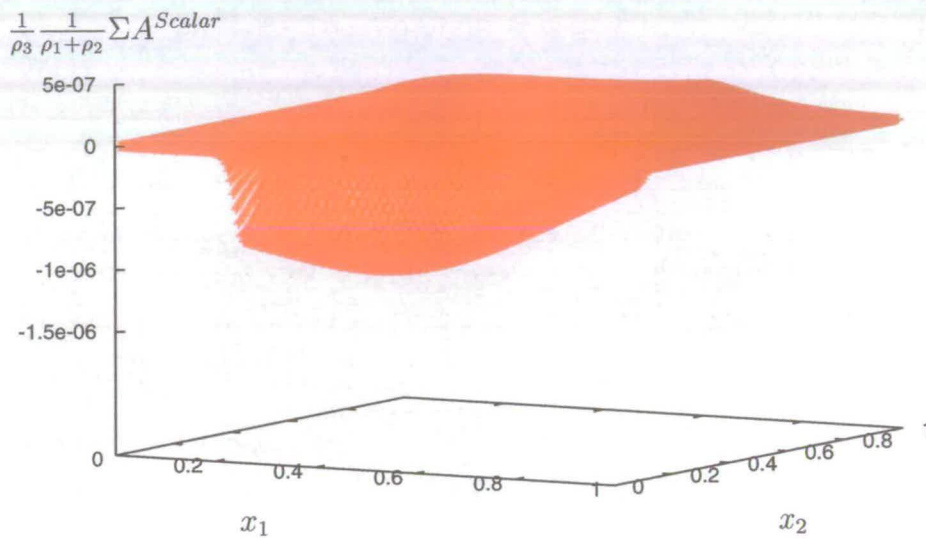


Figure 3.15.: Sections of the scalar integrand in the true sample space with $z_1 = 0.8$.

In each case a transformation for the external momentum needs to be performed,

$$\begin{aligned} |\vec{l}_4| &= E \left(\frac{1}{z_1} - 1 \right) \\ \cos \theta &= 2z_2 - 1 \\ \phi &= 2\pi z_3 \quad , \end{aligned} \quad (3.123)$$

which produces an inverse density,

$$\frac{1}{\rho_3} = 4\pi E |\vec{l}_4|^2 \left(\frac{|\vec{l}_4|}{E} + 1 \right)^2 \quad (3.124)$$

Again the value of E is arbitrary and an input parameter. This can be varied and does not affect the result analytically as it just scales the transformation. A value of 100 GeV was used in the numerical procedure. Combining these transformations produces two integrals. For method 1,

$$\int d\vec{z} \frac{1}{\rho_3} \int d\vec{x} \frac{1}{\rho_1 + \rho_2} \Sigma A^{Scalar} \quad (3.125)$$

and method 2,

$$\int d\vec{z} \frac{1}{\rho_3} \int d\vec{y} \frac{1}{\rho_1 + \rho_2} \Sigma A^{Scalar} \quad (3.126)$$

Combining the values obtained from both integrals gives the overall result (Tab. 3.2).

| | Method 1 | Error | Method 2 | Error |
|--------------|-------------------------|-------------------------|------------------------|------------------------|
| I^{Scalar} | -2.11×10^{-10} | 1.28×10^{-10} | 1.37×10^{-10} | 1.33×10^{-10} |
| | | Result | Error | |
| I^{Scalar} | | -1.84×10^{-11} | 9.25×10^{-11} | |

Table 3.2.: Results for the scalar vertex integral showing the numerical values and errors for the two sampling methods used.

This result provides good evidence for the soundness of the procedure.

3.4. Numerical Procedure for Dealing with UV Singularities

Numerical integrations are carried out using a whole number of dimensions. The analytic calculations carried out were performed in $4 - 2\epsilon$ dimensions so that they were UV

3. Numerical Methods

finite and could be renormalised simply by subtraction of appropriate terms according to the \overline{MS} scheme. In a numerical integration, this can be done by subtracting an integral that renders the result UV finite and produces the same result as the analytic procedure. This requires determining an integrand that depends on the same momenta as the UV divergent integral and integrates analytically in $4 - 2\epsilon$ dimensions to give the correct $\frac{1}{\epsilon}$ pole and accompanying finite parts.

As mentioned earlier the two UV divergent loop diagrams to be computed are the first order strong corrections to the quark-antiquark-photon vertex and the quark/antiquark self energies. Of these two corrections, the modification of the propagators require special care as they superficially belong to untruncated Feynman diagrams. In this section, the method of renormalisation will be shown using the massless fermion propagator as it is a fairly rich example and the vertex correction with massive or massless quarks will be left for the following chapter.

Through the evolution of Beowulf, the methods for evaluating the self energy correction have been adapted. The underlying principle for carrying out the calculation has remained the same. To begin evaluating the self energy correction, the spinor structure of the self energy correction has to be made explicit. Considering the self energy correction as a truncated diagram, it has one momentum integral and can only depend on the incoming momentum:

$$i\Sigma(q) = -g^2 \int \frac{d^n l}{(2\pi)^n} \frac{(2-n)(\not{q} - \not{l})}{((q-l)^2 + i\epsilon)(l^2 + i\epsilon)} \quad (3.127)$$

By inspection it is clear that the correction must be proportional to a single gamma matrix. After integration of the loop momenta it can only depend on the incoming quark momenta, q , so the self energy must be proportional to \not{q} (Eq. 3.128). This simplifies the expressions when the propagators on each side of the correction are included:

$$\Sigma(q) = \not{q} A(q^2) \quad (3.128)$$

$$\frac{\not{q}\Sigma(q)\not{q}}{q^2} = \not{q} A(q^2) \quad (3.129)$$

$$A(q^2) = ig^2 \int \frac{d^n l}{(2\pi)^n} \frac{(2-n)(q-l) \cdot q}{q^2((q-l)^2 + i\epsilon)(l^2 + i\epsilon)} \quad (3.130)$$

At this point there are different methods for manipulating the integral into a form that is suitable for numerical integration. The original procedure described by Soper

performed the energy integral by looking at the discontinuity of the integral [1]. An alternative method is to perform the energy integral directly by finding the poles of the propagator as considered previously. A piece of work by Krämer and Soper required a coordinate transformation to be performed on the resulting integral [4]. The variables used were elliptic coordinates based on the momentum within the integral:

$$\begin{aligned} A_+ &= \frac{1}{|\vec{q}|} (|\vec{l}| + |\vec{q} - \vec{l}|) & 1 < A_+ < \infty \\ A_- &= \frac{1}{|\vec{q}|} (|\vec{l}| - |\vec{q} - \vec{l}|) & -1 < A_- < \infty \\ \phi &= \phi & 0 < \phi < 2\pi. \end{aligned} \quad (3.131)$$

This procedure highlighted the fact that there were redundant terms within the original integrand as a term generated had a factor of A_- . The linear momentum term in the original integrand points to this fact as well. A simple way of avoiding the zero linear terms and the method adopted here will be through scalar decomposition as described by 't Hooft and Veltman [23]. Initially, momentum conservation has to be used on the numerator to generate terms akin to those in the denominator.

$$\begin{aligned} ((q-l) - q)^2 &= (q-l)^2 + q^2 - 2(q-l) \cdot q \\ \implies (q-l) \cdot q &= \frac{1}{2}(q^2 + (q-l)^2 - l^2) \end{aligned} \quad (3.132)$$

$$\begin{aligned} \implies A(q^2) &= ig^2 \int \frac{d^n l}{(2\pi)^n} \left(\frac{2-n}{2} \right) \left(\frac{1}{((q-l)^2 + i\epsilon)(l^2 + i\epsilon)} \right. \\ &\quad \left. + \frac{1}{q^2(l^2 + i\epsilon)} - \frac{1}{q^2((q-l)^2 + i\epsilon)} \right). \end{aligned} \quad (3.133)$$

At this point in the calculation, the last two terms of the integrand have a factor of q^2 in the denominator. This is a worrying factor especially when $q^2 = 0$ as the massless external quark is put on-shell. The previous methods removed this factor and this method does as well. To see this the last two terms are numerically equal to each other when the integration over the loop momentum is performed. This leads to a cancellation of these terms:

$$A(q^2) = ig^2 \int \frac{d^n l}{(2\pi)^n} \left(\frac{2-n}{2} \right) \left(\frac{1}{((q-l)^2 + i\epsilon)(l^2 + i\epsilon)} \right) \quad (3.134)$$

$$= g^2 \int \frac{d^{n-1} \vec{l}}{(2\pi)^{n-1}} \left(\frac{2-n}{2} \right) \left(\frac{|\vec{l}| + |\vec{q} - \vec{l}|}{2|\vec{l}||\vec{q} - \vec{l}|((q^0)^2 - (|\vec{q} - \vec{l}| + |\vec{l}|)^2)} \right) \quad (3.135)$$

From this point it is quite simple to find the counter term for the self energy. The UV singularity occurs due to high loop momentum, thus the form of the numerical counter

3. Numerical Methods

term can be found by ignoring q in equation (3.134) and introducing a renormalisation mass μ in the denominator to prevent a soft singularity. To gain the correct finite part as well, a term proportional to μ^2 has to be introduced:

$$\begin{aligned} A_{Counter}(q^2) &= -ig^2 \int \frac{d^n l}{(2\pi)^n} \left(\frac{2-n}{2} \right) \left(\frac{1}{(l^2 - \mu^2)^2} + \frac{S\mu^2}{(l^2 - \mu^2)^3} \right) \\ &= -\frac{g^2}{(4\pi)^{\frac{n}{2}}} (\mu^2)^{\frac{n}{2}-2} \left(\Gamma(\epsilon) - \Gamma(1+\epsilon) - \frac{S}{2} \Gamma(1+\epsilon) \right) \quad . \quad (3.136) \end{aligned}$$

To remove the finite part the constant S has to be -2 . The energy integral of the counter term can now be performed, however there are now multiple poles in the integral and so the residue must be found using an extension to the method used before and given by standard complex analysis:

$$i \int \frac{dl_0}{2\pi} \frac{f(l^0)}{(l^2 - m^2)^N} = \left[\frac{1}{(N-1)!} \left(\frac{\partial}{\partial l^0} \right)^{N-1} \frac{f(l^0)}{(l^0 + (|\vec{l}|^2 + m^2)^{\frac{1}{2}})^N} \right]_{l^0=(|\vec{l}|^2+m^2)^{\frac{1}{2}}} \quad (3.137)$$

$$\begin{aligned} \Rightarrow A_{Counter}(q^2) &= -g^2 \int \frac{d^{n-1} \vec{l}}{(2\pi)^{n-1}} \\ &\quad \times \left(\frac{2-n}{2} \right) \left(-\frac{1}{4(|\vec{l}|^2 + \mu^2)^{\frac{3}{2}}} - \frac{3}{8(|\vec{l}|^2 + \mu^2)^{\frac{5}{2}}} \right) \quad . \quad (3.138) \end{aligned}$$

By adding $A_{Counter}(q^2)$ to $A(q^2)$ the self energy is finite, renormalised in the \overline{MS} scheme and can be used in the numerical integration by setting $n = 4$.

3.5. Treatment of Scattering Singularities

The case examined has been quite special as the scattering singularities cancel. This is because all possible cuts are taken of the diagram and there were matching scattering singularities with the same momenta flowing through the loops. In the current versions of Beowulf only a subset of the possible cuts for the three loop strong correction of the photon propagator are considered and they do not contain all the required matching singularities. The subset contains all possible cuts involving three or four particles in the final state. While this is sufficient for cancellation of soft and collinear singularities in the three particle limit, it is not suitable for cancellation of soft or collinear singularities that occur in the two particle limit or certain scattering singularities. To accommodate these problems limits are placed on the choice of momenta so that the two particle limit

isn't reached and a contour deformation of the loop momentum involved in producing the scattering singularity is performed. This section will describe the basic aspects of the contour deformation procedure as although this is not of direct concern with this project it will be needed to discuss modifying Beowulf.

Contour deformation is an idea generated from the $i\epsilon$ prescription given by the Feynman rules. By keeping this complex component of the factor in the denominator that contains the scattering singularity, the integrand doesn't become singular. Due to the symmetric nature of the cutting, scattering singularities of the same type are found with both a $+i\epsilon$ and a $-i\epsilon$ factor. This ensures that any finite complex additions due to the inclusion of $i\epsilon$ cancel and the result is real. The procedure separates into three parts; finding the shape of the scattering singularity, choosing the direction of the deformation and determining the size of the deformation.

For a loop momentum, l , and an arbitrary momentum Q representing a combination of momenta the scattering singularity can be written in a generic form:

$$(l - Q)^2 + i\epsilon \quad (3.139)$$

$$\text{or} \quad (l - Q)^2 - i\epsilon \quad (3.140)$$

Using the conditions $l^2 = 0$, $(l - Q)^2 = 0$, $Q^0 > |\vec{Q}|$ and ignoring the $i\epsilon$ factor, the shape of the scattering singularity can be determined,

$$(l^0 - Q^0)^2 = |\vec{l} - \vec{Q}|^2 \quad (3.141)$$

$$(|\vec{l}| - Q^0)^2 = |\vec{l} - \vec{Q}|^2 \quad (3.142)$$

$$\implies |\vec{l}| + |\vec{l} - \vec{Q}| = Q^0 \quad (3.143)$$

This gives the familiar equation of an ellipse with foci at $\vec{l} = 0$ and $\vec{l} = \vec{Q}$. The integrand is enhanced on this surface and so the Beowulf program chooses the loop momentum using an elliptical coordinate system so that the density of points can be increased in this region [3]. A simple method for finding the transformation to an elliptical coordinate system is to use a two part procedure. Consider first that \vec{Q} is along the z -axis of the loop momentum. The loop momenta can be decomposed into l_z , l_T and ϕ which are components of the loop momentum in the direction of \vec{Q} , transverse to \vec{Q} and the azimuthal angle about the z -axis. This constitutes the standard cylindrical

3. Numerical Methods

polar coordinate system:

$$\vec{l} = l_T \cos \phi \hat{i} + l_T \sin \phi \hat{j} + l_z \hat{k} \quad (3.144)$$

$$d^3\vec{l} = dl_T dl_z d\phi l_T \quad (3.145)$$

New variables A_+ and A_- representing elliptic and orthogonal hyperbolic surfaces can be introduced and written in terms of l_T , l_z and $|\vec{Q}|$:

$$|\vec{l}| = (l_z^2 + l_T^2)^{\frac{1}{2}} \quad (3.146)$$

$$|\vec{l} - \vec{Q}| = ((l_z - |\vec{Q}|)^2 + l_T^2)^{\frac{1}{2}} \quad (3.147)$$

$$A_+ = \frac{1}{|\vec{Q}|} (|\vec{l}| + |\vec{l} - \vec{Q}|) \quad (3.148)$$

$$A_- = \frac{1}{|\vec{Q}|} (|\vec{l}| - |\vec{l} - \vec{Q}|) \quad (3.149)$$

$$l_T = \left(\frac{|\vec{Q}|}{2} \right) (A_+^2 - 1)^{\frac{1}{2}} (1 - A_-^2)^{\frac{1}{2}} \quad (3.150)$$

$$l_z = \left(\frac{|\vec{Q}|}{2} \right) (A_+ A_- + 1) \quad (3.151)$$

$$d^3\vec{l} = dA_+ dA_- d\phi \left(\frac{Q}{2} \right)^3 (A_+^2 - A_-^2) \quad (3.152)$$

By examining the limits of loop momentum, the limits $1 < A_+ < \infty$ and $-1 < A_- < 1$ can be determined. The task of choosing a high density of points on the elliptic surface corresponds to finding a mapping from $0 < x_1 < 1$ to $1 < A_+ < \infty$ that deforms the region about $A_+ = Q^0$ so that it is sampled frequently. A suitable transformation is of the type for selecting the radial component of a loop momentum, but with the constant adjusted so that the maximum density of points occur on the surface of the ellipse.

This is a simplified example that illustrates the procedure. In the real Beowulf program, more complex transformations are used to smooth the integrand further especially when scattering singularities are close to each other or soft singularity cancellations occur on the scattering surface. The exact choice of transformation is somewhat arbitrary yet tailored by hand to produce an efficient integration procedure

Now that the shape of the contour has been established and a route for creating a high density of points on the scattering surface determined, a method for introducing

the $i\epsilon$ factor must be found. The aim is to integrate along a contour for a complex loop momentum, l_C , that can be used instead of the original loop momentum l and includes the effects of the $i\epsilon$ prescription:

$$(l_C - Q)^2 \approx (l - Q)^2 + i\epsilon \quad (3.153)$$

$$\text{or } (l_C - Q)^2 \approx (l - Q)^2 - i\epsilon \quad (3.154)$$

To obtain this relation, a suitable form for \vec{l}_C must be postulated:

$$\vec{l}_C = \vec{l} - iC\vec{v} \quad (3.155)$$

The variable C is taken to be small compared to the magnitude of the loop momentum. This can now be introduced into equation (3.154) to determine the form of ϵ .

$$\begin{aligned} |\vec{l}_C| &= |\vec{l} - iC\vec{v}| \\ &\approx |\vec{l}| - iC \frac{\vec{v} \cdot \vec{l}}{|\vec{l}|} \end{aligned} \quad (3.156)$$

$$\begin{aligned} |\vec{l}_C - \vec{Q}| &= |\vec{l} - iC\vec{v} - \vec{Q}| \\ &\approx |\vec{l} - \vec{Q}| - iC \frac{\vec{v} \cdot (\vec{l} - \vec{Q})}{|\vec{l} - \vec{Q}|} \end{aligned} \quad (3.157)$$

$$\begin{aligned} \Rightarrow (l_C - Q)^2 &\approx (l - Q)^2 + 2iC\vec{v} \cdot \left(\frac{\vec{l}}{|\vec{l}|} + \frac{\vec{l} - \vec{Q}}{|\vec{l} - \vec{Q}|} \right) \\ &= (l - Q)^2 + 2iC\vec{v} \cdot \vec{A} \end{aligned} \quad (3.158)$$

Here \vec{A} is actually the normal to the scattering surface. To ensure that the size of the deformation is not controlled by \vec{v} , the vector is taken to be in the direction of \vec{A} . Controlling the size of the deformation is responsibility of C .

Altering the size of C is important to give sensible results. The contour deformation needs to be switched off at points where soft and collinear cancellations occur. If the external momenta are to be used in any physical calculations then no imaginary parts should enter the final state particles. The size of the deformation should also be small and disappear as the loop momentum is much bigger than the size of the scattering singularity. Each of these conditions can be met by a separate function and depending on the complexity of the singularity structure, several combinations may be required. As C is taken to be a function of the loop momentum, it also has an effect on the Jacobian of the transformation.

4. Numerical Calculations of Observables for Quark-Antiquark Production from Electron-Positron Annihilation up to $\mathcal{O}(\alpha_s)$

The previous two chapters have been concerned with setting up the procedure for numerically integrating the $\mathcal{O}(\alpha_s)$ correction for the process $e^+e^- \rightarrow q\bar{q}$ with massive quarks. Working towards this has shown that results can be obtained analytically and the systematics of the numerical integration procedure based on the work by Soper has been demonstrated using a scalar toy model. Now the final step of applying the procedure will be explained, results confirming the procedure given and additional information for extending the procedure discussed.

4.1. Integrands with Massive Fermions

Most of the ground work for determining the integrands has been developed in the analytic framework chapter. As has been seen, there are two graph topologies to be considered, one with a vertex correction and the other with a self energy correction, their respective cuts and renormalisation counter terms. To begin adapting them for use within the numerical integration scheme, the energy integrals must be performed akin to the method used in the previous chapter, however, remembering there is now a mass. This modifies the poles of the propagators and changes the on-shell delta

4. Numerical Calculations

functions, however, the principles of the integration remain the same:

$$\int \frac{dl^0}{(2\pi)} f(l^0) (2\pi) \delta(l^2 - m^2) \theta(l^0) = \frac{f((|\vec{l}|^2 + m^2)^{\frac{1}{2}})}{2(|\vec{l}|^2 + m^2)^{\frac{1}{2}}}$$

$$i \int \frac{dl^0}{2\pi} \frac{f(l^0)}{(l^2 - m^2)} = \frac{f((|\vec{l}|^2 + m^2)^{\frac{1}{2}})}{2(|\vec{l}|^2 + m^2)^{\frac{1}{2}}} \quad (4.1)$$

As shown above, the energy integration also affects the numerator of each topology. Although the numerator for a particular topology of graph is the same for each cut when written in terms of four momenta, the specific cut determines the energies of the four momenta within the numerator. When performing the energy integrals for the renormalisation terms, the above integrals are not quite sufficient. Due to the construction of these terms, multiple poles arise and so the residue must be found using standard complex analysis:

$$i \int dl^0 \frac{f(l^0)}{(l^2 - m^2)^N} = \left[\frac{1}{(N-1)} \left(\frac{\partial}{\partial l^0} \right)^{N-1} \frac{f(l^0)}{(l^0 + (|\vec{l}|^2 + m^2)^{\frac{1}{2}})^N} \right]_{l^0 = (|\vec{l}|^2 + m^2)^{\frac{1}{2}}} \quad (4.2)$$

These methods can now be utilised to obtain the required integrands.

4.1.1. Vertex Correction

As the vertex correction graph in the fermion case (Fig. 4.1) is topologically the same

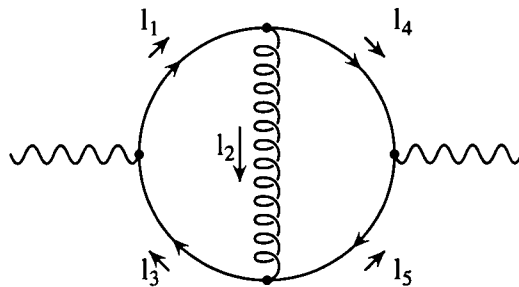
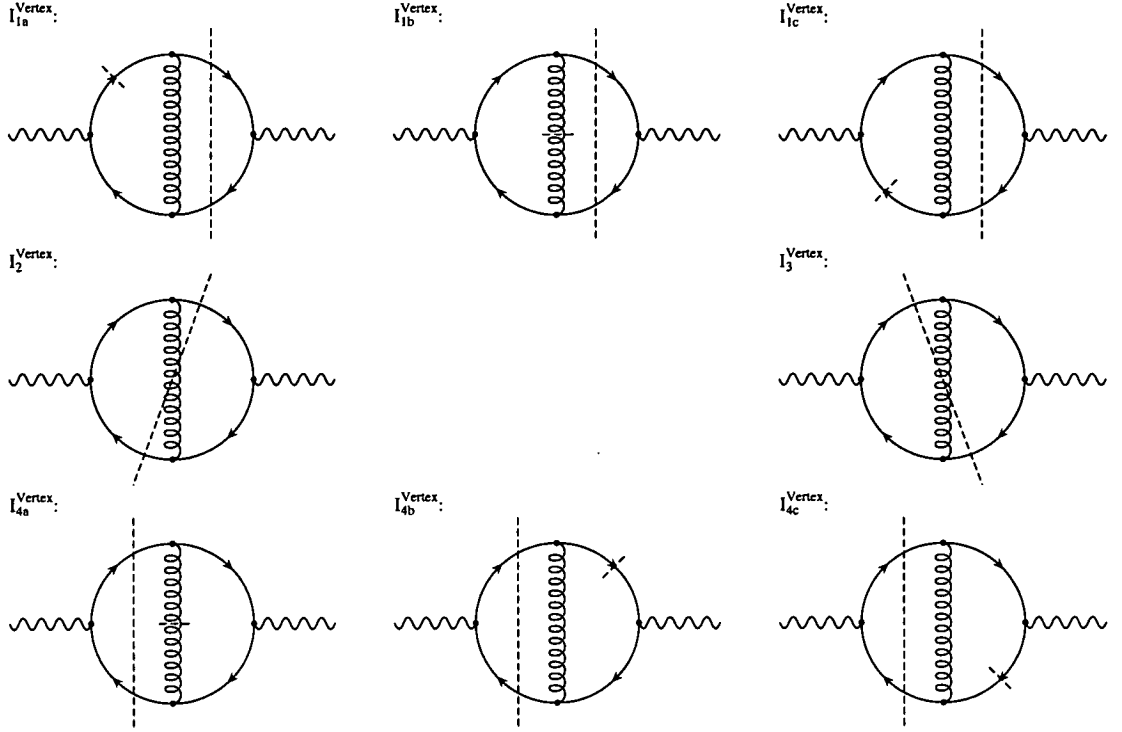


Figure 4.1.: Two loop $\mathcal{O}(\alpha_s)$ correction of the photon propagator containing the vertex correction.

as the scalar case, all momenta and equivalent cuts will be labelled in the same way as before. It is not surprising that after integrating out the energies the terms generated (Fig. 4.2) pictorially look very similar to the scalar case (Fig. 3.2 and 3.3) . For


 Figure 4.2.: Two and three particle cuts of the $\mathcal{O}(\alpha_s)$ correction to the photon propagator.

brevity, the numerator, N^{Vertex} , (Eq. 4.4) and momentum relations (Eq. 4.5) will be given once. Each cut is also accompanied by the momentum integrals

$$\int \frac{d^3\vec{l}_2}{(2\pi)^3} \int \frac{d^3\vec{l}_4}{(2\pi)^3} . \quad (4.3)$$

The energy relations and denominator, D^{Vertex} , will be given for each cut:

$$\begin{aligned} N^{Vertex} = & g^2 e^2 Q^2 \left(\frac{N_c^2 - 1}{2} \right) (-32 l_3 \cdot l_4 l_1 \cdot l_5 \\ & + 16 m^2 (l_3 \cdot l_5 + l_1 \cdot l_5 - l_1 \cdot l_3 + l_4 \cdot l_5 - l_3 \cdot l_4 - l_1 \cdot l_4) \\ & + 32 m^4) \end{aligned} \quad (4.4)$$

$$\vec{l}_1 = \vec{l}_2 + \vec{l}_4$$

$$\vec{l}_3 = \vec{l}_2 + \vec{l}_4$$

$$\vec{l}_5 = -\vec{l}_4 \quad (4.5)$$

4. Numerical Calculations

$$\begin{aligned}
l_1^0 &= (|\vec{l}_2 + \vec{l}_4|^2 + m^2)^{\frac{1}{2}} \\
l_2^0 &= (|\vec{l}_2 + \vec{l}_4|^2 + m^2)^{\frac{1}{2}} - (|\vec{l}_4|^2 + m^2)^{\frac{1}{2}} \\
l_3^0 &= (|\vec{l}_2 + \vec{l}_4|^2 + m^2)^{\frac{1}{2}} - (|\vec{l}_4|^2 + m^2)^{\frac{1}{2}} - (|\vec{l}_4|^2 + m^2)^{\frac{1}{2}} \\
l_4^0 &= (|\vec{l}_4|^2 + m^2)^{\frac{1}{2}} \\
l_5^0 &= (|\vec{l}_4|^2 + m^2)^{\frac{1}{2}} \\
D_{1a}^{Vertex} &= 8|l_1^0|l_2^2(l_3^2 - m^2)|l_4^0||l_5^0| \tag{4.6}
\end{aligned}$$

$$\begin{aligned}
l_1^0 &= |\vec{l}_2| + (|\vec{l}_4|^2 + m^2)^{\frac{1}{2}} \\
l_2^0 &= |\vec{l}_2| \\
l_3^0 &= |\vec{l}_2| - (|\vec{l}_4|^2 + m^2)^{\frac{1}{2}} \\
l_4^0 &= (|\vec{l}_4|^2 + m^2)^{\frac{1}{2}} \\
l_5^0 &= (|\vec{l}_4|^2 + m^2)^{\frac{1}{2}} \\
D_{1b}^{Vertex} &= 8(l_1^2 - m^2)|l_2^0|(l_3^2 - m^2)|l_4^0||l_5^0| \tag{4.7}
\end{aligned}$$

$$\begin{aligned}
l_1^0 &= (|\vec{l}_2 + \vec{l}_4|^2 + m^2)^{\frac{1}{2}} + 2(|\vec{l}_4|^2 + m^2)^{\frac{1}{2}} \\
l_2^0 &= (|\vec{l}_2 + \vec{l}_4|^2 + m^2)^{\frac{1}{2}} + (|\vec{l}_4|^2 + m^2)^{\frac{1}{2}} \\
l_3^0 &= (|\vec{l}_2 + \vec{l}_4|^2 + m^2)^{\frac{1}{2}} \\
l_4^0 &= (|\vec{l}_4|^2 + m^2)^{\frac{1}{2}} \\
l_5^0 &= (|\vec{l}_4|^2 + m^2)^{\frac{1}{2}} \\
D_{1c}^{Vertex} &= 8(l_1^2 - m^2)l_2^2|l_3^0||l_4^0||l_5^0| \tag{4.8}
\end{aligned}$$

$$\begin{aligned}
l_1^0 &= (|\vec{l}_2 + \vec{l}_4|^2 + m^2)^{\frac{1}{2}} \\
l_2^0 &= -|\vec{l}_2| \\
l_3^0 &= -|\vec{l}_2| - (|\vec{l}_4|^2 + m^2)^{\frac{1}{2}} \\
l_4^0 &= (|\vec{l}_2 + \vec{l}_4|^2 + m^2)^{\frac{1}{2}} + |\vec{l}_2| \\
l_5^0 &= (|\vec{l}_4|^2 + m^2)^{\frac{1}{2}} \\
D_2^{Vertex} &= 8|l_1^0||l_2^0|(l_3^2 - m^2)(l_4^2 - m^2)|l_5^0| \tag{4.9}
\end{aligned}$$

4.1. Integrands with Massive Fermions

$$\begin{aligned}
l_1^0 &= |\vec{l}_2| + (|\vec{l}_4|^2 + m^2)^{\frac{1}{2}} \\
l_2^0 &= |\vec{l}_2| \\
l_3^0 &= -(|\vec{l}_2 + \vec{l}_4|^2 + m^2)^{\frac{1}{2}} \\
l_4^0 &= (|\vec{l}_4|^2 + m^2)^{\frac{1}{2}} \\
l_5^0 &= |\vec{l}_2| + (|\vec{l}_2 + \vec{l}_4|^2 + m^2)^{\frac{1}{2}} \\
D_3^{Vertex} &= 8(l_1^2 - m^2)|l_2^0||l_3^0||l_4^0|(l_5^2 - m^2)
\end{aligned} \tag{4.10}$$

$$\begin{aligned}
l_1^0 &= (|\vec{l}_2 + \vec{l}_4|^2 + m^2)^{\frac{1}{2}} \\
l_2^0 &= -|\vec{l}_2| \\
l_3^0 &= -(|\vec{l}_2 + \vec{l}_4|^2 + m^2)^{\frac{1}{2}} \\
l_4^0 &= (|\vec{l}_2 + \vec{l}_4|^2 + m^2)^{\frac{1}{2}} + |\vec{l}_2| \\
l_5^0 &= (|\vec{l}_2 + \vec{l}_4|^2 + m^2)^{\frac{1}{2}} - |\vec{l}_2| \\
D_{4a}^{Vertex} &= 8|l_1^0||l_2^0||l_3^0|(l_4^2 - m^2)(l_5^2 - m^2)
\end{aligned} \tag{4.11}$$

$$\begin{aligned}
l_1^0 &= (|\vec{l}_2 + \vec{l}_4|^2 + m^2)^{\frac{1}{2}} \\
l_2^0 &= (|\vec{l}_2 + \vec{l}_4|^2 + m^2)^{\frac{1}{2}} - (|\vec{l}_4|^2 + m^2)^{\frac{1}{2}} \\
l_3^0 &= -(|\vec{l}_2 + \vec{l}_4|^2 + m^2)^{\frac{1}{2}} \\
l_4^0 &= (|\vec{l}_2 + \vec{l}_4|^2 + m^2)^{\frac{1}{2}} \\
l_5^0 &= 2(|\vec{l}_2 + \vec{l}_4|^2 + m^2)^{\frac{1}{2}} - (|\vec{l}_4|^2 + m^2)^{\frac{1}{2}} \\
D_{4b}^{Vertex} &= 8|l_1^0|l_2^2|l_3^0||l_4^0|(l_5^2 - m^2)
\end{aligned} \tag{4.12}$$

$$\begin{aligned}
l_1^0 &= (|\vec{l}_2 + \vec{l}_4|^2 + m^2)^{\frac{1}{2}} \\
l_2^0 &= -(|\vec{l}_2 + \vec{l}_4|^2 + m^2)^{\frac{1}{2}} - (|\vec{l}_4|^2 + m^2)^{\frac{1}{2}} \\
l_3^0 &= -(|\vec{l}_2 + \vec{l}_4|^2 + m^2)^{\frac{1}{2}} \\
l_4^0 &= 2(|\vec{l}_2 + \vec{l}_4|^2 + m^2)^{\frac{1}{2}} + (|\vec{l}_4|^2 + m^2)^{\frac{1}{2}} \\
l_5^0 &= -(|\vec{l}_4|^2 + m^2)^{\frac{1}{2}} \\
D_{4c}^{Vertex} &= 8|l_1^0|l_2^2|l_3^0|(l_4^2 - m^2)|l_5^0|
\end{aligned} \tag{4.13}$$

As can be seen, the massless denominators are easily modified by replacing $|\vec{l}|$ with $(|\vec{l}|^2 + m^2)^{\frac{1}{2}}$ for the massive fermions.

4. Numerical Calculations

Renormalisation of the vertex graph

From the form of the vertex graph, a UV counter term must be determined so that it has the same UV properties. To do this, the part of the integrand corresponding to the vertex is extracted and the limit of large loop momentum is taken. As described in the analytic framework chapter, power counting of the momentum leads to the renormalisation counter term being independent of the mass. Care must be taken when considering what to take as the loop momentum. The loop momentum of the left hand side vertex is easily found if momentum conservation is used to write the momenta in terms of l_2 , l_4 and l_5 :

$$\begin{aligned}
 V^\rho &= -g^2 e Q T^a T^a \int \frac{d^n l_2}{(2\pi)^n} \frac{\gamma^\mu (\not{l}_1 + m) \gamma^\rho (\not{l}_3 + m) \gamma_\mu}{(l_1^2 - m^2 + i\epsilon)(l_3^2 - m^2 + i\epsilon)(l_2^2 + i\epsilon)} \\
 &= -g^2 e Q T^a T^a \int \frac{d^n l_2}{(2\pi)^n} \frac{\gamma^\mu (\not{l}_2 + \not{l}_4 + m) \gamma^\rho (\not{l}_2 - \not{l}_5 + m) \gamma_\mu}{((l_2 + l_4)^2 - m^2 + i\epsilon)((l_2 - l_5)^2 - m^2 + i\epsilon)(l_2^2 + i\epsilon)} .
 \end{aligned} \tag{4.14}$$

By doing this, it is clear to see that l_2 is the only momentum flowing round the left hand vertex and the external legs of this loop are independent of it. Looking at the highest order of the loop momentum in the numerator and performing some algebra one can obtain an integral corresponding to the UV divergent part,

$$V^\rho \rightarrow -g^2 e Q T^a T^a \int \frac{d^n l_2}{(2\pi)^n} \frac{(2-n)(2\not{l}_2 l_2^\rho - l_2^2)}{((l_2 + l_4)^2 - m^2 + i\epsilon)((l_2 - l_5)^2 - m^2 + i\epsilon)(l_2^2 + i\epsilon)} . \tag{4.15}$$

To obtain the counter term required in the numerical integration, the UV limit of the denominator is taken, further simplifying the integrand. This would lead to a possible soft singularity dependent on the loop momentum, however a renormalisation scale, μ , can be introduced in the denominator taking the form of a mass proportional to the centre of mass energy thus preventing the soft singularity:

$$V^\rho \rightarrow -g^2 e Q T^a T^a \int \frac{d^n l_2}{(2\pi)^n} \frac{(2-n)(2\not{l}_2 l_2^\rho - l_2^2)}{(l_2^2 - \mu^2 + i\epsilon)^3} . \tag{4.16}$$

Calculating the analytic value of the above counter term in the \overline{MS} scheme gives a result that contains the required counter term along with an additional finite piece. This can be dealt with by subtracting a term proportional to μ^2 that produces the

correct counter term:

$$V_{Counter}^\rho \rightarrow g^2 e Q T^a T^a \int \frac{d^n l_2}{(2\pi)^n} \frac{(2-n)(2\sqrt{2}l_2^\rho - l_2^2 + 2\mu^2)}{(l_2^2 - \mu^2 + i\epsilon)^3} . \quad (4.17)$$

Before incorporating the correction term into the full graph, the energy integral of the loop momentum can be performed using the residue theorem:

$$V_{Counter}^\rho \rightarrow -ig^2 e Q T^a T^a \int \frac{d^{n-1} \vec{l}_2}{(2\pi)^{n-1}} \left[\frac{4\gamma^0 n^\rho - 8\gamma^\rho}{16(|\vec{l}_2|^2 + \mu^2)^{\frac{3}{2}}} - \frac{12\sqrt{2}\vec{l}_2^\rho + 6\mu^2\gamma^\rho}{16(|\vec{l}_2|^2 + \mu^2)^{\frac{5}{2}}} \right] . \quad (4.18)$$

A similar expression can be obtained for the counter term when the vertex is on the right hand side of the cut. However, the external momenta of the vertex are no longer l_4 and l_5 , but l_1 and $-l_3$. Thus, the vertex can be written in terms of l_1 , l_3 and l_2 :

$$\begin{aligned} V^\rho &= -g^2 e Q T^a T^a \int \frac{d^n l_2}{(2\pi)^n} \frac{\gamma^\mu (\not{l}_4 + m) \gamma^\rho (-\not{l}_5 + m) \gamma_\mu}{(l_4^2 - m^2 + i\epsilon)(l_5^2 - m^2 + i\epsilon)(l_2^2 + i\epsilon)} \\ &= -g^2 e Q T^a T^a \int \frac{d^n l_2}{(2\pi)^n} \frac{\gamma^\mu (\not{l}_1 - \not{l}_2 + m) \gamma^\rho (\not{l}_3 - \not{l}_2 + m) \gamma_\mu}{(l_1 - l_2)^2 - m^2 + i\epsilon)((l_3 - l_2)^2 - m^2 + i\epsilon)(l_2^2 + i\epsilon)} . \end{aligned} \quad (4.19)$$

Determining the counter term as before, the second counter term can easily be found. The counter terms now have to be incorporated into the full graph by including the expressions from the other side of the cut in each case. This generates expressions for the numerator and denominator for the counter term on the left hand side of the cut ($N_{Counter,LHS}^{Vertex}$ and $D_{Counter,LHS}^{Vertex}$) and for the right hand side of the cut ($N_{Counter,RHS}^{Vertex}$ and $D_{Counter,RHS}^{Vertex}$):

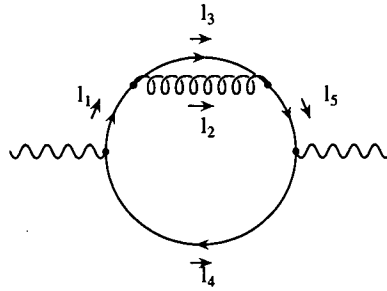
$$\begin{aligned} l_1^0 &= (|\vec{l}_1|^2 + m^2)^{\frac{1}{2}} \\ l_2^0 &= (|\vec{l}_2|^2 + \mu^2)^{\frac{1}{2}} \\ l_3^0 &= -(|\vec{l}_3|^2 + m^2)^{\frac{1}{2}} \\ N_{Counter,RHS}^{Vertex} &= -g^2 e^2 Q^2 \left(\frac{N_c^2 - 1}{2} \right) \\ &\quad \times 32(-2(l_2^0)^2(l_1^0 l_3^0 - 2m^2) + 3(2\vec{l}_1 \cdot \vec{l}_2 \vec{l}_3 \cdot \vec{l}_2 - 2\mu^2 l_1 \cdot l_3 + 3\mu^2 m^2)) \\ D_{Counter,RHS}^{Vertex} &= 128 |l_1^0| |l_3^0| |l_2^0|^5 \end{aligned} \quad (4.20)$$

4. Numerical Calculations

$$\begin{aligned}
l_2^0 &= (|\vec{l}_2|^2 + \mu^2)^{\frac{1}{2}} \\
l_4^0 &= (|\vec{l}_4|^2 + m^2)^{\frac{1}{2}} \\
l_5^0 &= (|\vec{l}_5|^2 + m^2)^{\frac{1}{2}} \\
N_{Counter,LHS}^{Vertex} &= g^2 e^2 Q^2 \left(\frac{N_c^2 - 1}{2} \right) \\
&\quad \times 32(-2(l_2^0)^2(l_4^0 l_5^0 + 2m^2) + 3(2\vec{l}_4 \cdot \vec{l}_2 \vec{l}_5 \cdot \vec{l}_2 - 2\mu^2 l_4 \cdot l_5 - 3\mu^2 m^2)) \\
D_{Counter,LHS}^{Vertex} &= 128 |l_4^0| |l_5^0| |l_2^0|^5 \quad . \quad (4.21)
\end{aligned}$$

4.1.2. Self Energy Correction

A little more thought is required when dealing with the graph containing the self energy (Fig. 4.3). As has been discussed, the self energy corrects the wave function and defines



$$\begin{aligned}
\vec{l}_3 &= \vec{l}_1 - \vec{l}_2 \\
\vec{l}_4 &= -\vec{l}_1 \\
\vec{l}_5 &= \vec{l}_1
\end{aligned}$$

(4.22)

Figure 4.3.: Two loop $\mathcal{O}(\alpha_s)$ correction of the photon propagator containing the self energy correction.

a new mass according to the position of the pole of the propagator. Due to symmetry, either the self energy that occurs on the left hand side of the cut or the right hand side of the cut needs to be considered. Similarly, either the quark self energy or the antiquark self energy has to be evaluated as each diagram will contribute the same value to the overall calculation. The quark self energy contribution will be considered with the overall contribution of the correction given.

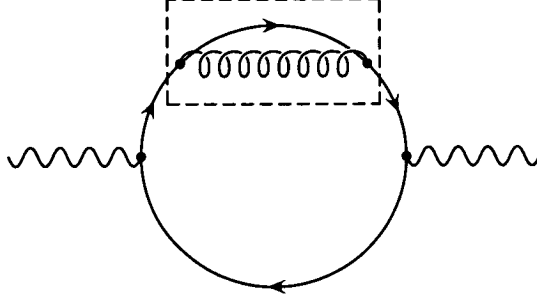


Figure 4.4.: Combined contribution from the self energy when the cuts are on the left and right hand side of it.

The self energy contributes by multiplying the lowest order two particle process, i.e. the Born cross section, by a factor. This correction has already been described in the analytic framework chapter, yet the exact form suitable for numerical calculation must be determined. Again scalar decomposition is used to generate the expressions required for the self energy. Similar to the massless case, there are terms that are numerically unstable, however, they are no longer simple cancellations. Instead the terms can be replaced with numerically equivalent integrands while maintaining the same singularity structure. This then gives the integral, I_1^{Self} , corresponding to the self energy contribution:

$$\begin{aligned}
 l_1^0 &= (|\vec{l}_1|^2 + m^2)^{\frac{1}{2}} \\
 l_2^0 &= |\vec{l}_2| \\
 l_3^0 &= (|\vec{l}_3|^2 + m^2)^{\frac{1}{2}} \\
 l_4^0 &= (|\vec{l}_4|^2 + m^2)^{\frac{1}{2}}
 \end{aligned} \tag{4.23}$$

$$\Sigma(l_1^2) = \not{l}_1 A(l_1^2) - m B(l_1^2) \tag{4.24}$$

$$A(l_1^2) = ig^2 T^a T^a \int \frac{d^n l_2}{(2\pi)^n} \frac{(2-n)l_3 \cdot l_1}{l_1^2 (l_3^2 - m^2 + i\epsilon)(l_2^2 + i\epsilon)} \tag{4.25}$$

$$B(l_1^2) = ig^2 T^a T^a \int \frac{d^n l_2}{(2\pi)^n} \frac{-n}{(l_3^2 - m^2 + i\epsilon)(l_2^2 + i\epsilon)} \tag{4.26}$$

4. Numerical Calculations

$$\begin{aligned}
\left(A - m \frac{\partial B}{\partial \psi_1} + m \frac{\partial A}{\partial \psi_1} \right) \Big|_{\psi_1=m} &= ig^2 T^a T^a \int \frac{d^n l_2}{(2\pi)^n} \left(\frac{2-n}{2} \right) \frac{1}{(l_3^2 - m^2) l_2^2} \\
&\quad - \left(\frac{2-n}{2} \right) \left(\frac{1}{(l_3^2 - m^2) l_2^2} + \frac{1}{m^2 l_2^2} - \frac{1}{m^2 (l_3^2 - m^2)} \right) \\
&\quad - 2 \left(\frac{2m^2}{(l_3^2 - m^2)^2 l_2^2} + \frac{1}{(l_3^2 - m^2) l_2^2} - \frac{1}{(l_3^2 - m^2)} \right) \\
&= ig^2 T^a T^a \int \frac{d^n l_2}{(2\pi)^n} \left(\frac{2-n}{2} \right) \frac{1}{(l_3^2 - m^2) l_2^2} \\
&\quad - \frac{2m^2}{(l_3^2 - m^2)^3} \\
&\quad - 2 \left(\frac{2m^2}{(l_3^2 - m^2)^2 l_2^2} - \frac{4m^2}{(l_3^2 - m^2)^3} \right) \\
&= ig^2 T^a T^a \int \frac{d^n l_2}{(2\pi)^n} \left(\frac{2-n}{2} \right) \frac{1}{(l_3^2 - m^2) l_2^2} + \frac{6m^2}{(l_3^2 - m^2)^3} \\
&\quad - \frac{4m^2}{(l_3^2 - m^2)^2 l_2^2} \\
&= g^2 T^a T^a \int \frac{d^{n-1} \vec{l}_2}{(2\pi)^{n-1}} \frac{l_2^0 + l_3^0}{2l_2^0 l_3^0 ((l_1^0)^2 - (l_2^0 + l_3^0)^2)} \\
&\quad - \frac{m^2}{(l_3^0)^3 ((l_1^0 + l_3^0)^2 - (l_2^0)^2)} - \frac{2m^2 (l_1^0 + l_3^0)}{(l_3^0)^2 ((l_1^0 + l_3^0)^2 - (l_2^0)^2)} \\
&\quad + \frac{2m^2}{l_2^0 ((l_1^0 - l_2^0)^2 - (l_3^0)^2)^2} - \frac{9m^2}{8((l_2^0)^2 + m^2)^{\frac{5}{2}}} \\
I_1^{Self} &= \left(A - m \frac{\partial B}{\partial \psi_1} + m \frac{\partial A}{\partial \psi_1} \right) \Big|_{\psi_1=m} \\
&\quad \times e^2 Q^2 \int \frac{d^3 \vec{l}_1}{(2\pi)^{n-1}} \frac{2(l_1 \cdot l_4 + 2m^2)}{(|\vec{l}_1|^2 + m^2)^{\frac{1}{2}} (|\vec{l}_4|^2 + m^2)^{\frac{1}{2}}} \quad (4.27)
\end{aligned}$$

For numerical stability, the three particle cut for this graph, I_2^{Self} has to be put into a similar form illustrated by placing a box around the self energy part of the diagram (Fig. 4.5). This involves taking the part of the scattering matrix that corresponds to

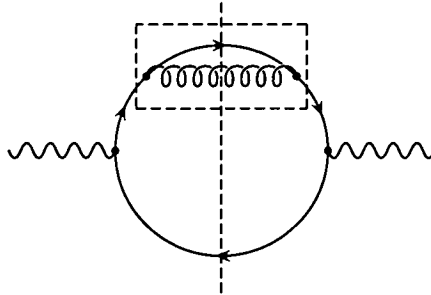


Figure 4.5.: Three particle cut of the graph containing the self energy.

the splitting and recombination of the quark and gluon, and giving it the same form as the self energy, $\not{l}_1 A - mB$. From the jet perspective, this is quite sensible as the decay of the photon into two fermions naturally describes two jets while the splitting of a gluon from one of the fermions gives the possibility of a third. However, it must be shown analytically possible to separate the splitting of the fermion into a fermion and a gluon from the underlying process:

$$\begin{aligned}
 I_2^{Self} &= -g^2 e^2 Q^2 \left(\frac{N_c^2 - 1}{2} \right) \int \frac{d^n l_2}{(2\pi)^n} \int \frac{d^n l_3}{(2\pi)^n} \int \frac{d^n l_4}{(2\pi)^n} \\
 &\quad Tr \left(\frac{\bar{u}(l_3) \gamma^\rho (\not{l}_1 + m) \gamma^\mu v(l_4) \bar{v}(l_4) \gamma_\mu (\not{l}_1 + m) \gamma_\rho u(l_3)}{(l_1^2 - m^2)^2} \right) \\
 &\quad (2\pi) \delta(l_2^2) \theta(l_2^0) (2\pi) \delta(l_3^2 - m^2) \theta(l_3^0) (2\pi) \delta(l_4^2 - m^2) \theta(l_4^0) \\
 &\quad (2\pi)^n \delta(q - l_2 - l_3 - l_4) \\
 &= -g^2 e^2 Q^2 \left(\frac{N_c^2 - 1}{2} \right) \int \frac{d^n l_1}{(2\pi)^n} \int \frac{d^n l_4}{(2\pi)^n} \int \frac{d^n l_2}{(2\pi)^n} \int \frac{d^n l_3}{(2\pi)^n} \\
 &\quad Tr \left(\frac{\bar{u}(l_3) \gamma^\rho (\not{l}_1 + m) \gamma^\mu v(l_4) \bar{v}(l_4) \gamma_\mu (\not{l}_1 + m) \gamma_\rho u(l_3)}{(l_1^2 - m^2)^2} \right) \\
 &\quad (2\pi) \delta(l_2^2) \theta(l_2^0) (2\pi) \delta(l_3^2 - m^2) \theta(l_3^0) (2\pi)^n \delta(l_1 - l_2 - l_3) \\
 &\quad (2\pi) \delta(l_4^2 - m^2) \theta(l_4^0) (2\pi)^n \delta(q - l_2 - l_3 - l_4) \quad (4.28) \\
 &= -g^2 e^2 Q^2 \left(\frac{N_c^2 - 1}{2} \right) \int \frac{d^n l_1}{(2\pi)^n} \int \frac{d^n l_2}{(2\pi)^n} \int \frac{d^n l_3}{(2\pi)^n} \int \frac{d^n l_4}{(2\pi)^n} \\
 &\quad Tr \left(\frac{(\not{l}_1 + m) ((2-n)\not{l}_4 - nm) (\not{l}_1 + m) [(2-n)\not{l}_3 + nm]}{(l_1^2 - m^2)^2} \right) \\
 &\quad (2\pi) \delta(l_2^2) \theta(l_2^0) (2\pi) \delta(l_3^2 - m^2) \theta(l_3^0) (2\pi) \delta(l_4^2 - m^2) \theta(l_4^0) \\
 &\quad (2\pi)^n \delta(q - l_2 - l_3 - l_4) (2\pi)^n \delta(l_1 - l_2 - l_3) \\
 \implies \not{l}_1 A - mB &= \int \frac{d^n l_2}{(2\pi)^n} \int \frac{d^n l_3}{(2\pi)^n} (2-n)\not{l}_3 + nm \\
 &\quad (2\pi) \delta(l_2^2) \theta(l_2^0) (2\pi) \delta(l_3^2 - m^2) \theta(l_3^0) (2\pi)^n \delta(l_1 - l_2 - l_3) \\
 A &= \int \frac{d^n l_2}{(2\pi)^n} \int \frac{d^n l_3}{(2\pi)^n} \left(\frac{2-n}{2} \right) \frac{(l_1^2 + l_3^2)}{l_1^2} \\
 &\quad (2\pi) \delta(l_2^2) \theta(l_2^0) (2\pi) \delta(l_3^2 - m^2) \theta(l_3^0) (2\pi)^n \delta(l_1 - l_2 - l_3) \quad (4.29) \\
 B &= \int \frac{d^n l_2}{(2\pi)^n} \int \frac{d^n l_3}{(2\pi)^n} -n \\
 &\quad (2\pi) \delta(l_2^2) \theta(l_2^0) (2\pi) \delta(l_3^2 - m^2) \theta(l_3^0) (2\pi)^n \delta(l_1 - l_2 - l_3) \quad (4.30)
 \end{aligned}$$

Obtaining the form for A and B , this may then be reinserted into the integrand

4. Numerical Calculations

and the required integrals may be performed:

$$\begin{aligned}
l_1^0 &= |\vec{l}_2| + (|\vec{l}_3|^2 + m^2)^{\frac{1}{2}} \\
l_2^0 &= |\vec{l}_2| \\
l_3^0 &= (|\vec{l}_3|^2 + m^2)^{\frac{1}{2}} \\
l_4^0 &= (|\vec{l}_4|^2 + m^2)^{\frac{1}{2}} \\
I_2^{Self} &= g^2 e^2 Q^2 \left(\frac{N_c^2 - 1}{2} \right) \int \frac{d^{n-1} \vec{l}_1}{(2\pi)^{n-1}} \int \frac{d^{n-1} \vec{l}_2}{(2\pi)^{n-1}} \\
&\quad \frac{(l_1 \cdot l_4 + 2m^2)(l_1^4 - 6m^2 l_1^2 + m^4)}{|\vec{l}_2^0| |\vec{l}_3^0| |\vec{l}_4^0| l_1^2 (l_1^2 - m^2)^2} + \frac{2(3m^2 l_1^2 - m^4)}{|\vec{l}_2^0| |\vec{l}_3^0| |\vec{l}_4^0| l_1^2 (l_1^2 - m^2)} \quad (4.31)
\end{aligned}$$

This gives both the contributions from the graph containing the unrenormalised self energy.

Renormalisation of the self energy graph

As stated previously, the renormalisation term is the same form as the massless wave function renormalisation since the mass renormalisation goes towards the running of the mass parameters. This has been calculated in the previous chapter and becomes a multiplicative factor of the Born cross section:

$$\begin{aligned}
l_1^0 &= (|\vec{l}_1|^2 + m^2)^{\frac{1}{2}} \\
l_4^0 &= (|\vec{l}_4|^2 + m^2)^{\frac{1}{2}} \\
I_{Counter}^{Self} &= e^2 Q^2 A_{Counter} \int \frac{d^{n-1} \vec{l}_1}{(2\pi)^{n-1}} \frac{2(l_1 \cdot l_4 + 2m^2)}{(|\vec{l}_1|^2 + m^2)^{\frac{1}{2}} (|\vec{l}_4|^2 + m^2)^{\frac{1}{2}}} \\
&= -g^2 e^2 Q^2 \left(\frac{N_c^2 - 1}{2} \right) \int \frac{d^{n-1} \vec{l}_1}{(2\pi)^{n-1}} \int \frac{d^{n-1} \vec{l}_2}{(2\pi)^{n-1}} \\
&\quad \times \left(-\frac{1}{4(|\vec{l}_2|^2 + \mu^2)^{\frac{3}{2}}} - \frac{3}{8(|\vec{l}_2|^2 + \mu^2)^{\frac{5}{2}}} \right) \frac{2(l_1 \cdot l_4 + 2m^2)}{(|\vec{l}_1|^2 + m^2)^{\frac{1}{2}} (|\vec{l}_4|^2 + m^2)^{\frac{1}{2}}} \quad (4.32)
\end{aligned}$$

Combining the renormalisation term with the other two cuts produces the finite contribution for the graph containing the self energy correction.

4.1.3. Comparison to the Massless Case

By taking the limit $m \rightarrow 0$ it is self evident that the basic integrands are the same as those obtained in the massless case. The corresponding renormalisation terms also have a smooth limit to the massless case and have the same structure as that used in the Beowulf program. Massive fermions remove the soft singularities that were associated with these particles and the collinear cancellation properties are no longer required. This suggests that only one sampling method concentrating points on the zero momentum gluon is required in this case. However, for simplicity, two sampling methods can still be used so that the transition between massive and massless fermions is apparent. It is also suitable as for small masses there is still an enhancement near to where the soft points would be.

4.2. Cancellation of Singularities Revisited

Before going any further, the integrands need to be checked to ensure that there are no singularities present. Most of the work towards this has been completed in the previous chapter when the scalar diagram was considered. As before there are soft, collinear and scattering singularities to consider plus another graph and masses to account for.

4.2.1. Vertex Graph

The difference between the vertex graph considered in this chapter and that of the scalar case in the previous chapter is in the numerator. Prior to integration of the energies, the numerators for each cut are identical. For cancellations to occur, the numerators of the cancelling integrands must be the same for the region of cancellation. It is sufficient to check that the energy terms in the massless case of the four-momenta involved in the numerator are the same for each cut in the required regions. There are four cases to consider; three collinear regions (Tab. 4.1, 4.2 and 4.3) and the scattering surface (Tab. 4.4). The soft points are end points of the collinear region and so do not need to be considered separately. The same collinear conventions will be used as in the previous chapter.

4. Numerical Calculations

| Integrand | l_1^0 | l_3^0 | l_4^0 | l_1^0 |
|------------------------------------|---------------------|---------------------|----------------------|----------------|
| $A_{1b}^{Vertex}, A_{1c}^{Vertex}$ | $(1-x) \vec{l}_4 $ | $-(1+x) \vec{l}_4 $ | $ \vec{l}_4 $ | $ \vec{l}_4 $ |
| $A_{4a}^{Vertex}, A_{4c}^{Vertex}$ | $-(1+x) \vec{l}_4 $ | $(1+x) \vec{l}_4 $ | $-(1+2x) \vec{l}_4 $ | $- \vec{l}_4 $ |

Table 4.1.: Energies for integrands with collinear singularity along $-\infty < x < -1$.

| Integrand | l_1^0 | l_3^0 | l_4^0 | l_1^0 |
|------------------------------------|--------------------|---------------------|---------------|---------------------|
| $A_{1a}^{Vertex}, A_3^{Vertex}$ | $(1+x) \vec{l}_4 $ | $(x-1) \vec{l}_4 $ | $ \vec{l}_4 $ | $ \vec{l}_4 $ |
| $A_{1b}^{Vertex}, A_2^{Vertex}$ | $(1-x) \vec{l}_4 $ | $-(1+x) \vec{l}_4 $ | $ \vec{l}_4 $ | $ \vec{l}_4 $ |
| $A_{4a}^{Vertex}, A_{4b}^{Vertex}$ | $(1+x) \vec{l}_4 $ | $-(1+x) \vec{l}_4 $ | $ \vec{l}_4 $ | $(1+2x) \vec{l}_4 $ |

Table 4.2.: Energies for integrands with collinear singularity along $-1 < x < 0$.

| Integrand | l_1^0 | l_3^0 | l_4^0 | l_1^0 |
|------------------------------------|--------------------|---------------------|---------------------|---------------------|
| $A_{1a}^{Vertex}, A_{1b}^{Vertex}$ | $(1+x) \vec{l}_4 $ | $(x-1) \vec{l}_4 $ | $ \vec{l}_4 $ | $ \vec{l}_4 $ |
| $A_2^{Vertex}, A_{4b}^{Vertex}$ | $(1+x) \vec{l}_4 $ | $-(1+x) \vec{l}_4 $ | $ \vec{l}_4 $ | $(1+2x) \vec{l}_4 $ |
| $A_3^{Vertex}, A_{4a}^{Vertex}$ | $(1+x) \vec{l}_4 $ | $-(1+x) \vec{l}_4 $ | $(1+2x) \vec{l}_4 $ | $ \vec{l}_4 $ |

Table 4.3.: Energies for integrands with collinear singularity along $0 < x < \infty$.

| Integrand | l_1^0 | l_3^0 | l_4^0 | l_1^0 |
|------------------------------------|---------------|----------------|---------------|---------------|
| $A_{1a}^{Vertex}, A_{4b}^{Vertex}$ | $ \vec{l}_4 $ | $- \vec{l}_4 $ | $ \vec{l}_4 $ | $ \vec{l}_4 $ |

Table 4.4.: Energies for integrands on the scattering singularity $|\vec{l}_2 + \vec{l}_4| = |\vec{l}_4|$.

Adding massive fermions to this analysis tends to simplify the singularity structure rather than complicate it. To begin with, the collinear singularities are removed as they only appear when the particles subtending from a vertex are all massless. This is due to simple energy conserving principles and can also be verified by performing the collinear analysis demonstrated in the previous chapter with masses on the appropriate momenta. The mass of the fermions prevents soft singularities occurring due to the fermions as they now have a minimum energy. Cancellation of the soft singularity due to the gluon occurs in exactly the same way as before since the mass of the propagator is applied consistently throughout the integrands and the numerator structure is the same for each integrand. Similarly, the scattering singularity cancels in the same way as before. The surface of the scattering singularity is the same as before.

4.2.2. Self Energy Graph

The graph containing the self energy is a much simpler example to consider as the terms split neatly into a massless and massive case and the massless case is proportional to the Born cross section that is free from soft and collinear divergences. To guide the analysis it is useful to consider some general aspects of soft and collinear singularities. Collinear singularities require two massless particles at the same vertex and so it is only possible to have a collinear singularity in the massless case. The integrands take a very simple form when the mass is set to zero:

$$\begin{aligned}
 I_1^{Self} &= g^2 e^2 Q^2 \left(\frac{N_c^2 - 1}{2} \right) \\
 &\quad \int \frac{d^3 \vec{l}_1}{(2\pi)^3} \int \frac{d^3 \vec{l}_2}{(2\pi)^3} \frac{h(|\vec{l}_1| + |\vec{l}_4|) l_1 \cdot l_4 (|\vec{l}_2| + |\vec{l}_3|)}{|\vec{l}_2| |\vec{l}_3| (|\vec{l}_2 + \vec{l}_3|^2 - (|\vec{l}_2| + |\vec{l}_3|)^2) |\vec{l}_2 + \vec{l}_3| |\vec{l}_4|} \\
 I_2^{Self} &= g^2 e^2 Q^2 \left(\frac{N_c^2 - 1}{2} \right) \\
 &\quad \int \frac{d^3 \vec{l}_1}{(2\pi)^3} \int \frac{d^3 \vec{l}_2}{(2\pi)^3} \frac{h(|\vec{l}_2| + |\vec{l}_3| + |\vec{l}_4|) l_1 \cdot l_4}{|\vec{l}_2| |\vec{l}_3| (|\vec{l}_2 + \vec{l}_3|^2 - |\vec{l}_2 + \vec{l}_3|^2) |\vec{l}_4|} \quad (4.33)
 \end{aligned}$$

To examine the collinear singularity it is useful to look at l_2 lying in the direction of l_3 with some small transversal momentum. Looking at the integrands, there is only one denominator that could cause a collinear divergence. Applying the representation

4. Numerical Calculations

of l_2 , one can determine the range for x where there is a collinear divergence:

$$\begin{aligned}
\vec{l}_2 &= x\vec{l}_3 + \vec{l}_T \\
|\vec{l}_2| &\approx |x||\vec{l}_3| \left(1 + \frac{|\vec{l}_T|^2}{2x^2|\vec{l}_3|^2} \right) \\
|\vec{l}_2 + \vec{l}_3| &\approx |1+x||\vec{l}_3| \left(1 + \frac{|\vec{l}_T|^2}{2(1+x)^2|\vec{l}_3|^2} \right) \\
|\vec{l}_2| + |\vec{l}_3| - |\vec{l}_2 + \vec{l}_3| &\approx |x||\vec{l}_3| \left(1 + \frac{|\vec{l}_T|^2}{2x^2|\vec{l}_3|^2} \right) + |\vec{l}_3| - |1+x||\vec{l}_3| \left(1 + \frac{|\vec{l}_T|^2}{2(1+x)^2|\vec{l}_3|^2} \right) \\
&= \frac{|\vec{l}_T|^2}{2|x||\vec{l}_3|} - \frac{|\vec{l}_T|^2}{2|1+x||\vec{l}_3|} \quad 0 \leq x < \infty \quad . \quad (4.34)
\end{aligned}$$

The range of x for which the collinear singularity exists includes $x = 0$ that corresponds to the gluon going soft, however, the gluon does not produce a soft singularity at this point. As the integrands for both cuts have a common factor, I_{Common}^{Self} , in the collinear region, it suffices to look at the combination of the factors that are different in the collinear region:

$$\begin{aligned}
I_1^{Self} + I_2^{Self} &= I_{Common}^{Self} \left(\frac{h(|\vec{l}_1| + |\vec{l}_4|)(|\vec{l}_2| + |\vec{l}_3|)}{|\vec{l}_2 + \vec{l}_3|} - h(|\vec{l}_2| + |\vec{l}_3| + |\vec{l}_4|) \right) \\
&= I_{Common}^{Self} \\
&\quad \times \left(\frac{h(|\vec{l}_2 + \vec{l}_3| + |\vec{l}_4|)(|\vec{l}_2| + |\vec{l}_3|) - h(|\vec{l}_2| + |\vec{l}_3| + |\vec{l}_4|)|\vec{l}_2 + \vec{l}_3|}{|\vec{l}_2 + \vec{l}_3|} \right) \quad . \quad (4.35)
\end{aligned}$$

In the collinear limit the smearing functions are dependent on the same momenta and so there is an exact cancellation between the numerator and denominator that removes the collinear singularity. When the fermions are massive, it is necessary to

check the soft cancellation again due to the additional terms:

$$\begin{aligned}
 |\vec{l}_2| &\approx \delta \\
 |\vec{l}_2 + \vec{l}_3| &\approx |\vec{l}_3| + \delta \vec{u}_2 \cdot \vec{u}_3 \\
 I_1^{Self} &\approx g^2 e^2 Q^2 \left(\frac{N_c^2 - 1}{2} \right) \int \frac{d^3 \vec{l}_1}{(2\pi)^3} \int \frac{d^3 \vec{l}_2}{(2\pi)^3} \left(\frac{1}{4\delta^2 (|\vec{l}_3| \vec{u}_2 \cdot \vec{u}_3 - (|\vec{l}_3|^2 + m^2)^{\frac{1}{2}})} \right. \\
 &\quad \left. - \frac{m^2}{2\delta (|\vec{l}_3|^2 + m^2)^{\frac{1}{2}} (|\vec{l}_3| \vec{u}_2 \cdot \vec{u}_3 - (|\vec{l}_3|^2 + m^2)^{\frac{1}{2}})} - \frac{m^2}{(|\vec{l}_3|^2 + m^2)^3} \right. \\
 &\quad \left. + \frac{m^2}{2\delta^3 (|\vec{l}_3| \vec{u}_2 \cdot \vec{u}_3 - (|\vec{l}_3|^2 + m^2)^{\frac{1}{2}})^2} - \frac{9}{8m^3} \right) \times \frac{2(l_1 \cdot l_4 + 2m^2)}{(|\vec{l}_3|^2 + m^2)^{\frac{1}{2}} (|\vec{l}_4|^2 + m^2)^{\frac{1}{2}}} \\
 I_2^{Self} &\approx g^2 e^2 Q^2 \left(\frac{N_c^2 - 1}{2} \right) \int \frac{d^3 \vec{l}_1}{(2\pi)^3} \int \frac{d^3 \vec{l}_2}{(2\pi)^3} \left(\frac{(l_1 \cdot l_4 + 2m^2)}{\delta (|\vec{l}_3|^2 + m^2)^{\frac{1}{2}} (|\vec{l}_4|^2 + m^2)^{\frac{1}{2}} m^2} \right. \\
 &\quad \left. - \frac{m^2 (l_1 \cdot l_4 + 2m^2)}{\delta^3 (|\vec{l}_3|^2 + m^2)^{\frac{1}{2}} (|\vec{l}_4|^2 + m^2)^{\frac{1}{2}} ((|\vec{l}_3|^2 + m^2)^{\frac{1}{2}} - |\vec{l}_3| \vec{u}_2 \cdot \vec{u}_3)^2} \right. \\
 &\quad \left. + \frac{3m^2}{\delta^2 (|\vec{l}_3|^2 + m^2)^{\frac{1}{2}} (|\vec{l}_4|^2 + m^2)^{\frac{1}{2}} ((|\vec{l}_3|^2 + m^2)^{\frac{1}{2}} - |\vec{l}_3| \vec{u}_2 \cdot \vec{u}_3)} \right. \\
 &\quad \left. - \frac{1}{\delta^2 (|\vec{l}_3|^2 + m^2)^{\frac{1}{2}} (|\vec{l}_4|^2 + m^2)^{\frac{1}{2}} ((|\vec{l}_3|^2 + m^2)^{\frac{1}{2}} - |\vec{l}_3| \vec{u}_2 \cdot \vec{u}_3)} \right)
 \end{aligned} \tag{4.36}$$

The soft singularities in these expressions are found in the terms with δ^3 in the denominator and are proportional to m^2 showing that these have been created by the introduction of mass. Effectively the collinear singularity of the massless case has turned into a soft singularity in the massive case. It is clear that when the two integrands are added together that the terms containing δ^3 in the denominator cancel and so no soft pole remains.

4.3. Obtaining Numerical Results

Evaluating these expressions requires some care. For the remainder of the chapter all the calculations will be performed using only one quark and ignoring the charge, Q . This is to simplify the checking of calculations and get a feeling for the effect of introducing mass, however by combining and interpolating the results, numbers can be obtained for several quarks. It should also be noted that a factor of

$$\frac{\alpha_s}{\pi} = \frac{g^2}{4\pi^2} \tag{4.37}$$

4. Numerical Calculations

has been factored out of the integrals as this corresponds to the massless $\mathcal{O}\alpha_s$ correction when $N_c = 3$.

The correction to the Born cross section is a function of the velocity,

$$v = \left(1 - \frac{4m^2}{s}\right)^{\frac{1}{2}}. \quad (4.38)$$

This means that for a given mass, different values of the centre of mass energy produce different values for the correction. Using a smearing function that is dependent on the centre of mass energy produces a weighted average of these corrections that is dependent on the shape of the smearing function. To determine the correction for a particular centre of mass energy requires a smearing function that is strongly peaked about the value to be considered. However, a smearing function that is too strongly peaked causes problems in terms of numerical stability.

The dependence of the correction to the Born cross section on the velocity is almost linear starting with a correction of π^2 for zero velocity and ending with 1 at a velocity of 1. This suggests that a sensible method of checking the validity of the expressions obtained would be to use a smearing function that averages over a small range of the velocities. The correction in each range can then be considered to be approximately linear and the average will give a good estimate of the central value of the range. To do this it is convenient to integrate over the velocity with a suitable smearing function. The Jacobian from this transformation introduces a factor that originates from the energy conserving delta function:

$$\begin{aligned} \int_0^1 dv h(v) I \delta(\sqrt{s} - \Sigma E) &= \int_0^1 dv h(v) I \delta\left(\frac{2m}{(1-v^2)^{\frac{1}{2}}} - \Sigma E\right) \\ &= \frac{(1-v^2)^{\frac{3}{2}} h(v) I}{2mv}. \end{aligned} \quad (4.39)$$

Averaging equally over a small range of velocities that lie between v_a and v_b requires the smearing function, $h(v)$, to take the form of a 'top hat',

$$h(v) = \frac{\theta(v - v_a) - \theta(v - v_b)}{v_b - v_a}. \quad (4.40)$$

It is suitable to use a width of 0.1 to verify the expressions obtained while avoiding numerical problems that arise due to narrow peaks. Choosing an arbitrary fixed mass

4.3. Obtaining Numerical Results

of 10 GeV the equivalent widths for the centre of mass energies can be determined (Tab. 4.5).

| Velocity | Extremal velocities | Energy | Extremal Energies | Difference |
|----------|---------------------|--------|-------------------|------------|
| 0.1 | 0.05 | 20.101 | 20.025 | -0.076 |
| | 0.15 | | 20.229 | +0.129 |
| 0.2 | 0.15 | 20.412 | 20.229 | -0.183 |
| | 0.25 | | 20.656 | +0.244 |
| 0.3 | 0.25 | 20.965 | 20.656 | -0.310 |
| | 0.35 | | 21.350 | +0.385 |
| 0.4 | 0.35 | 21.822 | 21.350 | -0.472 |
| | 0.45 | | 22.396 | +0.574 |
| 0.5 | 0.45 | 23.094 | 22.396 | -0.698 |
| | 0.55 | | 23.947 | +0.853 |
| 0.6 | 0.55 | 25.000 | 23.947 | -1.053 |
| | 0.65 | | 26.318 | +1.318 |
| 0.7 | 0.65 | 28.007 | 26.318 | -1.688 |
| | 0.75 | | 30.237 | +2.230 |
| 0.8 | 0.75 | 33.333 | 30.237 | -3.096 |
| | 0.85 | | 37.966 | +4.633 |
| 0.9 | 0.85 | 45.883 | 37.966 | -7.917 |
| | 0.95 | | 64.051 | +18.168 |

Table 4.5.: Velocity-energy correspondence for a fixed mass of 10 GeV. For the given velocity bins, the corresponding energies and difference from the energy corresponding to the central energy are given in GeV.

As can be seen, higher velocities have greater energy widths and the central value for the velocity corresponds to centre of mass energy that is towards the lower energies of the range. There is a good agreement between the results obtained using this method and the analytic values for the correction (Tab. 4.6). When this data is represented graphically (Fig. 4.6) the almost linear nature of the correction can be seen and the deviations of the numerical calculations away from the corrections can be attributed to

4. Numerical Calculations

| Velocity | $\left(\frac{\sigma_1(v)}{\sigma_0(v=1)}\right)_{Analytic}$ | $\left(\frac{\sigma_1(v)}{\sigma_0(v=1)}\right)_{Tophat}$ | Error |
|----------|---|---|-------|
| 0.1 | 9.105 | 9.110 | 0.010 |
| 0.2 | 8.275 | 8.325 | 0.013 |
| 0.3 | 7.545 | 7.560 | 0.016 |
| 0.4 | 6.678 | 6.651 | 0.020 |
| 0.5 | 5.743 | 5.726 | 0.016 |
| 0.6 | 4.753 | 4.738 | 0.017 |
| 0.7 | 3.731 | 3.773 | 0.016 |
| 0.8 | 2.719 | 2.726 | 0.013 |
| 0.9 | 1.773 | 1.785 | 0.011 |

Table 4.6.: Comparison of the value of $\frac{\sigma_1(v)}{\sigma_0(v=1)}$ for different velocities using analytic results and the top hat velocity smearing function.

the slight curvature. As the errors are quite small it is useful to look at the numerical results normalised to the analytic results (Fig. 4.7).

Using velocity smearing has properties useful for calculations beyond the one considered here. It provides a finite interval for integration to work within in contrast to using \sqrt{s} . Even if higher order corrections do not depend directly on the velocity, one would expect the corrections to change smoothly, maybe with isolated peaks as $\frac{m}{\sqrt{s}}$ varies. These properties will allow checking of higher order corrections using a sliding bin technique. By taking a suitably thin top hat function and gradually moving it along the values of velocity so that there is a large overlap between consecutive evaluations, the amount of variation in the correction for different velocities can be deduced.

The velocity top hat smearing method can be contrasted with the approach using a smooth smearing function that depends on the centre of mass energy. As described in the previous chapter, the Beowulf code uses a smearing function that is based on the method for choosing radial components in the spherical coordinate system. It may be

4. Numerical Calculations

modified to cater for the centre of mass threshold at an energy of $\sqrt{s} = 2m$:

$$\sqrt{s} = E \left(\frac{1}{X^A} - 1 \right)^B + 2m$$

$$\int_{2m}^{\infty} d\sqrt{s} h(\sqrt{s}) = \int_0^1 dX \frac{h(\sqrt{s}) A B E \left(\left(\frac{\sqrt{s}-2m}{E} \right)^{\frac{1}{B}} + 1 \right)^{1+\frac{1}{A}}}{\left(\frac{\sqrt{s}-2m}{E} \right)^{\frac{1}{B}-1}}$$

$$= 1 \tag{4.41}$$

$$\rightarrow h(\sqrt{s}) = \frac{\left(\frac{\sqrt{s}-2m}{E} \right)^{\frac{1}{B}-1}}{A B E \left(\left(\frac{\sqrt{s}-2m}{E} \right)^{\frac{1}{B}} + 1 \right)^{1+\frac{1}{A}}} \tag{4.42}$$

Again to fix the peak at a particular energy, the smearing function must be differentiated with respect to the centre of mass energy. The parameter E can then be fixed according to the value of energy required, the parameters A and B , and the mass:

$$\left. \frac{\partial h(\sqrt{s})}{\partial \sqrt{s}} \right|_{\sqrt{s}_{peak}} = \frac{\left(\frac{\sqrt{s}-2m}{E} \right)^{\frac{1}{B}-2}}{A B E \left(\left(\frac{\sqrt{s}-2m}{E} \right)^{\frac{1}{B}} + 1 \right)^{2+\frac{1}{A}}}$$

$$\times \left[\left(\frac{1}{B} - 1 \right) - \left(1 + \frac{1}{A B} \right) \left(\frac{\sqrt{s}-2m}{E} \right)^{\frac{1}{B}} \right] \Bigg|_{\sqrt{s}_{peak}}$$

$$= 0 \tag{4.43}$$

$$\Rightarrow E = (\sqrt{s}_{peak} - 2m) \left(\frac{1 + A B}{A(1 - B)} \right)^B \tag{4.44}$$

This gives a family of smearing functions for a fixed set of parameters but different masses. The peak of the function has to be greater than $2m$ for this procedure to work. Adjusting the parameters leads to changing the shape of the smearing function. The parameter A must be greater than zero and B ranges between zero and one. Broadly speaking smaller values of B create much more peaked distributions and smaller values of A leads to smaller widths and slightly changed shape. It is useful to consider plots of the smearing function for different values of $\frac{m}{\sqrt{s}_{peak}}$ and varying values of B to get an idea of the differences changing the parameters causes (Fig. 4.8 and 4.9).

Fixing A at 0.9, B can be varied to determine how well the values fit with the analytic values obtained for the velocity (Fig. 4.10). To see the effect of varying B more clearly, the correction produced by the numerical method can be divided by the analytic result for each value of B (Fig. 4.11 and 4.12). This illustrates the shape

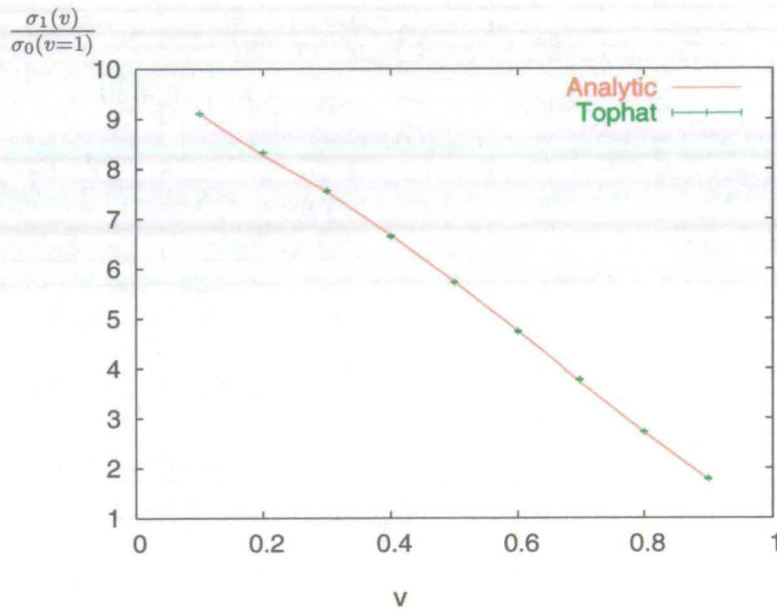


Figure 4.6.: Plot of $\frac{\sigma_1(v)}{\sigma_0(v=1)}$ for different velocities using analytic results and the top hat velocity smearing function.

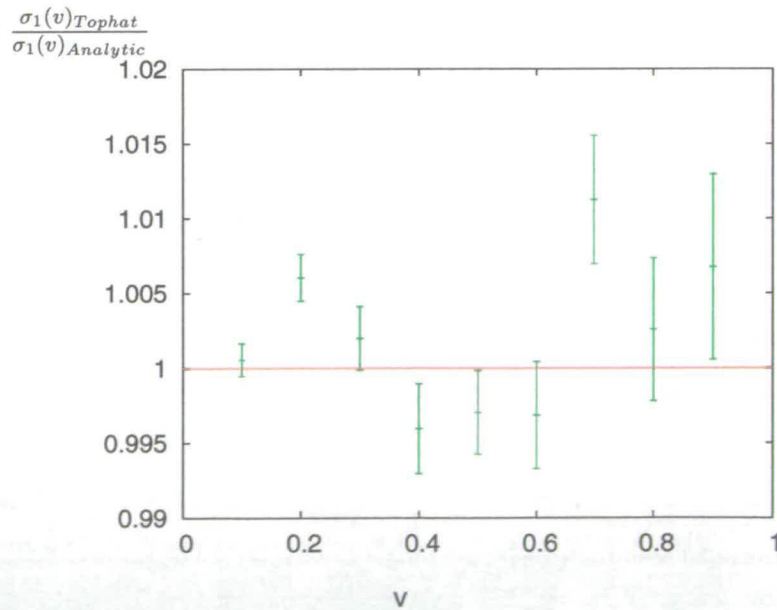


Figure 4.7.: Plot of $\frac{\sigma_1(v)_{Tophat}}{\sigma_1(v)_{Analytic}}$ for different velocities.

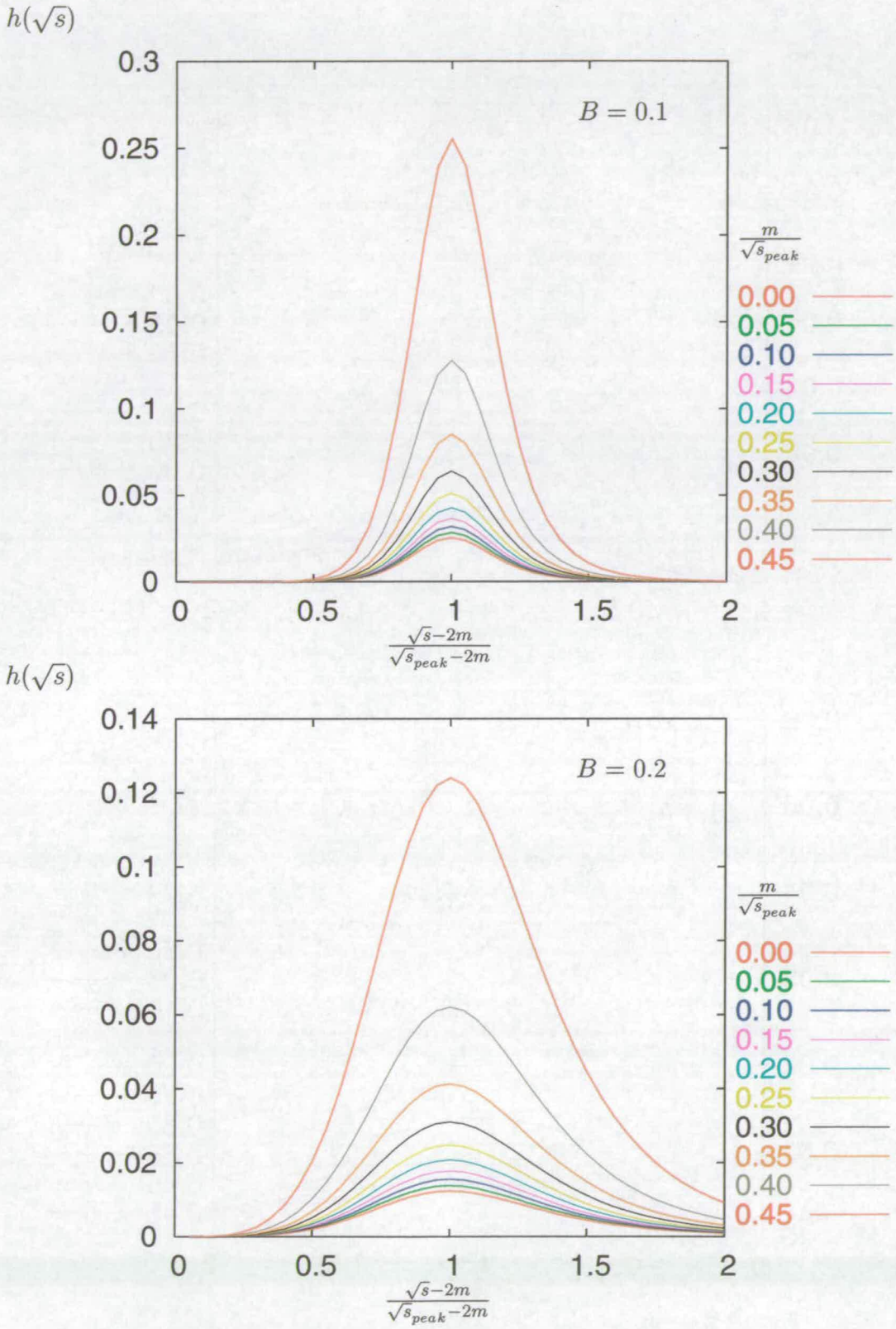


Figure 4.8.: Smearing functions with $A = 0.9$, $B = 0.1$ (Top) and $B = 0.2$ (Bottom) for $\frac{m}{\sqrt{s_{peak}}}$ between 0 and 0.45.

4. Numerical Calculations

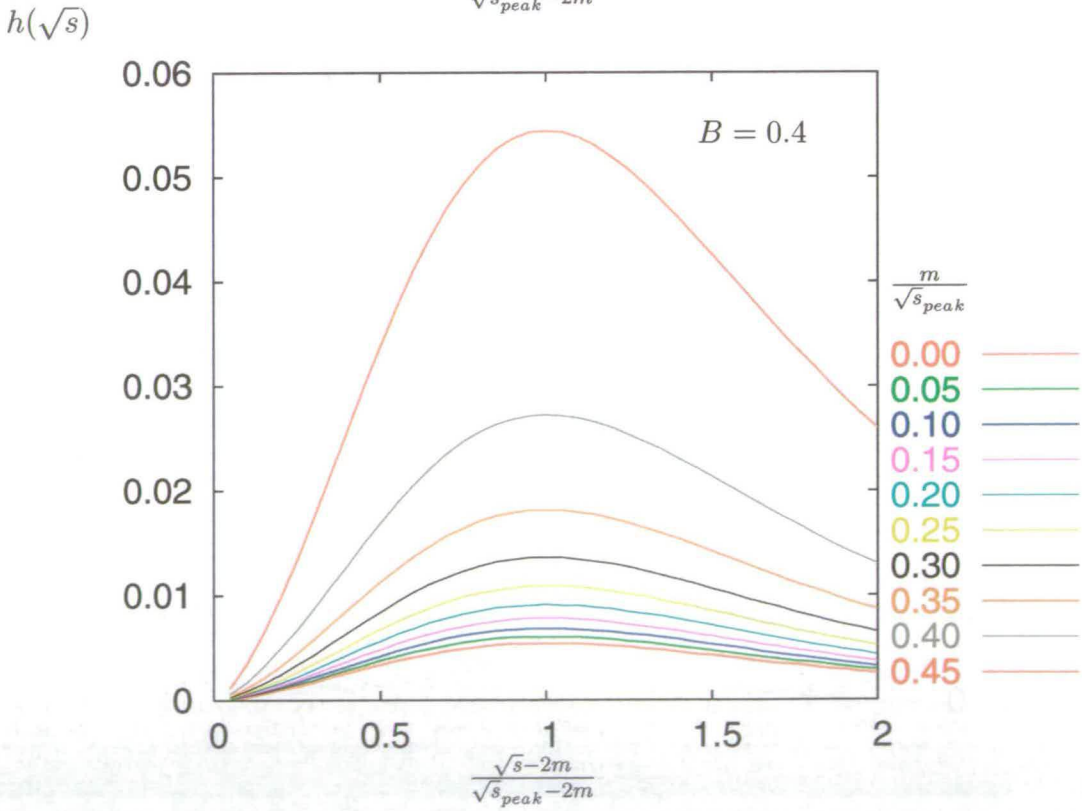
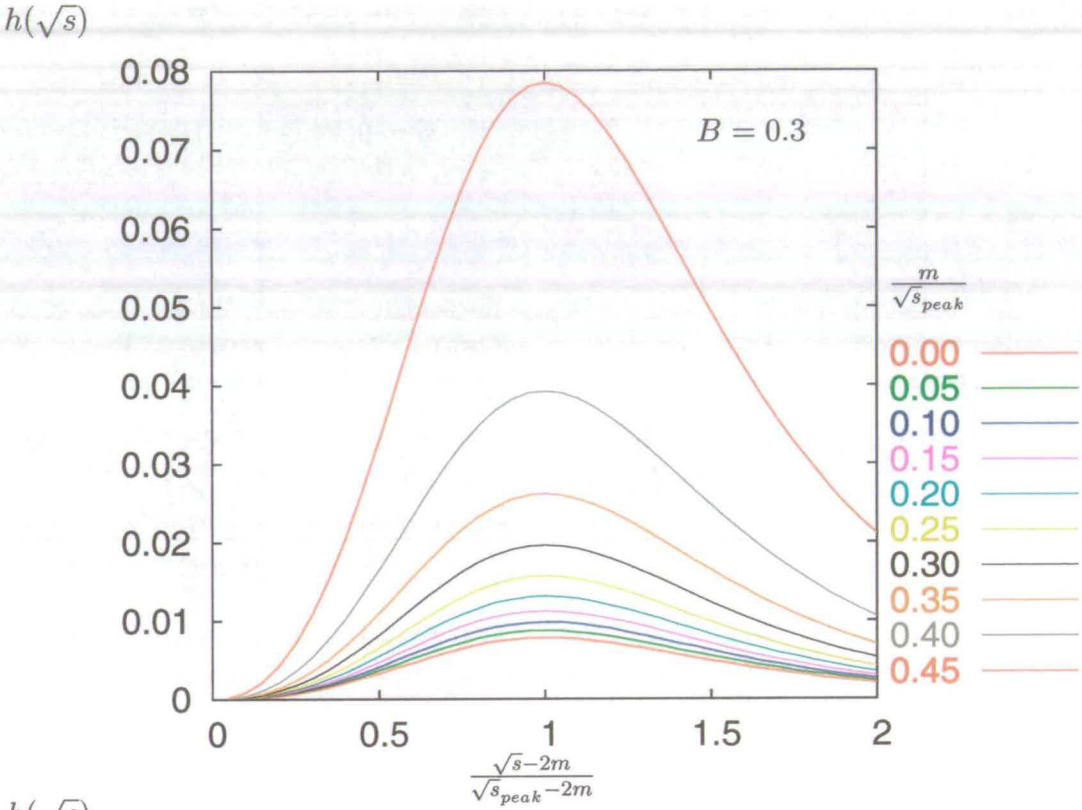


Figure 4.9.: Smearing functions with $A = 0.9$, $B = 0.3$ (Top) and $B = 0.4$ (Bottom) for $\frac{m}{\sqrt{s}_{peak}}$ between 0 and 0.45.

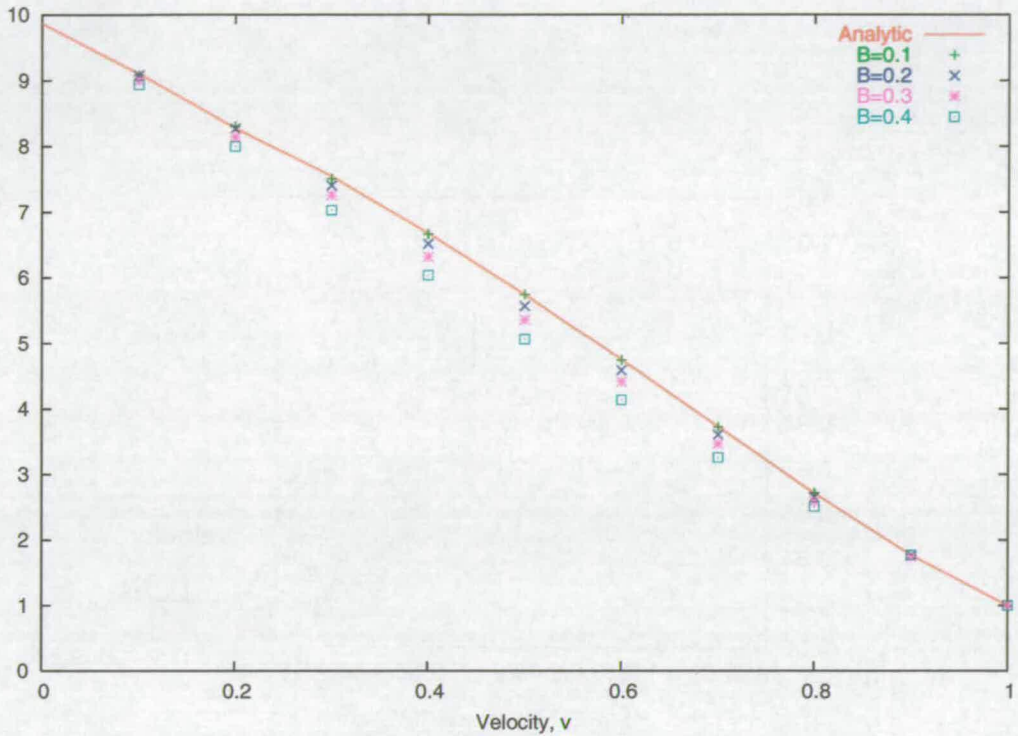


Figure 4.10.: Plot of correction produced for different values of B and velocity using the smooth smearing function.

dependence on the numerical values obtained. Results close to velocities of 0 and 1 are least dependent on the value for B as these are fixed points and least dependent on the mass. From the results obtained for $v = 1$ it can be seen that the results are independent of the smearing function used. Numerical instability prevents B from taking very small values and also appears to affect the accuracy of the calculations. This can be seen from the deviation of convergence to the analytic result as B is reduced to 0.05. The values obtained when $A = 0.9$ and $B = 0.1$ are within errors and as good as the values obtained using the top hat smearing function (Tab. 4.7).

The work described so far has all been in terms of velocities of particles and has shown that the numerical procedure produces results consistent with analytic values obtained over the full range of velocities. Although it has been useful to consider all the results in terms of the velocity, it is more normal to consider different centre of mass energies and masses of fermions. In addition, particles with velocities very much less than one could be strongly affected by higher order corrections. The processes producing low velocity particles are those created close to threshold.

4. Numerical Calculations

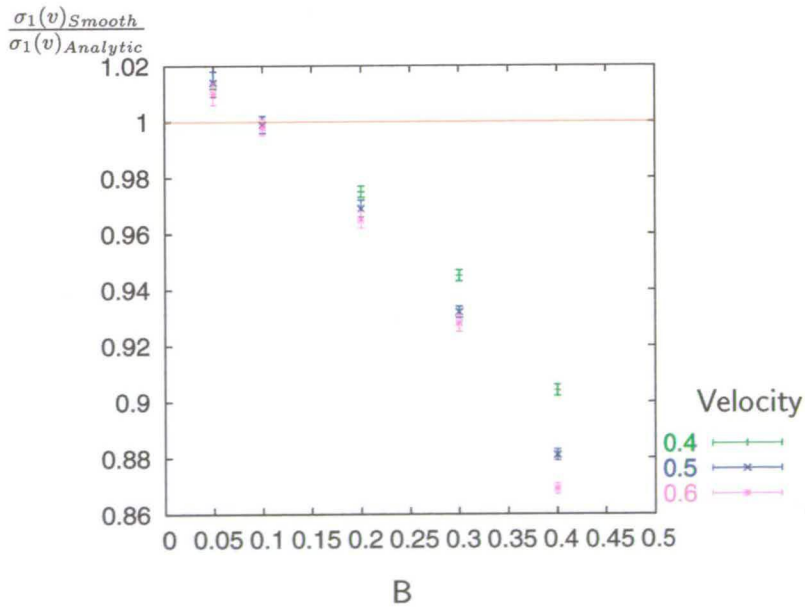
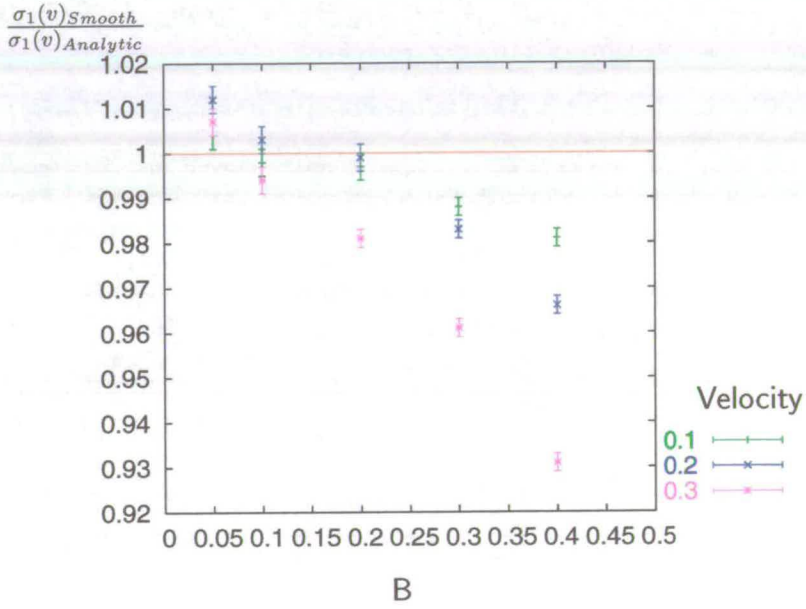


Figure 4.11.: Values of $\frac{\sigma_1(v)_{Smooth}}{\sigma_1(v)_{Analytic}}$ for B between 0.05 and 0.4, and v between 0.1 and 0.6

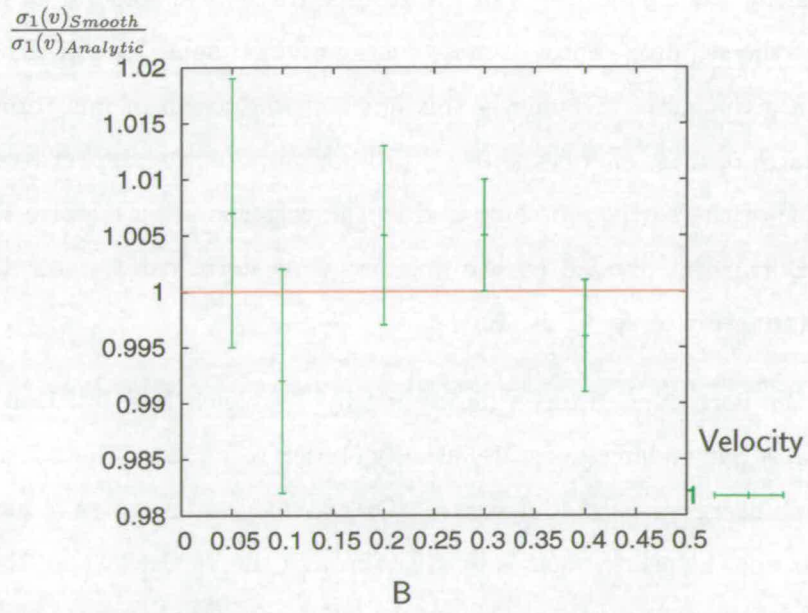
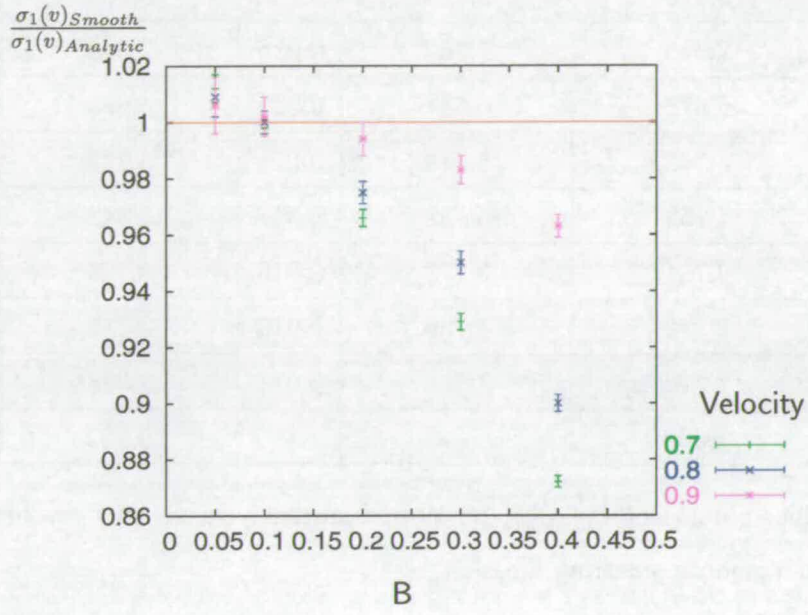


Figure 4.12.: Values of $\frac{\sigma_1(v)_{Smooth}}{\sigma_1(v)_{Analytic}}$ for B between 0.05 and 0.4, and v between 0.7 and 1

4. Numerical Calculations

| Velocity | $\left(\frac{\sigma_1(v)}{\sigma_0(v=1)}\right)_{Analytic}$ | $\left(\frac{\sigma_1(v)}{\sigma_0(v=1)}\right)_{Tophat}$ | Error | $\left(\frac{\sigma_1(v)}{\sigma_0(v=1)}\right)_{Smooth}$ | Error |
|----------|---|---|-------|---|-------|
| 0.1 | 9.105 | 9.110 | 0.010 | 9.083 | 0.026 |
| 0.2 | 8.275 | 8.325 | 0.013 | 8.303 | 0.022 |
| 0.3 | 7.545 | 7.560 | 0.016 | 7.503 | 0.020 |
| 0.4 | 6.678 | 6.651 | 0.020 | 6.663 | 0.018 |
| 0.5 | 5.743 | 5.726 | 0.016 | 5.738 | 0.016 |
| 0.6 | 4.753 | 4.738 | 0.017 | 4.742 | 0.013 |
| 0.7 | 3.731 | 3.773 | 0.016 | 3.725 | 0.012 |
| 0.8 | 2.719 | 2.726 | 0.013 | 2.718 | 0.011 |
| 0.9 | 1.773 | 1.785 | 0.011 | 1.778 | 0.012 |
| 1.0 | 1.000 | - | - | 0.992 | 0.010 |

Table 4.7.: Values obtained for $\frac{\sigma_1(v)}{\sigma_0(v=1)}$ obtained from analytic, velocity top hat smearing and a smooth smearing function.

By considering the fraction $\frac{m}{\sqrt{s}}$, all the results are kept as general as possible so one can choose the required centre of mass energy and get some idea of the correction produced for a given mass. Obviously this ignores production of jets through the Z channel for centre of mass energies above Z production. Another aspect to consider is the relative size of the correction compared to the corresponding massive Born term. The massive Born term divided by the massless Born term can be calculated quite easily and is a function of $\frac{m}{\sqrt{s}}$ (Tab. 4.8).

However, the correction term is multiplied by $\frac{\alpha_s}{\pi}$ which is a function of energy renormalised at a particular mass scale, usually chosen to be m_Z . There is a matter of choice for which energy is used to define α_s . One could use the centre of mass energy, however this is not the energy that is flowing through the vertices where the coupling takes place. Increasing the number of external particles for graphs without loops means less energy is flowing through the coupling, leading to higher values for the coupling constants. Between the energies of 1.2 GeV and M_Z , α_s is found to range between 0.35 and 0.12 by e^+e^- experiments [24]. Taking a value for the coupling constant of 0.25 the two particle cross section up to $\mathcal{O}(\alpha_s)$ normalised by the born cross section can be calculated for different values of $\frac{m}{\sqrt{s}}$ (Fig. 4.13).

4.3. Obtaining Numerical Results

| $\frac{m}{\sqrt{s}}$ | $\frac{\sigma_0(\frac{m}{\sqrt{s}})}{\sigma_0(\frac{m}{\sqrt{s}}=0)} + \frac{\alpha_s}{\pi} \frac{\sigma_1(\frac{m}{\sqrt{s}})}{\sigma_0(\frac{m}{\sqrt{s}}=0)}$ |
|----------------------|--|
| 0.00 | 1.079 |
| 0.05 | 1.082 |
| 0.10 | 1.091 |
| 0.15 | 1.104 |
| 0.20 | 1.122 |
| 0.25 | 1.141 |
| 0.30 | 1.162 |
| 0.35 | 1.175 |
| 0.40 | 1.170 |
| 0.45 | 1.119 |
| 0.50 | 0.785 |

$$\frac{\sigma_0(\frac{m}{\sqrt{s}})}{\sigma_0(\frac{m}{\sqrt{s}}=0)} + \frac{\alpha_s}{\pi} \frac{\sigma_1(\frac{m}{\sqrt{s}})}{\sigma_0(\frac{m}{\sqrt{s}}=0)}$$

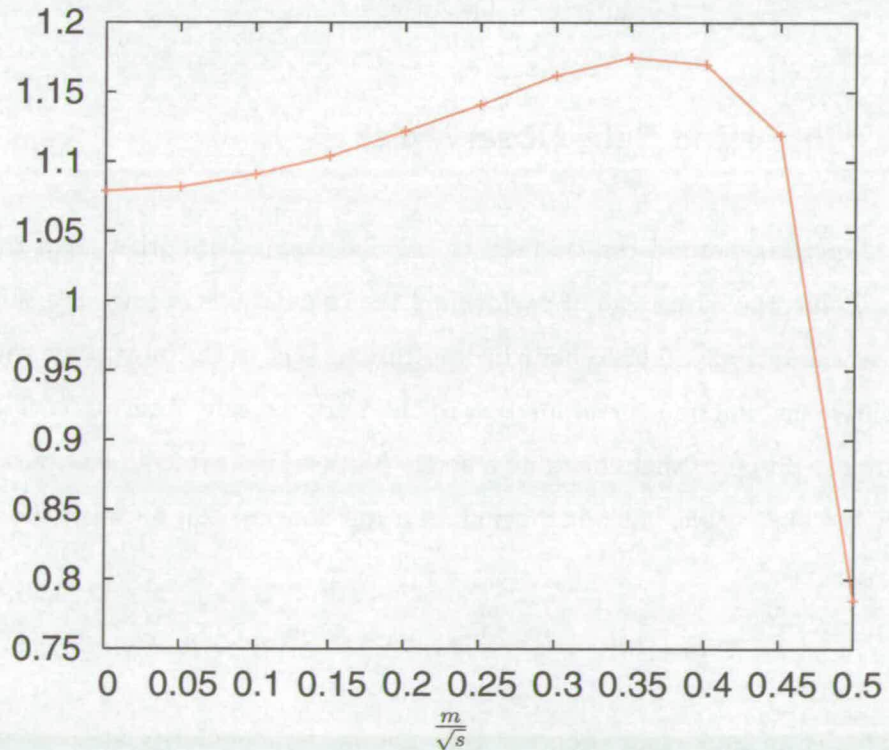


Figure 4.13.: The $\mathcal{O}(\alpha_s)$ two particle inclusive cross section for different values of $\frac{m}{\sqrt{s}}$ with $\alpha_s = 0.25$.

4. Numerical Calculations

| $\frac{m}{\sqrt{s}}$ | $\frac{\sigma_0(\frac{m}{\sqrt{s}})}{\sigma_0(\frac{m}{\sqrt{s}}=0)}$ | $\frac{\sigma_1(\frac{m}{\sqrt{s}})}{\sigma_0(\frac{m}{\sqrt{s}}=0)}$ | Error |
|----------------------|---|---|-------|
| 0 | 1.00000 | 0.99 | 0.01 |
| 0.05 | 0.99996 | 1.03 | 0.01 |
| 0.10 | 0.99939 | 1.15 | 0.01 |
| 0.15 | 0.99687 | 1.34 | 0.01 |
| 0.20 | 0.98984 | 1.66 | 0.01 |
| 0.25 | 0.97428 | 2.10 | 0.01 |
| 0.30 | 0.94400 | 2.74 | 0.01 |
| 0.35 | 0.88911 | 3.59 | 0.01 |
| 0.40 | 0.79200 | 4.75 | 0.01 |
| 0.45 | 0.61243 | 6.36 | 0.02 |
| 0.50 | 0.00000 | (π^2) | - |

Table 4.8.: Analytic values of $\frac{\sigma_0(\frac{m}{\sqrt{s}})}{\sigma_0(\frac{m}{\sqrt{s}}=0)}$ and numerical values of the coefficient of $\frac{\alpha_s}{\pi}$, $\frac{\sigma_1(\frac{m}{\sqrt{s}})}{\sigma_0(\frac{m}{\sqrt{s}}=0)}$, for different values of $\frac{m}{\sqrt{s}}$.

4.4. Infra-Red Safe Observables

The numerical method can be used to calculate quantities other than total cross sections. It has the advantage of performing the calculations of infra-red safe observables in a very simple way. This is done by multiplying each of the integrands with the desired measurement function corresponding to the infra-red safe observable. These functions satisfy the property that changing a single particle into two collinear particles does not affect the observable. This in turn gives a relationship [25] between the measurement functions used:

$$S_{n+1}(p_1, \dots, (1 - \lambda)p_n, \lambda p_n) = S_n(p_1, \dots, p_n) \quad . \quad (4.45)$$

This is an important property that allows the singularity analysis previously described to hold. A measurable quantity that can be used to produce a function that is infrared safe is the thrust [26, 27] which is described straightforwardly through the momentum of the final state particles:

$$\mathcal{T}_n(p_1, \dots, p_n) = \max(\vec{u}) \frac{\sum_i |\vec{p}_i \cdot \vec{u}|}{\sum_i |\vec{p}_i|} \quad . \quad (4.46)$$

As there are only two different final states, two particle and three particle, this reduces to two thrust functions:

$$\begin{aligned} \mathcal{T}_2(p_1, p_2) &= 1 \\ \mathcal{T}_3(p_1, p_2, p_3) &= \frac{2\max(|\vec{p}_1|, |\vec{p}_2|, |\vec{p}_3|)}{|\vec{p}_1| + |\vec{p}_2| + |\vec{p}_3|} . \end{aligned} \quad (4.47)$$

Due to conservation of momentum in the centre of mass frame the two particle final state always produce pencil like events. Whereas, the three particle final state can produce events ranging from three particles with an equal magnitude of momenta to two particle like events. Thus by momentum conservation the thrust can vary between two thirds and one for three particle final states. In general the thrust ranges between a half for spherical events and one for pencil like events. To get an idea of how much a contribution to the total cross section each value of thrust gives the differential of the cross section with respect to thrust can be performed for various values of thrust. As the calculations are to be performed numerically, it is more suitable to bin the events for a small range of thrusts (Tab. 4.9 and 4.10).

The thrust distribution highlights some properties of the leading order calculation. As the two particle final states can only produce events with a thrust of one, it can be seen that the three particle final states provide a positive contribution to the correction that increases as it approaches thrusts close to one. As $\frac{m}{\sqrt{s}}$ increases this contribution reduces. The two particle final states produce the most variation in contribution. For lower values of $\frac{m}{\sqrt{s}}$ the contribution is large and negative and as $\frac{m}{\sqrt{s}}$ increases so does the contribution becoming large and positive. To view how the correction affects the overall thrust distribution, the distribution can be combined with the lowest order quark anti-quark production and weighted against the total combined lowest and leading order correction (Appendix C).

The thrust distributions (Fig. 4.14) can be further changed by taking smaller bins for values of thrust close to one. However, in this region large logarithms exist and hadronisation corrections become large [28]. The bin size has the effect of smearing the contributions of the two and three particle final states in the final bin. To gain a better thrust distribution parton showering should be included to smooth the contributions more naturally. By taking the thrust average of this correction, the two particle contribution can be emphasised (Tab. 4.11).

4. Numerical Calculations

| Thrust Bin | $\frac{m}{\sqrt{s}}$ | | | | |
|------------|-----------------------|-----------------------|-----------------------|-----------------------|-----------------------|
| | 0.00 | 0.05 | 0.10 | 0.15 | 0.20 |
| 0.66-0.68 | 2.12×10^{-1} | 2.06×10^{-1} | 1.90×10^{-1} | 1.65×10^{-1} | 1.31×10^{-1} |
| 0.68-0.70 | 1.13×10^0 | 1.10×10^0 | 1.01×10^0 | 8.73×10^{-1} | 7.00×10^{-1} |
| 0.70-0.72 | 2.17×10^0 | 2.10×10^0 | 1.93×10^0 | 1.66×10^0 | 1.33×10^0 |
| 0.72-0.74 | 3.30×10^0 | 3.21×10^0 | 2.94×10^0 | 2.53×10^0 | 2.03×10^0 |
| 0.74-0.76 | 4.60×10^0 | 4.47×10^0 | 4.08×10^0 | 3.51×10^0 | 2.81×10^0 |
| 0.76-0.78 | 5.83×10^0 | 5.96×10^0 | 5.45×10^0 | 4.69×10^0 | 3.75×10^0 |
| 0.78-0.80 | 8.02×10^0 | 7.79×10^0 | 7.09×10^0 | 6.11×10^0 | 4.88×10^0 |
| 0.80-0.82 | 1.04×10^1 | 1.00×10^1 | 9.12×10^0 | 7.87×10^0 | 6.31×10^0 |
| 0.82-0.84 | 1.35×10^1 | 1.31×10^1 | 1.18×10^1 | 1.02×10^1 | 8.19×10^0 |
| 0.84-0.86 | 1.77×10^1 | 1.71×10^1 | 1.55×10^1 | 1.33×10^1 | 1.07×10^1 |
| 0.86-0.88 | 2.36×10^1 | 2.27×10^1 | 2.06×10^1 | 1.75×10^1 | 1.43×10^1 |
| 0.88-0.90 | 3.24×10^1 | 3.11×10^1 | 2.80×10^1 | 2.38×10^1 | 1.95×10^1 |
| 0.90-0.92 | 4.58×10^1 | 4.39×10^1 | 3.93×10^1 | 3.36×10^1 | 2.73×10^1 |
| 0.92-0.94 | 6.94×10^1 | 6.63×10^1 | 5.86×10^1 | 4.98×10^1 | 4.09×10^1 |
| 0.94-0.96 | 1.18×10^2 | 1.11×10^2 | 9.76×10^1 | 8.26×10^1 | 6.75×10^1 |
| 0.96-0.98 | 2.54×10^2 | 2.36×10^2 | 2.04×10^2 | 1.70×10^2 | 1.38×10^2 |
| 0.98-1.00 | -5.61×10^2 | -5.24×10^2 | -3.95×10^2 | -3.62×10^2 | -2.66×10^2 |

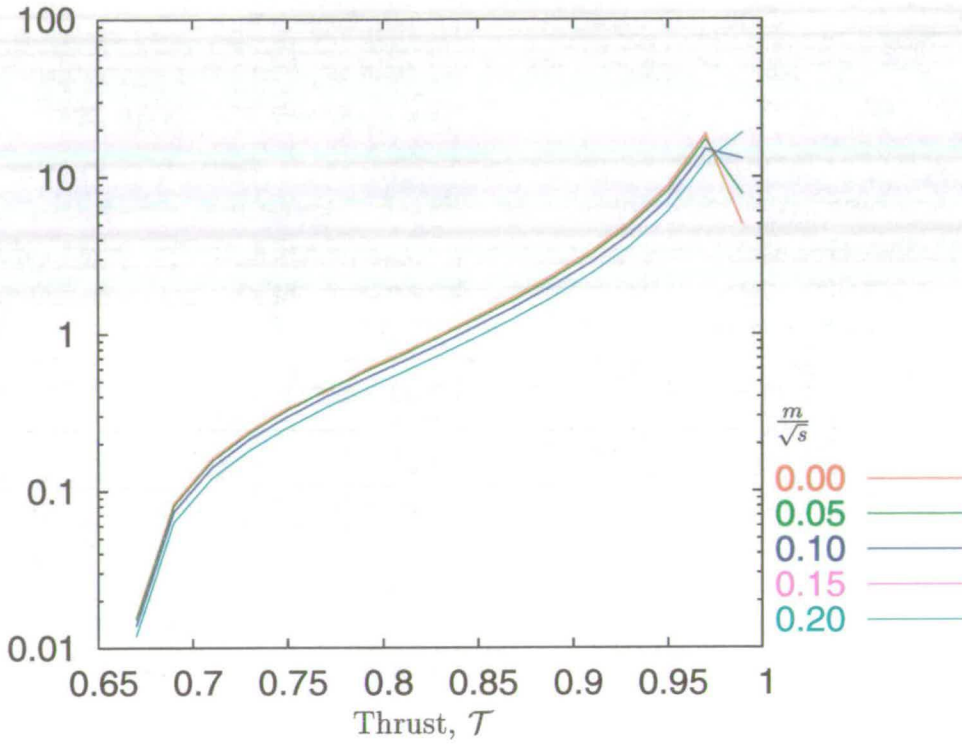
Table 4.9.: Values of the coefficient of $\frac{\alpha_s}{\pi}$ for different thrusts in bins for values of $\frac{m}{\sqrt{s}}$ between 0 and 0.20.

| Thrust Bin | $\frac{m}{\sqrt{s}}$ | | | | |
|------------|-----------------------|-----------------------|-----------------------|-----------------------|-----------------------|
| | 0.25 | 0.30 | 0.35 | 0.40 | 0.45 |
| 0.66-0.68 | 9.70×10^{-2} | 6.72×10^{-2} | 3.30×10^{-2} | 1.17×10^{-2} | 1.58×10^{-3} |
| 0.68-0.70 | 5.13×10^{-1} | 3.34×10^{-1} | 1.77×10^{-1} | 6.12×10^{-2} | 8.25×10^{-3} |
| 0.70-0.72 | 9.82×10^{-1} | 6.36×10^{-1} | 3.38×10^{-1} | 1.20×10^{-1} | 1.81×10^{-2} |
| 0.72-0.74 | 1.49×10^0 | 9.74×10^{-1} | 5.16×10^{-1} | 1.85×10^{-1} | 2.79×10^{-2} |
| 0.74-0.76 | 2.08×10^0 | 1.36×10^0 | 7.16×10^{-1} | 2.70×10^{-1} | 3.70×10^{-2} |
| 0.76-0.78 | 2.77×10^0 | 1.82×10^0 | 9.92×10^{-1} | 4.05×10^{-1} | 5.89×10^{-2} |
| 0.78-0.80 | 3.64×10^0 | 2.40×10^0 | 1.35×10^0 | 5.21×10^{-1} | 9.29×10^{-2} |
| 0.80-0.82 | 4.72×10^0 | 3.16×10^0 | 1.83×10^0 | 7.50×10^{-1} | 1.34×10^{-1} |
| 0.82-0.84 | 6.18×10^0 | 4.19×10^0 | 2.45×10^0 | 1.02×10^0 | 1.92×10^{-1} |
| 0.84-0.86 | 8.10×10^0 | 5.58×10^0 | 3.35×10^0 | 1.51×10^0 | 3.05×10^{-1} |
| 0.86-0.88 | 1.09×10^1 | 7.67×10^0 | 4.66×10^0 | 2.17×10^0 | 4.81×10^{-1} |
| 0.88-0.90 | 1.49×10^1 | 1.06×10^1 | 6.52×10^0 | 3.21×10^0 | 7.89×10^{-1} |
| 0.90-0.92 | 2.11×10^1 | 1.52×10^1 | 9.75×10^0 | 4.86×10^0 | 1.29×10^0 |
| 0.92-0.94 | 3.19×10^1 | 2.34×10^1 | 1.52×10^1 | 7.84×10^0 | 2.37×10^0 |
| 0.94-0.96 | 5.26×10^1 | 3.89×10^1 | 2.56×10^1 | 1.38×10^1 | 4.17×10^0 |
| 0.96-0.98 | 1.08×10^2 | 8.01×10^1 | 5.34×10^1 | 3.00×10^1 | 1.00×10^1 |
| 0.98-1.00 | -1.65×10^2 | -6.08×10^1 | 5.22×10^0 | 1.70×10^2 | 2.99×10^2 |

Table 4.10.: Values of the coefficient of $\frac{\alpha_s}{\pi}$ for different thrusts in bins for values of $\frac{m}{\sqrt{s}}$ between 0.25 and 0.45.

4. Numerical Calculations

$$\frac{1}{\sigma} \frac{d\sigma}{dT}$$



$$\frac{1}{\sigma} \frac{d\sigma}{dT}$$

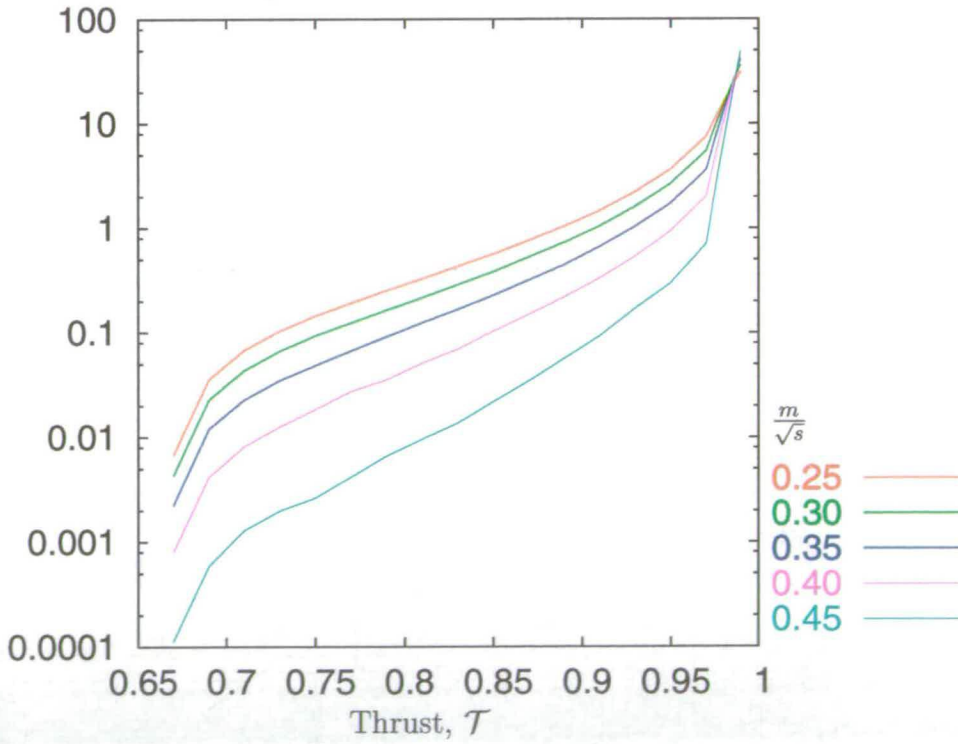


Figure 4.14.: Combined $\mathcal{O}(1)$ and $\mathcal{O}(\alpha_s)$ values of thrust in different bins for values of $\frac{m}{\sqrt{s}}$ between 0 and 0.45.

| $\frac{m}{\sqrt{s}}$ | Weighted Thrust | Error |
|----------------------|-----------------|-------|
| 0 | -0.04 | 0.01 |
| 0.05 | -0.03 | 0.01 |
| 0.10 | 0.06 | 0.01 |
| 0.15 | 0.30 | 0.01 |
| 0.20 | 0.62 | 0.01 |
| 0.25 | 1.06 | 0.01 |
| 0.30 | 1.65 | 0.01 |
| 0.35 | 2.41 | 0.01 |
| 0.40 | 3.38 | 0.01 |

Table 4.11.: Weighted thrust average for different values of $\frac{m}{\sqrt{s}}$.

Another way of examining the two particle and three particle contributions is through jet algorithms. As mentioned in chapter two, two of the commonly used algorithms are the JADE and Durham algorithms. They both set a limit on what is recognised as a two jet or three jet event according to a given parameter, y_{cut} , that can be fixed between zero and one, where one includes all contributions from the three particle final states and zero includes only those in the two particle limit. However the way y_{cut} is defined for each algorithm is slightly different. The JADE algorithm looks at the four-momentum dot product between particles and if they are all less than a predetermined fraction of the centre of mass energy then it is classed as a three jet event:

$$\begin{aligned}
 y_{cut_{ij}}^J &= \frac{2p_i \cdot p_j}{s} \\
 &= \frac{2E_i E_j}{s} (1 - \cos \theta_{ij}) \quad .
 \end{aligned}
 \tag{4.48}$$

The Durham algorithm, in contrast, replaces the energies of the particle by the smallest energy of the particles to be considered and then proceeds as the JADE algorithm:

$$y_{cut_{ij}}^D = \frac{2\min(E_i^2, E_j^2)}{s} (1 - \cos \theta_{ij}) \quad .
 \tag{4.49}$$

Using the same y_{cut} parameters, the two algorithms predict different contributions to a two jet process. The JADE algorithm (Tab. 4.12) is more affected by the contri-

4. Numerical Calculations

| y_{cut} | $\frac{m}{\sqrt{s}}$ | | | | | | | | | |
|-----------|----------------------|-------|-------|-------|-------|------|------|------|------|------|
| | 0.00 | 0.05 | 0.10 | 0.15 | 0.20 | 0.25 | 0.30 | 0.35 | 0.40 | 0.45 |
| 1.000 | 0.99 | 1.03 | 1.15 | 1.34 | 1.66 | 2.10 | 2.74 | 3.59 | 4.75 | 6.36 |
| 0.200 | 0.87 | 0.92 | 1.07 | 1.31 | 1.69 | 2.18 | 2.84 | 3.67 | 4.78 | 6.36 |
| 0.100 | 0.30 | 0.40 | 0.67 | 1.11 | 1.70 | 2.35 | 3.11 | 3.95 | 4.97 | 6.40 |
| 0.075 | -0.44 | -0.30 | 0.09 | 0.67 | 1.08 | 2.17 | 3.05 | 4.03 | 5.10 | 6.44 |
| 0.050 | -1.83 | -1.61 | -1.03 | -0.23 | 0.70 | 1.7 | 2.78 | 3.94 | 5.16 | 6.52 |
| 0.025 | -5.06 | -4.58 | -3.54 | -2.28 | -0.90 | 0.53 | 1.96 | 3.54 | 5.06 | 6.65 |

Table 4.12.: Coefficient of $\frac{\alpha_s}{\pi}$ for different values of y_{cut} and $\frac{m}{\sqrt{s}}$ using the JADE jet algorithm.

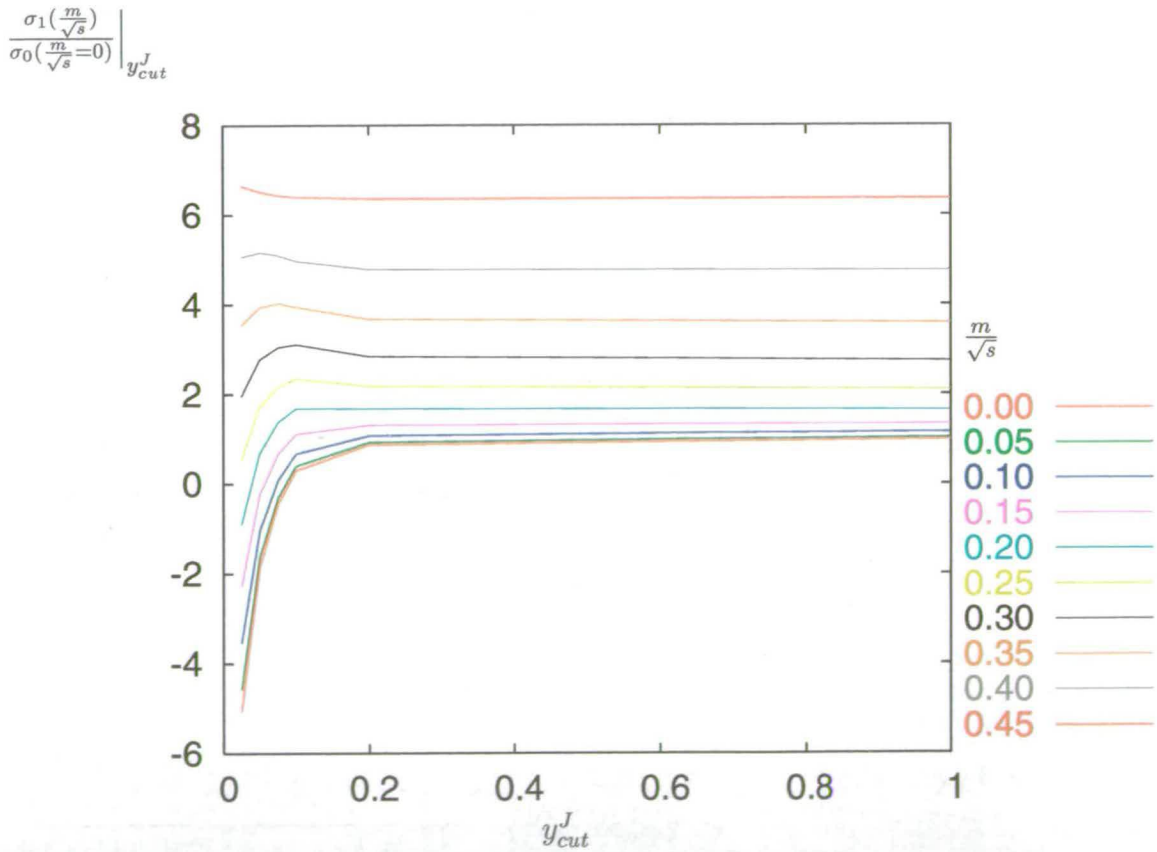


Figure 4.15.: Coefficient of $\frac{\alpha_s}{\pi}$ for different values of y_{cut} and $\frac{m}{\sqrt{s}}$ using the JADE algorithm

| y_{cut} | $\frac{m}{\sqrt{s}}$ | | | | | | | | | |
|-----------|----------------------|-------|-------|-------|------|------|------|------|------|------|
| | 0.00 | 0.05 | 0.10 | 0.15 | 0.20 | 0.25 | 0.30 | 0.35 | 0.40 | 0.45 |
| 1.000 | 0.99 | 1.03 | 1.15 | 1.34 | 1.66 | 2.10 | 2.74 | 3.59 | 4.75 | 6.36 |
| 0.200 | 0.94 | 0.98 | 1.11 | 1.32 | 1.65 | 2.13 | 2.77 | 3.60 | 4.75 | 6.36 |
| 0.100 | 0.74 | 0.80 | 0.99 | 1.28 | 1.71 | 2.24 | 2.89 | 3.69 | 4.77 | 6.36 |
| 0.075 | 0.51 | 0.57 | 0.81 | 1.17 | 1.67 | 2.26 | 2.93 | 3.74 | 4.79 | 6.36 |
| 0.050 | -0.03 | 0.09 | 0.38 | 0.87 | 1.48 | 2.17 | 2.93 | 3.79 | 4.84 | 6.36 |
| 0.025 | -1.47 | -1.28 | -0.75 | -0.01 | 0.82 | 1.70 | 2.67 | 3.74 | 4.91 | 6.38 |

Table 4.13.: Coefficient of $\frac{\alpha_s}{\pi}$ for different values of y_{cut} and $\frac{m}{\sqrt{s}}$ using the Durham jet algorithm.

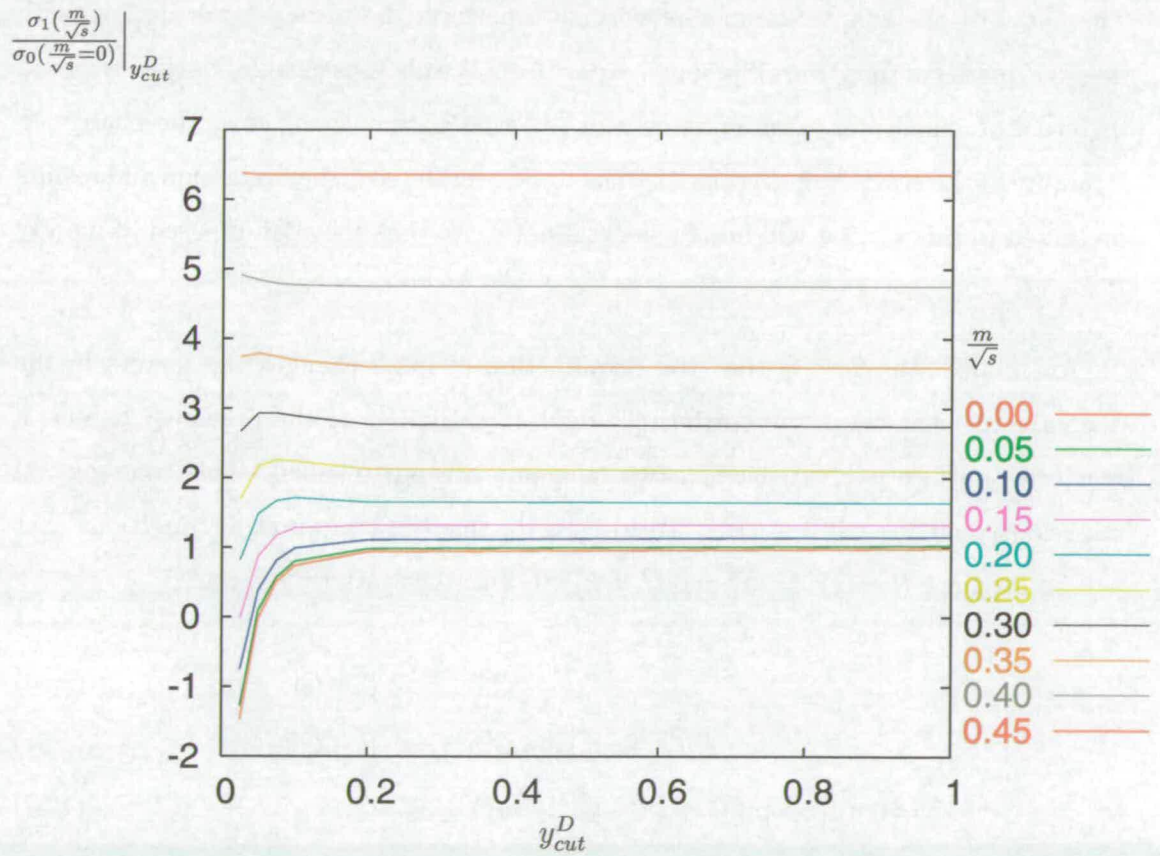


Figure 4.16.: Coefficient of $\frac{\alpha_s}{\pi}$ for different values of y_{cut} and m keeping $\sqrt{s} = 100$ using the Durham algorithm

4. Numerical Calculations

butions of two particle final states than the Durham algorithm (Tab. 4.13). When $\frac{m}{\sqrt{s}}$ is small, small values of y_{cut} and lead to a negative contribution to two jet production. It also means that for certain parameters there is a zero contribution from the strong corrections. For the larger values of $\frac{m}{\sqrt{s}}$ the correction is less dependent on the y_{cut} parameter for both algorithms. To see the effect of using different values of y_{cut} on the two jet cross section, the ratio between the Born cross section plus the contribution for a particular value of y_{cut} and the complete up to $\mathcal{O}(\alpha_s)$ jet calculation can be determined for both the JADE (Fig. 4.17) and Durham (Fig. 4.18) jet algorithms.

4.5. Ground Work for Future Calculations

The next obvious adaptation of this work is to perform the three jet calculations with massive quarks in the Beowulf scheme. Apart from the obvious changes to the integrand in terms of numerator, denominator and renormalisation conditions, the change in structure of the scattering singularities has to be considered. The discussion and results presented in this section will be of a general nature so that they can be used to modify Beowulf.

An immediate effect is that the introduction of mass changes the factors in the denominator that cause the scattering singularity. Similar to the previous chapter, a scattering surface is created when two momenta are put on-shell. This time general masses m_1 and m_2 will be used. To investigate this the two on shell conditions that will be used are $(l - Q)^2 = m_1^2$ and $l^2 = m_2^2$ to find the scattering surface:

$$(l^0 - Q^0)^2 = |\vec{l} - \vec{Q}|^2 + m_1^2 \quad (4.50)$$

$$((|\vec{l}|^2 + m_2^2)^{\frac{1}{2}} - Q^0)^2 = |\vec{l} - \vec{Q}|^2 + m_1^2 \quad (4.51)$$

$$\implies (|\vec{l}|^2 + m_2^2)^{\frac{1}{2}} + (|\vec{l} - \vec{Q}|^2 + m_1^2)^{\frac{1}{2}} = Q^0 \quad (4.52)$$

It is difficult to see what the shape of the scattering singularity is using this representation. A simple method for determining the shape is to get rid of the square roots and take \vec{Q} to lie on the z axis of the loop momentum. Performing this operation one finds that the scattering singularities are once again ellipses, but the foci and size of

4. Numerical Calculations

| y_{cut} | $\frac{m}{\sqrt{s}}$ | | | | | | | | | |
|-----------|----------------------|-------|-------|-------|-------|-------|-------|-------|-------|-------|
| | 0.00 | 0.05 | 0.10 | 0.15 | 0.20 | 0.25 | 0.30 | 0.35 | 0.40 | 0.45 |
| 1.000 | 1.000 | 1.000 | 1.000 | 1.000 | 1.000 | 1.000 | 1.000 | 1.000 | 1.000 | 1.000 |
| 0.200 | 0.998 | 0.998 | 0.999 | 0.999 | 1.000 | 1.001 | 1.001 | 1.000 | 1.000 | 1.000 |
| 0.100 | 0.991 | 0.991 | 0.994 | 0.998 | 1.002 | 1.005 | 1.006 | 1.004 | 1.001 | 1.000 |
| 0.075 | 0.982 | 0.983 | 0.988 | 0.994 | 1.001 | 1.006 | 1.007 | 1.005 | 1.002 | 1.000 |
| 0.050 | 0.962 | 0.965 | 0.971 | 0.983 | 0.994 | 1.003 | 1.007 | 1.007 | 1.003 | 1.000 |
| 0.025 | 0.907 | 0.913 | 0.929 | 0.950 | 0.969 | 0.985 | 0.997 | 1.005 | 1.006 | 1.001 |

$$\frac{\sigma(\frac{m}{\sqrt{s}})}{\sigma_0(\frac{m}{\sqrt{s}}=0)} \Big|_{y_{cut}^D}$$

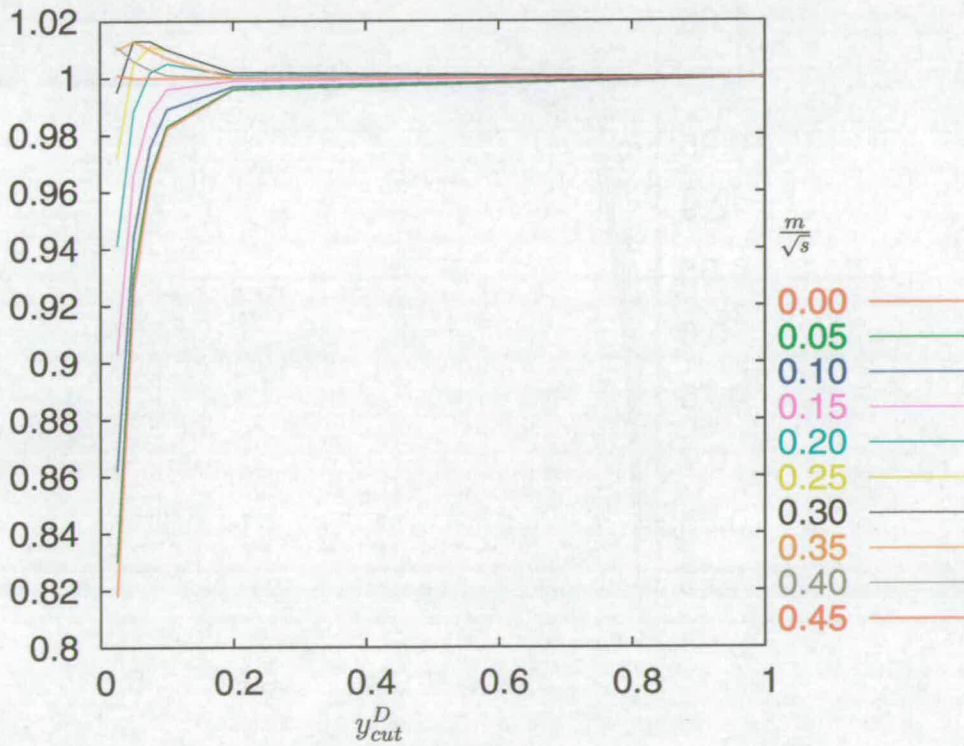


Figure 4.18.: Weighted jet cross section for different values of y_{cut} against combined $\mathcal{O}(1)$ and $\mathcal{O}(\alpha_s)$ cross section using the Durham algorithm.

| y_{cut} | $\frac{m}{\sqrt{s}}$ | | | | | | | | | |
|-----------|----------------------|-------|-------|-------|-------|-------|-------|-------|-------|-------|
| | 0.00 | 0.05 | 0.10 | 0.15 | 0.20 | 0.25 | 0.30 | 0.35 | 0.40 | 0.45 |
| 1.000 | 1.000 | 1.000 | 1.000 | 1.000 | 1.000 | 1.000 | 1.000 | 1.000 | 1.000 | 1.000 |
| 0.200 | 0.996 | 0.996 | 0.997 | 0.999 | 1.001 | 1.003 | 1.004 | 1.003 | 1.001 | 1.000 |
| 0.100 | 0.974 | 0.976 | 0.982 | 0.992 | 1.002 | 1.009 | 1.014 | 1.013 | 1.009 | 1.002 |
| 0.075 | 0.946 | 0.950 | 0.960 | 0.975 | 0.990 | 1.003 | 1.011 | 1.017 | 1.014 | 1.003 |
| 0.050 | 0.894 | 0.901 | 0.919 | 0.942 | 0.966 | 0.985 | 1.001 | 1.013 | 1.016 | 1.007 |
| 0.025 | 0.773 | 0.789 | 0.825 | 0.866 | 0.906 | 0.943 | 0.971 | 0.998 | 1.012 | 1.013 |

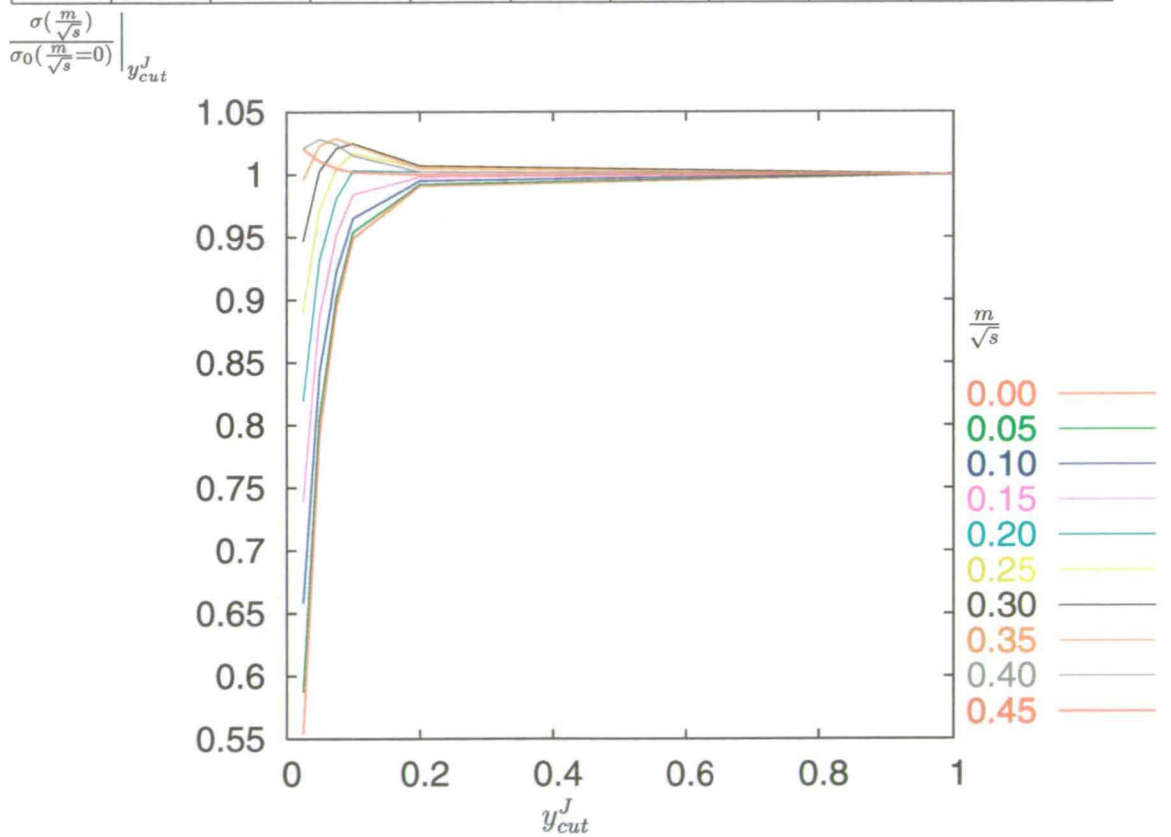


Figure 4.17.: Weighted jet cross section for different values of y_{cut} against combined $\mathcal{O}(1)$ and $\mathcal{O}(\alpha_s)$ cross section using the JADE algorithm.

the ellipse are a function of the masses and the momenta:

$$\begin{aligned} (r^2 + z^2 + m_2^2)^{\frac{1}{2}} + (r^2 + (z - Q)^2 + m_1^2)^{\frac{1}{2}} &= Q^0 \\ \implies \frac{(z + d)^2}{a^2} + \frac{r^2}{b^2} &= c^2 \end{aligned} \tag{4.53}$$

$$\begin{aligned} a &= Q^0 \\ b &= ((Q^0)^2 - Q^2)^{\frac{1}{2}} \\ c &= \frac{(((Q^0)^2 - Q^2)^2 + m_1^4 + m_2^4 - 2((Q^0)^2 - Q^2)m_1^2 - 2((Q^0)^2 - Q^2)m_2^2 - 2m_1^2m_2^2)^{\frac{1}{2}}}{2((Q^0)^2 - Q^2)} \\ d &= \frac{Q((Q^0)^2 - Q^2 + m_1^2 - m_2^2)}{2((Q^0)^2 - Q^2)} \end{aligned} \tag{4.54}$$

The values of a , b , c and d can be used to define the length of the major axis, minor axis and the centre of the ellipse given by ac , bc and $z = -d$ respectively. Using standard relations of the ellipse the foci are located at $-d \pm \sqrt{(ac)^2 - (bc)^2}$. This then gives the forms for A_+ and A_- required for an orthogonal elliptical coordinate system where the scattering singularity occurs at $A_+ = \frac{a}{\sqrt{a^2 + b^2}}$:

$$\begin{aligned} A_{\pm} &= \frac{1}{2\sqrt{(ac)^2 + (bc)^2}} \\ &\times ((z + d - \sqrt{(ac)^2 + (bc)^2})^2 + r^2)^{\frac{1}{2}} \pm (z + d + \sqrt{(ac)^2 + (bc)^2})^2 + r^2)^{\frac{1}{2}} \end{aligned} \tag{4.55}$$

The need for contour deformation appears because of the type of calculation being performed. As the three jet calculation at next to leading order does not contain all possible cuts of the three loop QCD correction to the photon, the integrands that provide the required cancellations for the scattering singularities are not generated. Within the set graphs there are a few that do not require contour deformation, namely those that have two self energies or corrections to one of the parent quarks. As well as the scattering singularity not all of the collinear singularities would cancel in as neat a way either as the two loop corrections to two parton production would not be included. The cancellations not catered for will be cut out by the jet algorithm that will remove the two jet-like processes. If all the possible cuts were used, then the complete $\mathcal{O}(\alpha_s^2)$ two jet process would also be calculated.

5. Conclusions

This thesis has explored the calculations of the leading order perturbative corrections to the production of two jet processes. An analysis of the photon decay into two massless quarks has been given with attention paid to analytic properties of scattering processes. With analytic results of the massless and massive two jet processes in mind, an alternative numerical method of calculation akin to the procedure developed by Soper was sought after. The principles behind numerical integrations were discussed along with the different methods for enhancing the numerical integration procedure. By extracting the tools developed in the Beowulf program, adapting and utilising them, numerical integrations of perturbative processes can be performed in conjunction with VEGAS. Other adaptations for further work have also been considered.

The major aim of the thesis was to establish the viability of extending the Beowulf procedure to include massive quarks. From the work performed, the viability has been established up to an approximation. As the corrections due to massive quarks depend on the centre of mass energy, and the smearing function varies with energy, then for an arbitrary smearing function only an approximation can be gained. Results obtained showed good agreement for the smearing functions used and as it is a numerical integration, there is a degree of approximation inherent to the procedure. The real issue of the accuracy is how important it is compared to the experimental measurements and the corrections due to the neglected higher order corrections. It is possible to use a smearing function that would analytically produce the actual correction but this would require a smearing function that depends on the analytic result that is to be found. This approach seems to defeat the object in terms of the simplicity of the procedure.

Investigating this problem has led to a variation of the Beowulf code being created.

5. Conclusions

The procedure used has had several benefits in terms of diagnostic and calculating purposes. Each graph could be considered separately and the convergence of the integrals checked. This allowed the ‘catching’ of spurious terms and the checking of divergence cancellation. As a different numerical integration is required for each choice of coordinates, an error in one of the integrations points towards an error in soft cancellation. Having multiple integrals gives greater control over the required accuracy of the integration. Beowulf controls errors through the specification of length of time for computation. Using VEGAS each integral can be computed to a required accuracy, which is useful when contributions from different integrals differ in size so the absolute error of each integrand compared to the sum of the integrals is important. There is still an element of judgement required using VEGAS when choosing sample sizes and the number of iterations for both the warm up integrations and main integration routines. Choosing too few points per sample can lead to ignoring parts of the sample space that are quite important while choosing too many can result in sampling regions that are strongly affected by cancellations between integrands and the inherent finite accuracy of the computer.

The introduction of massive quarks and the use of VEGAS has required some technical additions to the Beowulf arsenal. Beowulf’s ‘bare hands’ approach led to the integration of integrals on ‘face value’. Difficulties due to large cancellations around soft points are dealt with using cuts on the domain of integration. Because the integrand is finite, it would be nice to numerically integrate without cuts. For this to work using VEGAS a much more sensitive approach has to be employed as it homes in on the parts of integrals that have the most variance. This has been done by finding equivalent representations for the graph containing the self energy. To begin with the self energy has been manipulated using scalar decomposition. Large cancellations between terms generated required finding numerically equivalent integrands that preserved the singularity structure. This had a knock on effect on the three particle cuts that required manipulation to obtain the same spinor structure as the self energy.

By considering this particular process insight into the nature of the scattering singularities has been provided. Treatment of the scattering singularities in the Beowulf program used contour deformation to render the integrals finite. This process, however, shows that there are cancellations of scattering singularities. For certain graphs

in the three jet process described by Beowulf, use of this fact can remove some calculating burden of using complex momenta. There still remain scattering singularities in the three jet calculation, but this is because only the three and four particle cuts are included.

To improve this procedure so that quantities calculated are physically more significant, the work on the Coulomb gauge for the gluon and parton showering as now used in Beowulf should be included. The Coulomb gauge will affect the structure of the integrands and so more work on the representation of the integrands may be required. Parton showering which does not affect the soft, collinear or scattering singularities should not pose a problem in terms of implementation and should make the thrust distributions more realistic as it will smooth the contributions due to the two and three particle cuts.

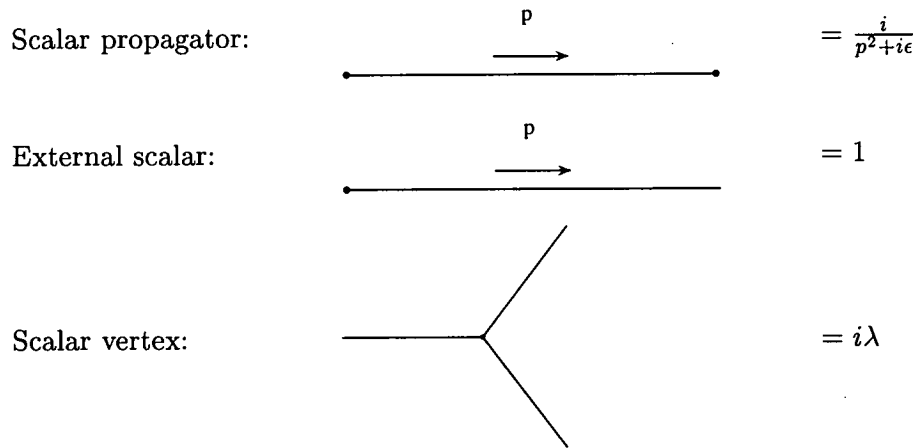
Including massive partons at $\mathcal{O}(\alpha_s^2)$ using the Coulomb gauge and parton showering will obviously further improve the physical calculations. To do this it would be better to incorporate the integrand manipulations discussed in this study into the Beowulf scheme as it contains the methods to cater for the scattering singularities and can cope with complex momenta. This method just needs adapting to take into consideration the shapes of the scattering singularities as discussed in the previous chapter. The full $\mathcal{O}(\alpha_s^2)$ calculation including the two loop contributions should contain sufficient cancellations between scattering singularities, however, this would require investigation.

In summary, massive particles can be included in numerical perturbative calculations. There is also plenty of scope for further investigation and development of this technique to explore the properties of particles as observed in particle physics experiments.

A. Feynman Rules

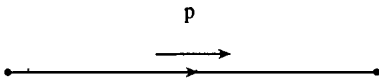
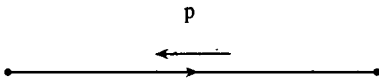
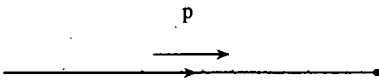
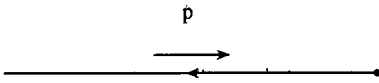
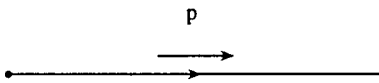
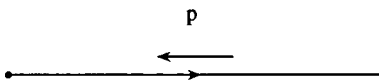
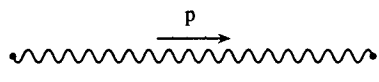
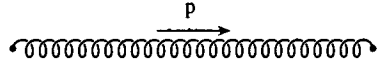
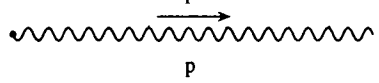
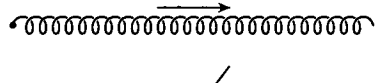
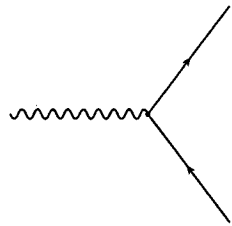
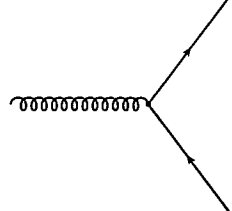
The Feynman rules for the gluons and quarks presented in this appendix have their colour algebra suppressed apart from the quark-antiquark-gluon vertex where the colour matrix T_{ij}^a has been written explicitly. To complete the rules, the quark and gluon propagator need to be multiplied by δ_{ij} and δ^{ab} respectively.

A.1. ϕ^3 Rules



A. Feynman Rules

A.2. Required rules for QED and QCD

| | | |
|------------------------------------|---|---|
| Fermion propagator: |  | $= \frac{i(\not{p}+m)}{p^2-m^2+i\epsilon}$ |
| Antifermion propagator: |  | $= \frac{i(-\not{p}+m)}{p^2-m^2+i\epsilon}$ |
| Incoming fermions: |  | $= u(p)$ |
| Incoming antifermions: |  | $= \bar{v}(p)$ |
| Outgoing fermions: |  | $= \bar{u}(p)$ |
| Outgoing antifermions: |  | $= v(p)$ |
| Boson propagators: |  | $= \frac{-i}{p^2+i\epsilon} \left(g^{\mu\nu} - \eta \frac{p^\mu p^\nu}{p^2} \right)$ |
| |  | $\eta = +1, \text{ Landau gauge}$ |
| External bosons: |  | $= \epsilon^\mu(p)$ |
| |  | |
| Fermion-antifermion-photon vertex: |  | $= iQ_e \gamma^\mu$ |
| Quark-antiquark-gluon vertex: |  | $= igT_{ij}^a \gamma^\mu$ |

- Introduce a factor of minus one for every closed fermion loop.

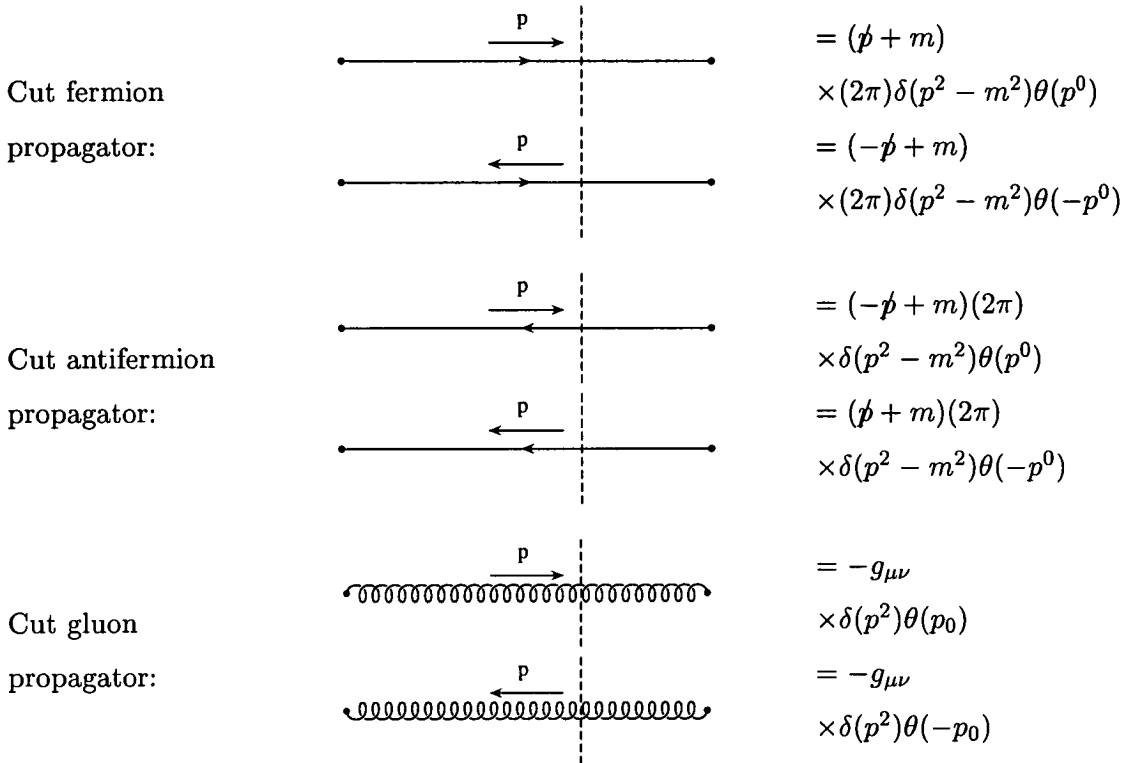
A.3. Cutkosky Cutting Rules in the Feynman Gauge

- Include an integral,

$$\int \frac{dl}{(2\pi)^n} , \quad (\text{A.1})$$

for each loop momentum.

A.3. Cutkosky Cutting Rules in the Feynman Gauge



- Complex conjugate all the propagators and vertices on the right hand side of the cut.
- Introduce a factor of minus one for every fermion loop even if it is cut.

Alternatively the standard Feynman rules can be used to write the un-cut graph then the following rules applied:

- For the propagators crossing the cuts replace the factors of,

$$\frac{i}{p^2 - m^2 + i\epsilon} \quad (\text{A.2})$$

A. Feynman Rules

with,

$$(2\pi)\delta(p^2 - m^2)\theta(\pm p^0) \tag{A.3}$$

where $\pm p^0$ is positive if the momentum is pointing to the right across the cut and negative if pointing left.

- Introduce a factor of minus one for each closed fermion loop even if it is cut.

B. Integrand Algebra

B.1. Gamma Matrices in n Dimensions

Using the defining commutation relation for the γ matrices in n dimensions,

$$\{\gamma^\mu, \gamma^\nu\} = 2g^{\mu\nu} \quad . \quad (\text{B.1})$$

relations for the contracted gamma matrices,

$$\gamma^\mu \gamma_\mu = n \quad (\text{B.2})$$

$$\gamma^\mu \gamma^\rho \gamma_\mu = (2 - n)\gamma^\rho \quad (\text{B.3})$$

$$\gamma^\mu \gamma^\rho \gamma^\sigma \gamma_\mu = 4g^{\rho\sigma} + (n - 4)\gamma^\rho \gamma^\sigma \quad (\text{B.4})$$

$$\gamma^\mu \gamma^\nu \gamma^\rho \gamma^\sigma \gamma_\mu = -2\gamma^\sigma \gamma^\rho \gamma^\nu - (n - 4)\gamma^\nu \gamma^\rho \gamma^\sigma \quad (\text{B.5})$$

and traced gamma matrices,

$$\text{Tr}(\gamma^\mu \gamma^\nu) = 4g^{\mu\nu} \quad (\text{B.6})$$

$$\text{Tr}(\gamma^\mu \gamma^\nu \gamma^\rho \gamma^\sigma) = 4(g^{\mu\nu} g^{\rho\sigma} - g^{\mu\rho} g^{\nu\sigma} + g^{\mu\sigma} g^{\nu\rho}) \quad (\text{B.7})$$

can be obtained.

B.2. Feynman Parameters

Denominators of an integrand can be combined simply using Feynman parameters, $x_1 \cdots x_n$, through integration [7]:

$$\frac{1}{A_1^{m_1} A_2^{m_2} \cdots A_n^{m_n}} = \int_0^1 dx_1 \cdots dx_n \delta(\sum x_i - 1) \frac{\prod x_i^{m_i - 1}}{[\sum x_i A_i]^{\sum m_i}} \frac{\Gamma(m_1 + \cdots + m_n)}{\Gamma(m_1) \cdots \Gamma(m_n)} \quad . \quad (\text{B.8})$$

B.3. n Dimensional Integrals

To evaluate n dimensional integrals it is useful to be able to integrate the redundant angular integrals. Consider

$$\begin{aligned}
 (\sqrt{\pi})^n &= \left(\int dx e^{-x^2} \right)^n \\
 &= \int d^n x \exp \left(- \sum_{i=1}^n x_i^2 \right) \\
 &= \int d\Omega_n \int_0^\infty dr r^{n-1} e^{-r^2} \\
 &= \frac{1}{2} \int d\Omega_n \int_0^\infty d(r^2) (r^2)^{\frac{n}{2}-1} e^{-r^2} \\
 &= \frac{1}{2} \int d\Omega_n \int_0^\infty dy y^{\frac{n}{2}-1} e^{-y} \tag{B.9}
 \end{aligned}$$

$$= \frac{1}{2} \int d\Omega_n \Gamma\left(\frac{n}{2}\right) \tag{B.10}$$

$$\Rightarrow \int d\Omega_n = \frac{2\pi^{\frac{n}{2}}}{\Gamma(\frac{n}{2})} \tag{B.11}$$

This can then be used to integrate the momentum integrals in n -spherical polar coordinates:

$$\int \frac{d^n K}{(2\pi)^n} \frac{K^{2M}}{(K^2 + \Delta)^L} = \int \frac{d\Omega_n}{(2\pi)^n} \int dK \frac{K^{2M+n-1}}{(K^2 + \Delta)^L} \tag{B.12}$$

$$= \frac{1}{(4\pi)^{\frac{n}{2}} \Gamma(\frac{n}{2})} \int dr \frac{r^{M+\frac{n}{2}-1}}{(r + \Delta)^L} \tag{B.13}$$

Let

$$s = \frac{\Delta}{r + \Delta} \tag{B.14}$$

Then

$$\begin{aligned}
 \frac{1}{(4\pi)^{\frac{n}{2}} \Gamma(\frac{n}{2})} \int dr \frac{r^{M+\frac{n}{2}-1}}{(r + \Delta)^L} &= \frac{1}{(4\pi)^{\frac{n}{2}} \Gamma(\frac{n}{2})} \int ds \Delta^{M+\frac{n}{2}-L} s^{L-M-\frac{n}{2}-1} (1-s)^{M+\frac{n}{2}-1} \\
 &= \frac{\Delta^{M+\frac{n}{2}-L} \Gamma(L-M-\frac{n}{2}) \Gamma(M+\frac{n}{2})}{(4\pi)^{\frac{n}{2}} \Gamma(\frac{n}{2}) \Gamma(L)} \tag{B.15}
 \end{aligned}$$

B.4. Gamma Functions

Integrals in n dimensions involving massless particles give results in terms of the Γ function defined as

$$\Gamma(x) = \int_0^\infty dy e^{-y} y^{x-1} \tag{B.16}$$

In the calculations performed in this thesis they have appeared in combinations due to integrals such as

$$\int_0^1 dx x^{M-1}(1-x)^{N-1} = \frac{\Gamma(M)\Gamma(N)}{\Gamma(M+N)} \quad (\text{B.17})$$

The Γ function has properties;

$$\Gamma(x+1) = x\Gamma(x) \quad (\text{B.18})$$

$$\Gamma(2x) = \frac{2^{2x-1}}{\sqrt{\pi}}\Gamma(x)\Gamma\left(x+\frac{1}{2}\right) \quad (\text{B.19})$$

$$\Gamma(1) = 1 \quad (\text{B.20})$$

$$\Gamma\left(\frac{1}{2}\right) = \sqrt{\pi} \quad (\text{B.21})$$

$$(\text{B.22})$$

which can be used to simplify the expressions obtained.

B.5. Colour Factors

The only elements of the $SU(N_c)$ lie algebra encountered here have been the traceless generators T_{ij}^a and the unit matrices δ_{ij} and δ^{ab} . Here the subscripts can take N_c different values and the superscripts $N_c^2 - 1$ different values. The structure constants f^{abc} can be defined through the commutation relation,

$$[T^a, T^b]_{ij} = if^{abc}T_{ij}^c, \quad (\text{B.23})$$

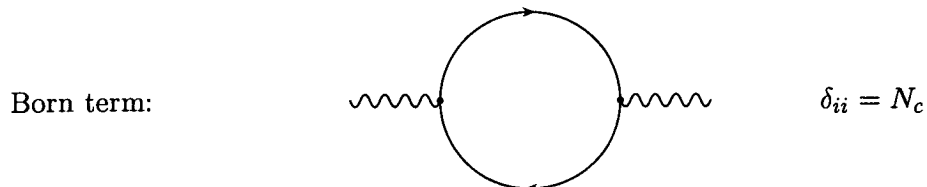
however it is the anti-commutation relation,

$$\{T^a, T^b\}_{ij} = \delta^{ab}\delta_{ij}, \quad (\text{B.24})$$

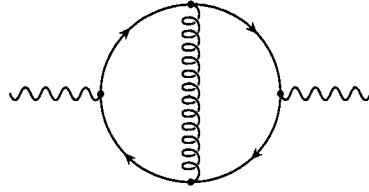
that gives the required factor for the graphs containing a gluon,

$$T_{ij}^a T_{ji}^a = \frac{N_c^2 - 1}{2}. \quad (\text{B.25})$$

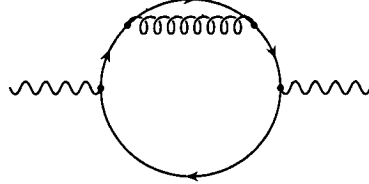
Graphically, the two colour factors used are:



B. Integrand Algebra



$\mathcal{O}(\alpha_s)$ terms:



$$T_{ij}^a T_{ji}^a = \frac{N_c^2 - 1}{2}$$

When the number of colours, N_c , is taken to be three this gives a colour factor of three for the Born term and four for the $\mathcal{O}(\alpha_s)$ terms.

C. Binned Thrust Values

| Thrust Bin | $\frac{m}{\sqrt{s}}$ | | | | |
|------------|-----------------------|-----------------------|-----------------------|-----------------------|-----------------------|
| | 0.00 | 0.05 | 0.10 | 0.15 | 0.20 |
| 0.66-0.68 | 1.56×10^{-2} | 1.52×10^{-2} | 1.38×10^{-2} | 1.19×10^{-2} | 9.32×10^{-3} |
| 0.68-0.70 | 8.32×10^{-2} | 8.08×10^{-2} | 7.36×10^{-2} | 6.30×10^{-2} | 4.97×10^{-2} |
| 0.70-0.72 | 1.60×10^{-1} | 1.55×10^{-1} | 1.41×10^{-1} | 1.20×10^{-1} | 9.43×10^{-2} |
| 0.72-0.74 | 2.43×10^{-1} | 2.36×10^{-1} | 2.15×10^{-1} | 1.82×10^{-1} | 1.44×10^{-1} |
| 0.74-0.76 | 3.39×10^{-1} | 3.29×10^{-1} | 2.98×10^{-1} | 2.53×10^{-1} | 2.00×10^{-1} |
| 0.76-0.78 | 4.30×10^{-1} | 4.38×10^{-1} | 3.98×10^{-1} | 3.39×10^{-1} | 2.67×10^{-1} |
| 0.78-0.80 | 5.91×10^{-1} | 5.73×10^{-1} | 5.17×10^{-1} | 4.41×10^{-1} | 3.47×10^{-1} |
| 0.80-0.82 | 7.63×10^{-1} | 7.37×10^{-1} | 6.65×10^{-1} | 5.68×10^{-1} | 4.48×10^{-1} |
| 0.82-0.84 | 9.92×10^{-1} | 9.61×10^{-1} | 8.60×10^{-1} | 7.35×10^{-1} | 5.82×10^{-1} |
| 0.84-0.86 | 1.31×10^0 | 1.26×10^0 | 1.13×10^0 | 9.57×10^{-1} | 7.62×10^{-1} |
| 0.86-0.88 | 1.74×10^0 | 1.67×10^0 | 1.50×10^0 | 1.27×10^0 | 1.02×10^0 |
| 0.88-0.90 | 2.39×10^0 | 2.29×10^0 | 2.05×10^0 | 1.72×10^0 | 1.39×10^0 |
| 0.90-0.92 | 3.38×10^0 | 3.23×10^0 | 2.86×10^0 | 2.43×10^0 | 1.94×10^0 |
| 0.92-0.94 | 5.11×10^0 | 4.88×10^0 | 4.27×10^0 | 3.59×10^0 | 2.90×10^0 |
| 0.94-0.96 | 8.67×10^0 | 8.13×10^0 | 7.12×10^0 | 5.96×10^0 | 4.79×10^0 |
| 0.96-0.98 | 1.87×10^1 | 1.73×10^1 | 1.49×10^1 | 1.23×10^1 | 9.79×10^0 |
| 0.98-1.00 | 4.98×10^0 | 7.70×10^1 | $1.30E \times 10^1$ | 1.90×10^1 | 2.53×10^1 |

Table C.1.: Combined $\mathcal{O}(1)$ and $\mathcal{O}(\alpha_s)$ values of thrust in different bins for values of $\frac{m}{\sqrt{s}}$ between 0 and 0.20.

C. Binned Thrust Values

| Thrust Bin | $\frac{m}{\sqrt{s}}$ | | | | |
|------------|-----------------------|-----------------------|-----------------------|-----------------------|-----------------------|
| | 0.25 | 0.30 | 0.35 | 0.40 | 0.45 |
| 0.66-0.68 | 6.76×10^{-3} | 4.29×10^{-3} | 2.23×10^{-3} | 7.97×10^{-4} | 1.12×10^{-4} |
| 0.68-0.70 | 3.58×10^{-2} | 2.29×10^{-2} | 1.20×10^{-2} | 4.16×10^{-3} | 5.87×10^{-4} |
| 0.70-0.72 | 6.85×10^{-2} | 4.36×10^{-2} | 2.29×10^{-2} | 8.19×10^{-3} | 1.29×10^{-3} |
| 0.72-0.74 | 1.04×10^{-1} | 6.67×10^{-2} | 3.50×10^{-2} | 1.26×10^{-2} | 1.98×10^{-3} |
| 0.74-0.76 | 1.45×10^{-1} | 9.34×10^{-2} | 4.85×10^{-2} | 1.84×10^{-2} | 2.63×10^{-3} |
| 0.76-0.78 | 1.93×10^{-1} | 1.24×10^{-1} | 6.72×10^{-2} | 2.75×10^{-2} | 4.19×10^{-3} |
| 0.78-0.80 | 2.54×10^{-1} | 1.64×10^{-1} | 9.12×10^{-2} | 3.54×10^{-2} | 6.61×10^{-3} |
| 0.80-0.82 | 3.29×10^{-1} | 2.16×10^{-1} | 1.24×10^{-1} | 5.10×10^{-2} | 9.57×10^{-3} |
| 0.82-0.84 | 4.31×10^{-1} | 2.87×10^{-1} | 1.66×10^{-1} | 6.92×10^{-2} | 1.36×10^{-2} |
| 0.84-0.86 | 5.64×10^{-1} | 3.82×10^{-1} | 2.27×10^{-1} | 1.03×10^{-1} | 2.17×10^{-2} |
| 0.86-0.88 | 7.63×10^{-1} | 5.25×10^{-1} | 3.16×10^{-1} | 1.48×10^{-1} | 3.42×10^{-2} |
| 0.88-0.90 | 1.04×10^0 | 7.26×10^{-1} | 4.42×10^{-1} | 2.18×10^{-1} | 5.61×10^{-2} |
| 0.90-0.92 | 1.47×10^0 | 1.04×10^0 | 6.61×10^{-1} | 3.31×10^{-1} | 9.21×10^{-2} |
| 0.92-0.94 | 2.22×10^0 | 1.60×10^0 | 1.03×10^0 | 5.34×10^{-1} | 1.69×10^{-1} |
| 0.94-0.96 | 3.67×10^0 | 2.66×10^0 | 1.73×10^0 | 9.37×10^{-1} | 2.97×10^{-1} |
| 0.96-0.98 | 7.54×10^0 | 5.49×10^0 | 3.61×10^0 | 2.04×10^0 | 7.12×10^{-1} |
| 0.98-1.00 | 3.12×10^1 | 3.65×10^1 | 4.14×10^1 | 4.54×10^1 | 4.86×10^1 |

Table C.2.: Combined $\mathcal{O}(1)$ and $\mathcal{O}(\alpha_s)$ values of thrust in different bins for values of $\frac{m}{\sqrt{s}}$ between 0.25 and 0.45.

Bibliography

- [1] Davison E. Soper. QCD calculations by numerical integration. *Physical Review Letters*, 81:2638–2641, 1998.
- [2] R. K. Ellis, D. A. Ross, and A. E. Terrano. The perturbative calculation of jet structure in $e^+ e^-$ annihilation. *Nuclear Physics*, B178:421, 1981.
- [3] Davison E. Soper. Choosing integration points for QCD calculations by numerical integration. *Physical Review*, D64:034018, 2001.
- [4] Michael Krämer and Davison E. Soper. Next-to-leading order numerical calculations in coulomb gauge. *Physical Review*, D66:054017, 2002.
- [5] Michael Krämer and Davison E. Soper. Next-to-leading order QCD calculations with parton showers 1: Collinear singularities. *Physical Review*, D69:054019, 2004.
- [6] Davison E. Soper. Next-to-leading order QCD calculations with parton showers 2: Soft singularities. *Physical Review*, D69:054020, 2004.
- [7] Michael E. Peskin and Daniel V. Schroeder. *An Introduction to Quantum Field Theory*. Perseus Books, Reading Massachusetts, 1995.
- [8] G. 't Hooft and M. Veltman. Regularization and renormalization of gauge fields. *Nuclear Physics*, B144:189–213, 1972.
- [9] G. 't Hooft. Dimensional regularization and renormalization group. *Nuclear Physics*, B61:455–468, 1973.
- [10] J. C. Ward. An identity in quantum electrodynamics. *Physical Review*, 78:182, 1950.

Bibliography

- [11] R. E. Cutkosky. Singularities and discontinuities of feynman amplitudes. *Journal of Mathematical Physics*, 1(5):429–433, 1960.
- [12] Richard D. Field. *Applications of Perturbative QCD*. Addison-Wesley Publishing Company, Reading, Massachusetts, 1995.
- [13] T. Muta. *Foundations of Quantum Chromdynamics*. World Scientific, Singapore, 1998.
- [14] JADE collaboration, S. Bethke, et al. Experimental investigation of the energy dependence of the strong coupling strength. *Physics Letters*, B213:235, 1988.
- [15] S. Catani, Yu. L. Dokshitzer, M. Olsson, G. Turnock, and B. R. Webber. New clustering algorithm for multi-jet cross sections in $e^+ e^-$ annihilation. *Physics Letters*, B269:432–438, 1991.
- [16] F. Bloch and A. Nordsieck. Note on the radiation field of the electron. *Physical Review*, 52:54–59, 1937.
- [17] T. Kinoshita. Mass singularities of feynman amplitudes. *Journal of Mathematical Physics*, 3:650–677, 1962.
- [18] T. D. Lee and M. Nauenberg. Degenerate systems and mass singularities. *Physical Review*, B133:1549–1562, 1964.
- [19] G. Grunberg, Yee Jack Ng, and S. H. H. Tye. Angular distributions of heavy quark jets in e^+e^- annihilation. *Physical Review*, D21:62, 1980.
- [20] Davison E. Soper. Techniques for QCD calculations by numerical integration. *Physical Review D*, 563:153–199, 1999.
- [21] William H. Press et al. *Numerical Recipes in Fortran 77: The Art of Scientific Computing*. Cambridge University Press, 1992.
- [22] G. P. Lepage. A new algorithm for adaptive multidimensional integration. *Journal of Computational Physics*, 27:192–203, 1978.
- [23] G. 't Hooft and M. Veltman. Scalar one-loop integrals. *Nuclear Physics*, B153:365–401, 1979.
- [24] S. Eidelman et al. *Physics Letters*, B592:1, 2004.

- [25] Zoltan Kunszt and Davison E. Soper. Calculations of jet cross sections in hadron collisions at order α_s^3 . *Physical Review D*, 46(1):192–221, 1992.
- [26] S. Brandt, C. Peyrou, R. Sosnowski, and A. Wroblewski. The principle axis of jets. An attempt to analyze high-energy collisions as two-body processes. *Physics Letters*, 12:57–61, 1964.
- [27] E. Farhi. A QCD test for jets. *Physical Review Letters*, 39:1587–1588, 1977.
- [28] R.K. Ellis, W.J. Stirling, and B.R. Webber. *QCD and Collider Physics*. Cambridge University Press, Cambridge, 1996.